STUDY ON ATMOSPHERIC PRESSURE PLASMA JET FOR PLASMA PATTERNING TOWARD CELL CULTURING

(プラズマパターニングの細胞培養応用に向けた大気圧プラズマジェットに関する研究)

A dissertation presented as a partial fulfillment of the requirements
for the degree of Doctor of Philosophy

by

WANNAKUWATHTHAWADUGE THOMAS LEON
SUGANDA FERNANDO

長岡技術科学大学
Nagaoka University of Technology

Department of Energy and Environment Science
Nagaoka University of Technology
August 2020

Statement of Authenticity

I certify that the work presented in this dissertation is original. I hereby declare that I have not submitted this material towards the fulfillment of a degree or diploma at any university or other institute. I confirm that all sources on which this work is based have been acknowledged in the bibliography.

Supervised by

Associate Professor SASAKI Toru (Chief Supervisor)
Department of Electrical Engineering,
Nagaoka University of Technology, 1603-1 Kamitomioka, Nagaoka, Niigata 940-2188, Japan.
e-mail: sasakit@vos.nagaokaut.ac.jp
TEL&FAX: +81-258-47-9559

Associate Professor KIKUCHI Takashi
Department of Electrical Engineering and Department of Nuclear System Safety Engineering,
Nagaoka University of Technology, 1603-1 Kamitomioka, Nagaoka, Niigata 940-2188, Japan.
e-mail: tkikuchi@vos.nagaokaut.ac.jp
TEL&FAX: +81-258-47-9506

Assistant Professor TAKAHASHI Kazumasa
Department of Electrical Engineering,
Nagaoka University of Technology, 1603-1 Kamitomioka, Nagaoka, Niigata 940-2188, Japan.
e-mail: kazumasa@vos.nagaokaut.ac.jp,
TEL&FAX: +81-258-47-9899

Examined by

Professor HARADA Nobuhiro
President,
National Institute of Technology, Nagaoka College, 888 Nishikatakai, Nagaoka, Niigata 940-8532, Japan.
e-mail: nobh@nagaoka-ct.ac.jp, TEL: +81-258-32-6435

Professor JIANG Weihua
Extreme Energy-Density Research Institute,
Nagaoka University of Technology, 1603-1 Kamitomioka, Nagaoka, Niigata 940-2188, Japan.
e-mail: jiang@vos.nagaokaut.ac.jp, TEL&FAX: +81-258-47-9890

Associate Professor OHNUMA Kiyoshi Department of Bioengineering and Department of Science of Technology Innovation,
Nagaoka University of Technology, 1603-1 Kamitomioka, Nagaoka, Niigata 940-2188, Japan.
e-mail: kohnuma@vos.nagaokaut.ac.jp, Tel: +81-258-47-9454, Fax: +81-258-47-9401

Associate Professor SASAKI Toru
Department of Electrical Engineering,
Nagaoka University of Technology, 1603-1 Kamitomioka, Nagaoka, Niigata 940-2188, Japan.
e-mail: sasakit@vos.nagaokaut.ac.jp, TEL&FAX: +81-258-47-9559

Associate Professor KIKUCHI Takashi
Department of Electrical Engineering and Department of Nuclear System Safety Engineering,
Nagaoka University of Technology, 1603-1 Kamitomioka, Nagaoka, Niigata 940-2188, Japan.
e-mail: tkikuchi@vos.nagaokaut.ac.jp, TEL&FAX: +81-258-47-9506

Assistant Professor TAKAHASHI Kazumasa
Department of Electrical Engineering,
Nagaoka University of Technology, 1603-1 Kamitomioka, Nagaoka, Niigata 940-2188, Japan.
e-mail: kazumasa@vos.nagaokaut.ac.jp, TEL&FAX: +81-258-47-9899

Abstract

In recent years, the development of new techniques for drug screening, modeling and the investigation of diseases, gene-editing technology, and regenerative medicine, has been investigated using cell cultures. The materials used in these investigations should exhibit specific properties such as the replication of the microenvironment of cells, cell-cell interactions, cell-substrate interactions, and spatiotemporal distribution of soluble factors. Polydimethylsiloxane (PDMS) is a notable material that is used in the field of biology to investigate these properties. However, it has a low adhesion property for cell-substrate interaction. Therefore, this material is typically subjected to surface modification processes to improve its hydrophilicity properties. Given that a low-pressure discharge plasma source in combination with a mask is used to create patterns on the surface of PDMS, this process several disadvantages such as the requirement of expensive vacuum pumps, sealed cascades, and mask charging, which limits its broad applicability.

In this investigation, a novel approach using atmospheric pressure plasma jet (APPJ) instead of low-pressure plasma for mask-free plasma patterning was experimentally investigated in cell cultures. In addition, control of the plasma patterning size was also experimentally investigated to determine the parameters of the electrode configuration, capillary tube diameter, and the use of a mask as a function of the irradiation time.

The glow discharge APPJs used in this study consist of parallel-electrode and double-electrode configurations. The double electrode APPJ configuration was further modified by including an additional grounded pin electrode at the bottom of the plasma jet. The electrode configuration, electrode polarity, capillary tube diameter, gas flow rate, and applied voltage were investigated using the double electrode APPJ to determine its impact on plasma jet properties and radical generation and propagation. The parallel electrode configured APPJ was used to achieve mask-free plasma patterning whereas the double electrode configured APPJ with and without an additional ground connected floating pin electrode was used to investigate the control of plasma pattern sizes.

The interaction between the direction of the applied electric field and the flow direction of the discharge plasma affects the plasma jet length and the radical generation. A longer plasma jet length and a high density of radicals can be obtained using the parallel interaction compared to the perpendicular interaction. The inclusion of an additional grounded pin electrode at the bottom of the plasma jet provides a physical potential point in the atmosphere, and results in secondary radical generation to further improve the jet length and increase the density of the propagation radicals.

The behavior of the plasma jet flow depends on the capillary tube diameter and the gas flow rate. The plasma jets that occurred in the laminar regime exhibited a longer plasma jet with a cone shape behavior, whereas in the turbulent regime, the length tends to fluctuate while deviating from the cone shape. The generation and propagation of radicals along with the plasma jet were also affected by this flow behavior, as the increase of the flow rate caused an increase of the density in the laminar regime and a decrease in the turbulent regime. The electric field strength increased with the density of generated and propagating radicals.

The oxidization of the surface of PDMS was performed using reactive oxygen in a discharge plasma. Hence, plasma etching was performed on the surface of PDMS using oxygen low-pressure plasma. Optical emission spectroscopy of the APPJ revealed its presence along with the plasma jet. Its density increased with the gas flow rate in the laminar regime, and the voltage applied to the double electrode configuration with an additional grounded pin electrode.

In this work, the author experimentally confirmed the oxidization of the surface of PDMS due to APPJ irradiation. The contact angle was measured as a function of the hydrophilicity of fabricated PDMS surfaces. The experimental results confirm that the irradiation time and the gas flow rate affect the wettability as the increase of these parameters cause a decrease of the contact angle. The area of the mask-free plasma pattern increased as irradiation time increased in the order of a few millimeters. The increase of the gas flow rate affected the increase of the wetting size for a considered irradiation time. Experimental evidence collected in this study confirmed human induced Pluripotent Stem Cells (hiPSCs) cultivation on mask-free plasma patterned PDMS surfaces using APPJ, and its cluster sizes were similar for respective wetting sizes as a function of irradiation time.

Compared to the parallel electrode, the double electrode APPJ generated a longer plasma jet with an increase of optical emission from radicals. The addition of a grounded pin electrode at the bottom of the plasma jet further enhanced these properties. Mask-free plasma patterning was performed using these sources. The experimental evidence revealed that the double electrode configured APPJs with or without a ground connected additional pin electrode facilitated mask-free plasma patterning for cell cultivation. Although the additional grounded pin electrode configuration improved the plasma jet properties, it did not result in variation of the plasma pattern size as a function of the irradiation time. A reduction of the capillary tube diameter caused a decrease of the diameter and jet length of the plasma jet. However, this decrease was also experimentally determined to be ineffective in reducing the pattern size as a function of the irradiation time. The experimental results revealed that the use of a mask and APPJ irradiation reduced the pattern size to less than the mask size for low irradiation times.

Based on the findings of this study, it was confirmed that APPJ can be

used for mask-free plasma patterning and cell cultivation. Moreover, it can be used as an alternative approach to low-pressure plasma patterning with a mask. The plasma pattern size can be controlled down to a few hundred micrometers using APPJ irradiation for lower irradiation times with a mask.

Acknowledgement

First, I would like to express my deepest gratitude to my family, Mrs. Achini Pullaperuma and my dearest son Master Denith Fernando for their tremendous support and their sacrifices in every aspect during this study period.

I am grateful to my late farther Mr. Laksiri Fernando, my mother Mrs. Padmi Fernando, my brothers Mr. Shihan Fernando and Mr. Alban Fernando, and my in-laws Mr. and Mrs. Pullaperuma and their family members for their support in this period.

I would like to express my intensive gratitude to my supervisor, Associate Professor Toru Sasaki of the Department of Electric, Electrical, and Information Engineering at Nagaoka University of Technology, not only for his kindness, guidance and intelligence during my studies, but also for his bountiful support and endurance throughout all the difficulties, I encountered. His technical and editorial advice was essential to the completion of this dissertation.

I am grateful to Associate Professor Takashi Kikuchi from the Department of Nuclear System Safety Engineering cum Department of Electric, Electrical, and Information Engineering, and Assistant Professor Kazumasa Takahashi from Department of Electric, Electrical, and Information Engineering at Nagaoka University of Technology, for mentoring me through my difficulties, and providing me with the support I needed to complete my studies, as well as their invaluable kindness and friendly support.

I am grateful to Professor Nob Harada, the president of the National Institute of Technology Nagaoka College for directing me to persuade my doctoral studies and mentoring me in difficult times in his best capacity, and connecting me to the communities in Fukazawa, Nagaoka for lifelong memories of Japan.

I would like to thank Associate Professor Kiyoshi Ohnuma from the Department of Bioengineering and the Department of Science of Technology for his kindness, guidance, mentoring, and his assistance in the completion of this dissertation.

I would like to thank Professor Weihua Jiang from the Department of Electrical, Electronics and Information Engineering and the Department of Nuclear System Safety Engineering, for using his valuable time to evaluate my studies and his

thoughtful comments to improve my work. I am grateful to Dr. Piumi Ishanka from the Department of Computer and Information System at Sabaragamuwa University of Sri Lanka for opening this path for me to pursue my graduate studies at Nagaoka University of Technology.

I wish to thank my friends Dr. Fumihiro Tamura, Mr. Kimura and his family, Mr. Kunii, and the community of the Fukazawa for having me as their family member and the long-lasting memories. I wish to thank my dear friends, Dr. Phouc, Mr. Thanet, Dr. Uchida, Dr. Mai, and Ms. James for their good company and friendship throughout my studies.

I would like to give special thanks to Mr. Ryo Kobayashi for being by my side throughout my studies and for his tremendous support to complete my studies. There are no words to express my gratitude to the past and present members of the MHD laboratory for their friendship, brotherhood, and their assistance when I had trouble with Japanese language during my studies.

I would like to thank the Sri Lankan community for their support during my many challenges and for their assistance with the transition of living in Japan.

I am profoundly indebted to the scholarship donor, Monbugakusho scholarship from the Government of Japan via the Japanese Ministry of Education, Culture, Sports, Science, and Technology (MEXT), for providing financial support during my studies at Nagaoka University of Technology. Moreover, thanks to the university, its staff and the country of Japan for providing me with these opportunities and the worthwhile experiences to aid me as I venture into the world and face the many challenges of life.

Finally, thank you to all who I mentioned here and missed for their support and kindness; without your help this will be impossible.

Japan, Nagaoka, August 2020
Leon Fernando

Contents

List of Figures

List of Tables

List of Publications

Journal Publications

[1]. W. T. L. S. Fernando, G. Kato, S. Miyazaki, K. Maruyama, K. Takahashi,T. Kikuchi, K. Ohnuma, and T. Sasaki, “Mask-free plasma patterning forbiocompatible material using atmospheric pressure plasma jet,” *IEEE Trans-actions on Radiation and Plasma Medical Sciences*, vol. 4, no. 1, pp. 108–112,2020.

[2]. W. T. L. S. Fernando, K. Takahashi, T. Kikuchi, and T. Sasaki, “Effect ofadditional pin electrode placing at the bottom of the plasma jet and flow be-havior on radical generation and propagation,” *IEEE Transactions on Plasma Science*, pp. 1–8, Article DOI: 10.1109/TPS.2020.3000570, 2020.

Conference Publications

[1]. W. T. L. S. Fernando, K. Morito, G. Kato, K. Ohnuma, K. Takahashi, T. Sasaki, and T. Kikuchi, ”Effect of the additional ground electrode in double electrode configuration in maintaining stable atmospheric pressure plasma jet for bio-applications,” in *Cheminas37*, Tsukuba, Japan, 2018.

[2]. W. T. L. S. Fernando, R. Kobayashi, K. Takahashi, T. Kikuchi, K. Ohnuma, and T. Sasaki, ”Effect of electrode polarity to atmospheric pressure plasma jet and its applicability to surface modification of bio-compatible material,” in *NIFS workshop on New developments in plasma beam physics and applications developed by new generation pulsed power technology*, Gifu, Japan, January 2019.

[3]. W. T. L. S. Fernando, K. Takahashi, T. Kikuchi, and T. Sasaki, ”Behavior of Atmospheric Pressure Plasma Jet using Double Electrode with Additional Ground Electrode,” in *XXXIV ICPIG & ICRP-10, ISBN 978-4-900986-19-0*, Sapporo, Hokkaido, Japan, 2019.

[4]. W. T. L. S. Fernando, K. Takahashi, T. Kikuchi, and T. Sasaki, ”Radical distribution along the plasma jet for double electrode APPJ with additional pin ground electrode,” in *APSPT-11*, Kanazawa, Japan, 2019.

[5]. K. Thanet, W. T. L. S. Fernando, K. Takahashi, T. Kikuchi, and T. Sasaki,

”Determination of Helium discharge atmospheric pressure plasma parameters,” in *XXXIV ICPIG & ICRP-10, ISBN 978-4-900986-19-0*, Sapporo, Hokkaido, Japan, 2019.

Publications under review (Journal)

[1]. W. T. L. S. Fernando, K. Takahashi, T. Kikuchi, and T. Sasaki, “Effect of additional pin ground electrode to the double electrode configuration on the properties of He atmospheric pressure plasma jets,” *IEEE Transactions on Plasma Science*, revision submitted 07.07.2020, (TPS12916).

Chapter 1

Introduction

This chapter focuses on understanding the physical phenomena related to the atmospheric pressure plasma jet and its applicability to plasma patterning without a mask. Background, motivation, and the scope of this study are discussed in this chapter in addition to the introduction of this dissertation.

The fourth state of matter is known to be "plasma," which consists of ionized gases containing charged particles of electrons, positive ions, negative ions, and excited atoms, in addition to molecules. Thermal energy provided through electrical circuits or electromagnetic radiation is able to dislocate the bond of neutral gases to generate highly ionized gases [1] - [2]. Depending on the supplied energy and the energy transferred to the plasma, its properties are may change. Variation of the electron density and electron temperature allow the different categories of plasmas to be distinguished and their classification is as shown in Figure 1.1.

Considering the thermal properties of these plasmas, they are classified into thermal and non-thermal plasmas. Non-thermal plasma sometimes called "cold plasma," possesses the thermal properties of a high electron temperature and a low gas temperature. Deviation from the thermodynamic equilibrium of these plasmas defines a category called non-equilibrium plasma. In this type of plasma, the gas temperature remains close to room temperature, which facilitates its use for thermally sensitive applications, especially in the field of biology. The development of sources that operate under atmospheric conditions has attracted significant attention in plasma technology, and primarily entails atmospheric pressure plasma (APP). The absence of the requirement of expensive vacuum equipment, the easy assemble of the setup, low manufacturing cost, portability, and ability to be modified according to requirements, provide value addition to these sources. Currently, these APP sources are used in a vast number of applications such as surface treatment, nano-particle synthesis, and in the field of biomedicine [3] [4] [5] [6].

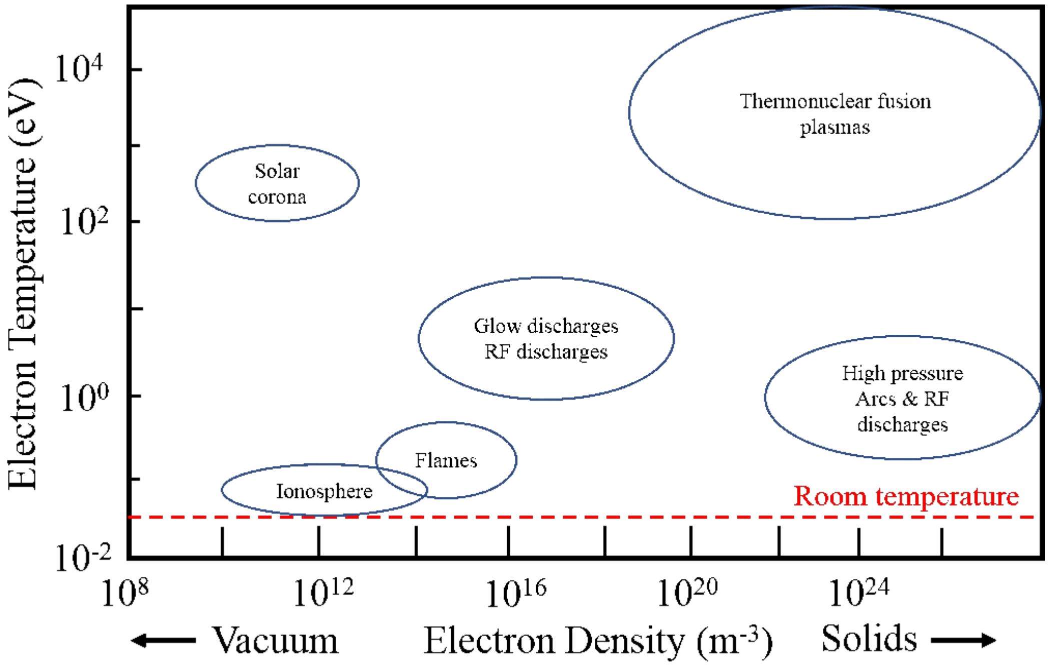

Figure 1.1: Classification of plasma (electron temperature vs electron density) [1]

Dielectric barrier discharge (DBD) is the main technique used to generate the APP. The application of high voltage pulses between two electrodes separated by an insulating dielectric barrier filled with air or rare gas at atmospheric pressure to generate an electrical discharge, results in the ionization of the gases to the plasma state. Different electrode configurations along with different applied voltage waveforms in the frequency range from radio-frequency to DC have been investigated based on the DBD technique to generate APP. Out of all the DBD plasma sources, atmospheric pressure plasma jet (APPJ) stands out because of its simplicity of design and convenience of use. The ability to localize and the generation of reactive species and radicals under atmospheric conditions renders these sources as useful, especially for surface treatment applications [7] [8] [9]. Such plasma jets can be used to fabricate biocompatible materials without a mask for the culturing of cells.

Fabrication of biocompatible materials for the culturing of biological cells is only possible if the fabrication technique satisfies certain conditions. To achieve these conditions according to the application requirement, the physical characteristics of APPJs must generally be varied. The characteristics of these plasmas are affected by various parameters such as the gas flow rate, working gas, arrangement of the DBD reactor, and the electrode configurations. Variations of these characteristics affect the generation and propagation of the reactive and excited species along the plasma jet.

Plasma treatments on biocompatible surfaces can change the hydrophilicity condition to improve cell attachment for cell culture applications. Polydimethylsiloxane (PDMS) is a widely using biocompatible materials for cell culturing, although the surface of PDMS is hydrophobic. One way to improve the wettability of PDMS has been reported using low-pressure plasma irradiation with a patterned mask. However, plasma patterning using low-pressure plasma limits the controllability of the pattern size. To overcome this limitation, the use of APPJ as a source to pattern the PDMS surface without a mask needs to be investigated.

Considering the pros of using APPJ for mask-free plasma patterning for cell culturing, this chapter is focused on understanding the properties of APPJ and its discharge behavior for the breakdown mechanism. The importance of spectroscopy in understanding the thermodynamic properties and the identification of radicals from APPJ sources will be discussed. The properties of biocompatible materials with modified surfaces for cell culturing with and without a mask will also be investigated. Finally, the scope of this study and the structure of this dissertation will be discussed in addition to the motivation for this work.

1.1 Atmospheric pressure plasma

In this study, non-equilibrium plasmas generated in open systems or under atmospheric conditions from electric discharge are considered as APP. In such plasmas, the application of an electric field transmits electrical energy to the electrons of the working gas to increase their kinetic energy. As these energetic electrons travel through the electric field, they undergo elastic and inelastic collisions with neutral species to generate excited species and ions [10].

The application of a large electric field in short periods in the case of air or feeding gas can generate plasma between the dielectric coated electrodes. This mechanism is known as dielectric barrier discharge (DBD) and variation of the electrode configuration in these models result in different properties of the plasma. This section discusses the basics of DBD plasma techniques along with the plasma jet and its use in bio-applications.

1.1.1 Dielectric Barrier Discharge and Plasma jet

DBDs are considered as self-sustaining electric discharges that occur between two electrodes supported by an insulator medium. Dielectric mediums such as glass, quartz, and ceramics are widely used in these systems with insulator mediums of air, rare gases, molecular gases, or a mixture of gases to generate non-thermal plasma [11]. . As the applied voltage exceeds the breakdown voltage of the insulator medium, it is converted into a conducting medium to generate a discharge plasma. DBD plasma characteristics depend on the capacitive character of discharge

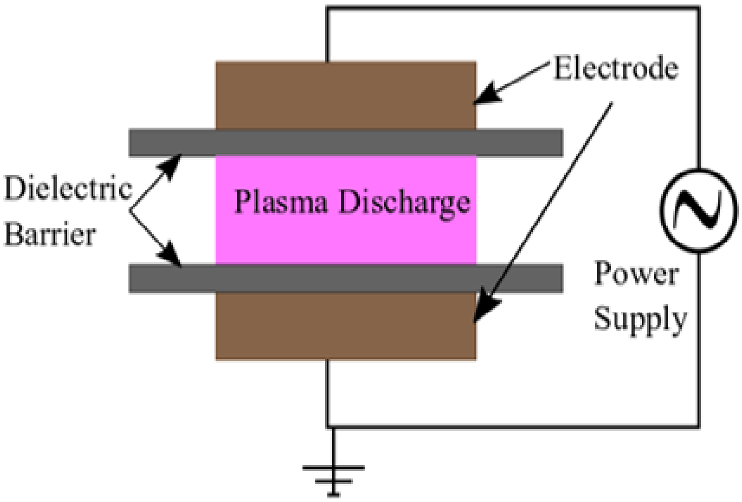

Figure 1.2: Schematic system of DBD configuration

alignment and the properties of the voltage source. Figure 1.2 shows the schematic system of a general DBD configuration.

The breakdown voltage in DBD systems was experimentally investigated by Paschen and Friedrich as a function of pressure and gap length [12] [13] [14]. The relationship between theses parameters is described by Paschen's law, which is expressed as equation (1.1) [14]:

$$V_{\mathrm{b}} = \frac{Bpd}{ln[Apd - ln[ln(1+\frac{1}{\gamma})]]} \tag{1.1}$$

where, V_b is the breakdown voltage (V), p is the pressure (Pa), d is the gap distance between the electrodes (m), and γ is the secondary-electron-emission coefficient. A and B are constants, where A is the saturation ionization of the gas at a certain $\frac{E}{p}$ (electric field/pressure) and B is related to the excitation and ionization energies.

As indicated by the equation 1.1, the breakdown voltage depends on product of p and d for a given gas. Figure 1.3 shows the Paschen curves for the helium, argon, and neon using the equation 1.1.

Considering the DBD sources, atmospheric pressure plasma jet (APPJ) stands out among the APP sources. Using capillary tubes and electrodes, APPJ sources were designed. In these designs, one end of a capillary tube was connected to a working gas, and plasma was generated inside the tube using an electric discharge. After the plasma is generated inside the tube, the working gas pushes plasma plumes to the atmosphere through the other end of the capillary tube. As it propagates, it interacts with the species in the atmosphere to generate excited and reactive radicals along their path. A unique jet shape and coaxial symmetry along the plasma plume facilitates the use of these devices in surface treatments on substrates away from the source. Figure 1.4 shows a typical APPJ configuration used to generate plasma for biological applications [15] [16] [17].

The main feature of these sources is the ability to propagate plasma as a jet with properties such as a cone shape in the propagation direction and a circular shape in the perpendicular plane to the propagation direction. These features allow for modification at a localized point on substrates without a mask. In addition to these properties, many studies have demonstrated that these plasma plumes propagate as plasma bullets and interact with species in the atmosphere [18] [19] [20]. This leads to the generation of different chemical species according to the plasma bullet properties.

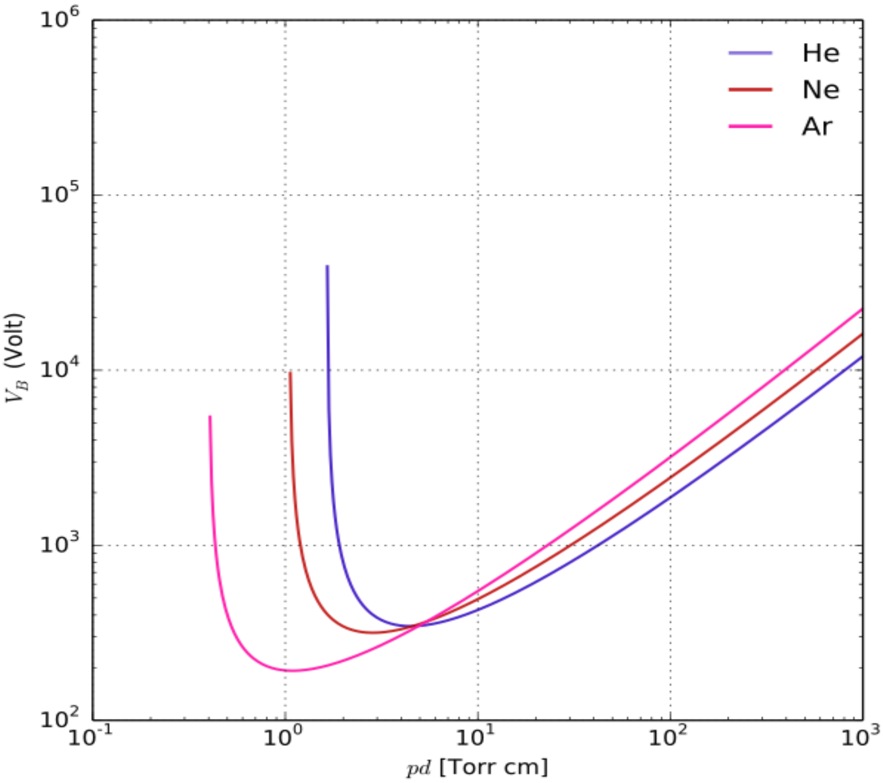

Figure 1.3: Paschen curves for helium, argon, and neon [14]

1.1.2 APPJ in bio-applications

Bio-applications are mostly performed in temperature-sensitive environment since cells and bio-sensitive materials can be decomposed at high temperatures. In these studies, cell detachments, sterilization, and wound healings have been shown to be affected by the reactive species at room temperature. For such requirements, it is essential to produce reactive species at room temperature without affecting the bio-environment. Given that APPJs generate reactive species at room temperature, these plasma sources are ideal for bio-applications.

The main advantage associated with the use of APPJs for bio-applications is that they generate excited radicals and reactive species under atmospheric conditions, at near room temperature. Dielectric barrier discharge plasma sources, which spread plasma equally over a surface, require masks to expose only specific areas. Compared to such sources, APPJs provide the ability to focus plasma on a localized point or treatment area without a mask.

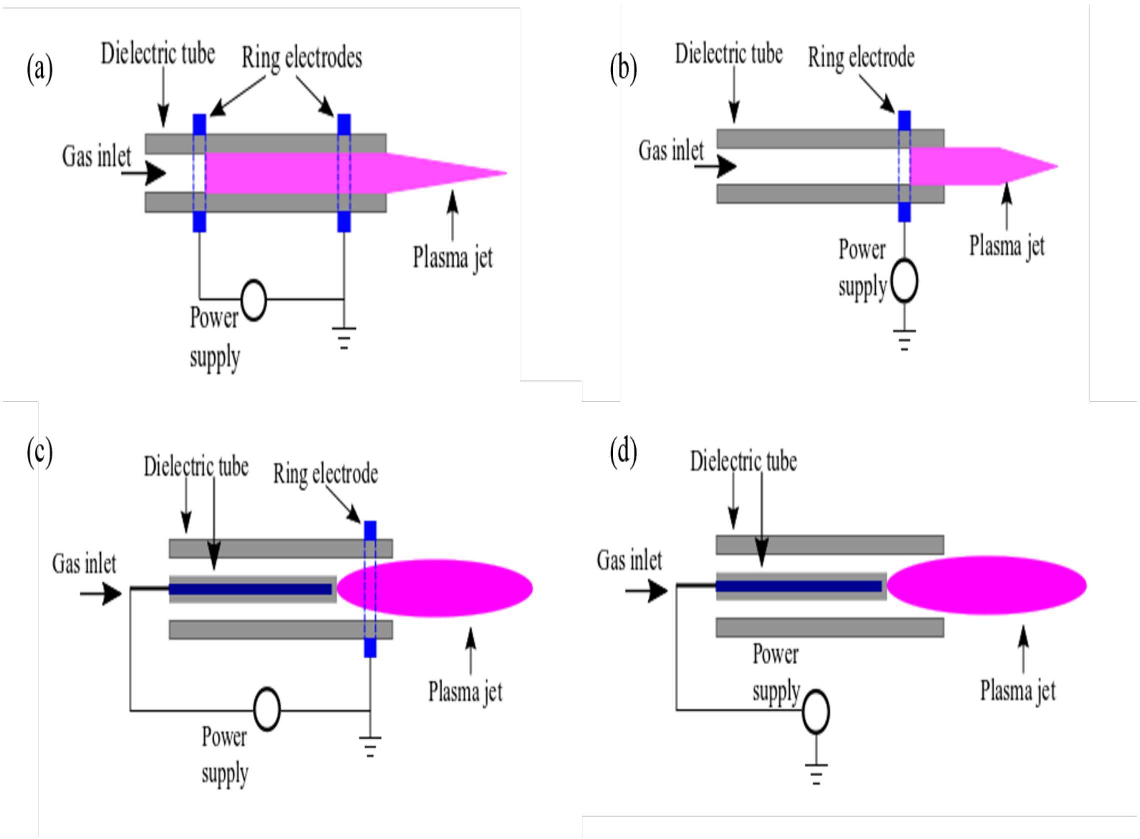

Figure 1.4: Typical plasma jets configurations [15]

1.2 Types of discharge

This section discusses the breakdown mechanism, and features of the discharges obtained from APP. A common approach that is used to generate APP is the application of an electric field between two electrodes using a dielectric medium to produce an electric discharge through the non-conductive medium. However, the electric field strength and surrounding environment affect the type of discharge such as arc, glow, and corona [21].

As the applied voltage reaches the breakdown voltage, electrons have enough velocity to be liberated and undergo collision to generate plasma. The generation of positive and negative ions and their density throughout the discharge process affect the discharge current waveform characteristics. Sustainability of the plasma depends on the avoidance of recombination processes. Therefore, it is necessary to supply enough energy via the voltage waveform to achieve sustainability. This will be discussed further in the following sections. A summary of these discharges can be illustrated using the voltage and current characteristics as express in Figure 1.5 [22].

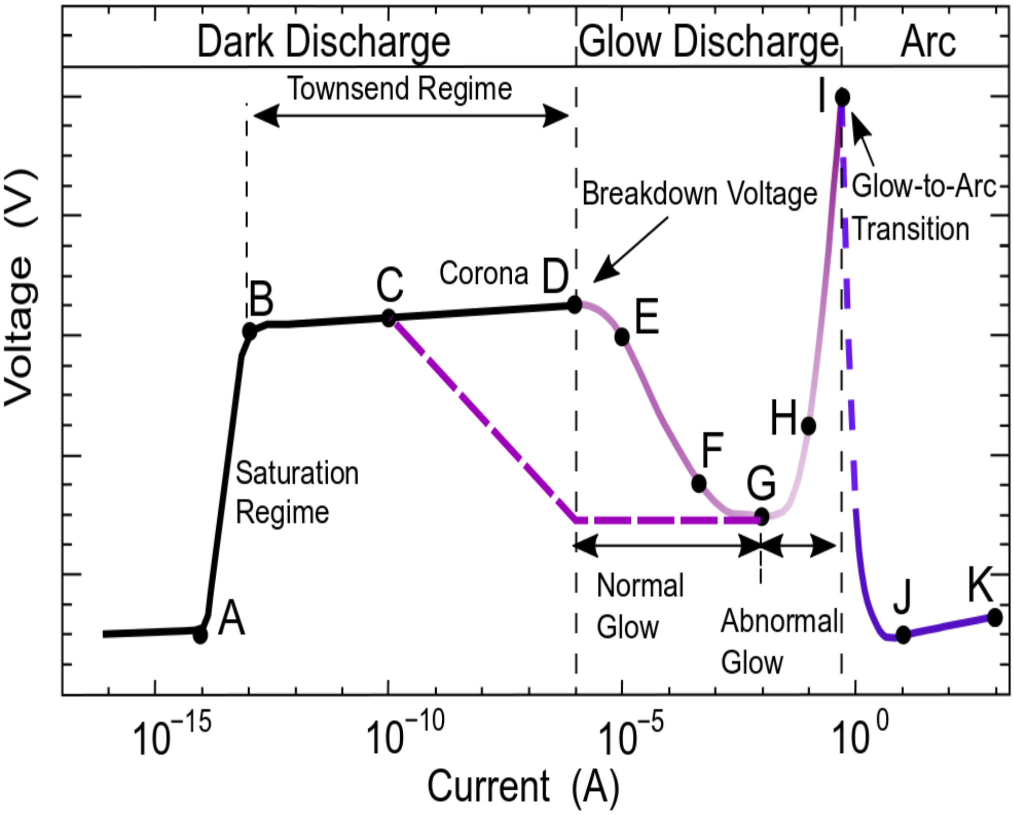

Figure 1.5: Voltage-current characteristics of an electrical discharge [22]

1.2.1 Arc discharge

Electrical breakdown of the working fluid occurs because the electrical discharge can cause an increase of thermionic, which is known as an electrical arc [23]. Such a discharge possesses a high current density as presented in Figure 1.5, due to the generation of additional ions from the thermionic emission. In arc discharge APPJs, electrons emitting from the cathode undergo collisions with the feeding gas to generate secondary ions. Positive and negative ions travel along the applied electric field direction and undergo further collision to increase the density of the charge ions. As the feeding gas flows to the atmosphere, it carries some of the ionized particles along with it to generate Arc APPJs, as presented in Figure 1.6.

This breakdown mechanism leads to an increase in the electric field strength of the plasma along the propagation direction. However, exhaustion of charged ions to the atmosphere avoids the continuation of ionization to equilibrium, inside the discharge vessel and causes the density of the ionized particles in the cell to be less

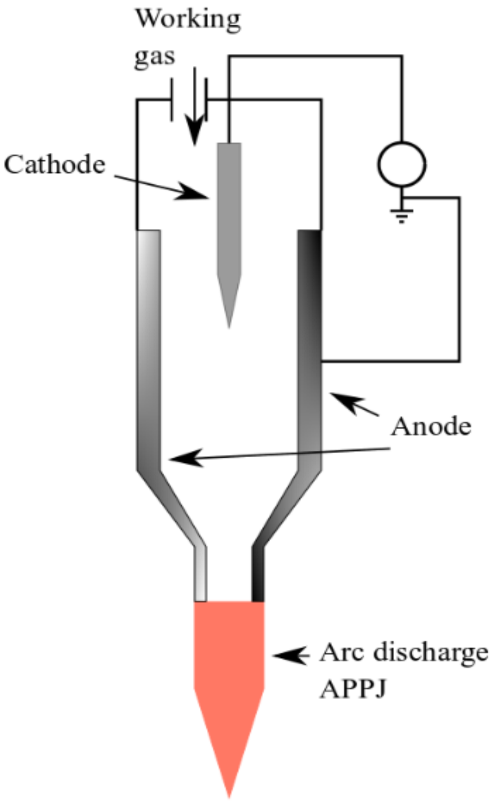

Figure 1.6: Schematic of Arc discharge APPJ

than that of the neutral species. In these sources, due to thermionic emission from the cathode, the density of the ionized particles is high compared to the other APPJ sources. Hence, its thermodynamic properties are also high. A schematic of the arc discharge APPJ is illustrated in Figure 1.6.

Arc discharges are widely using in melting, cutting, and welding of condensed materials [21] [24] [25] [26]. In these discharge sources, the fabricated material is normally used as one of the electrodes. When the active electrodes achieve a sufficiently high voltage to discharge the electrons through the working gas with minimal resistance, the flow of electrons rapidly heat up the fluid to generate plasma.

1.2.2 Glow discharge

As presented in Figure 1.5, when the applied voltage between the two electrodes reaches the breakdown voltage of the working gas, a glow discharge is produced. The important feature of this discharge is that the density of the ionized particles is lower than that of the neutral species. Applying a constant gas flow to

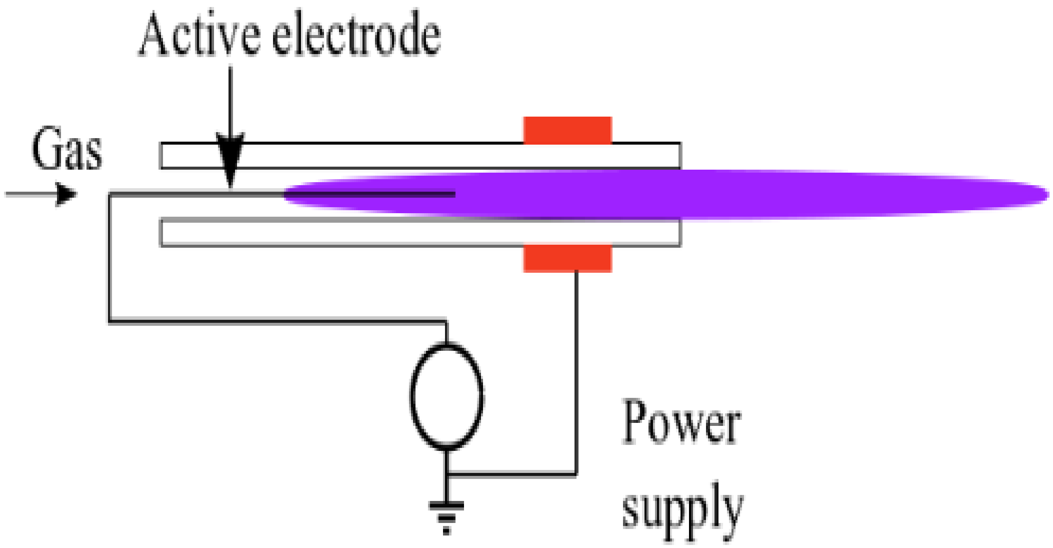

Figure 1.7: Schematic of glow discharge APPJ

such a discharge maintains the low density of the ionized species compares to the neutral species between the electrode [27].

In glow discharges, positive ions are accelerated towards the cathode and release secondary electron emission due to electron bombardment. As electrons arrive in the plasma, they cause excitation and ionization collisions. Excitation collisions generate subsequent radiative decay to the lower energy levels of the excited species and emit characteristics light, which is observed as a glow. The optical characteristics changes with the properties of the working gas. Figure 1.7 shows the schematic of a glow discharge plasma jet.

Ionization collision improves the ion-electron pairs to sustain the plasma as it propagates through the atmosphere as a plasma bullet [17] [28]. These plasma bullets have their own electric potential, which is sufficient to react with the neutral species to create excited and reactive species on their way. Given that these discharges maintain their optical characteristics, they are widely used in sign boards.

1.2.3 Corona discharge

Corona discharge can be considered as Townsend discharge or negative glow discharge associated with the strong electric field near a conductor [21] [29]

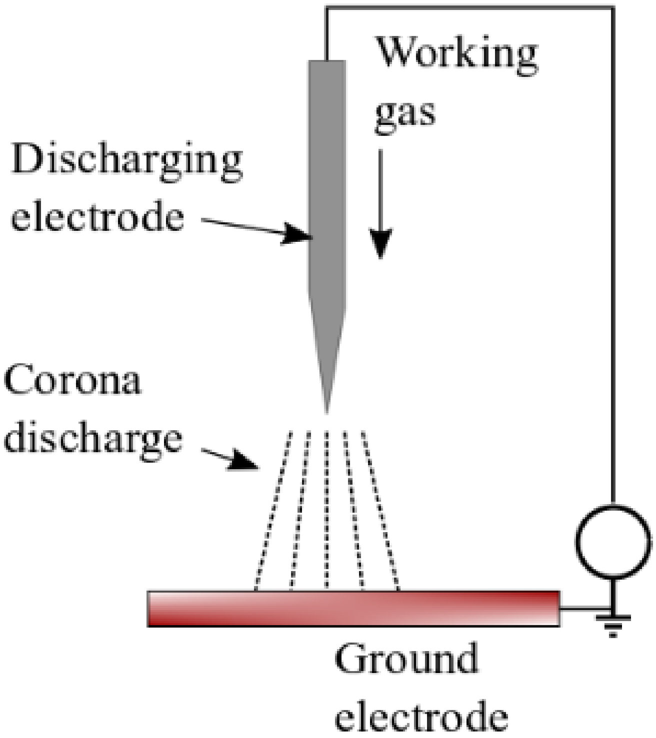

Figure 1.8: Schematic of corona discharge APPJ

[30]. These discharges appear as a localized bluish luminous glow. The electric field strength around a conductor is high enough to form a conductive region, but not sufficiently high for an electrical breakdown to initiate a sustainable plasma condition.

In corona discharges, large electric potential gradients cause the ionization of the working gas in a short region, but as it moves further, the electric potential gradient becomes smaller, thereby diminishing the corona discharge at longer range. Therefore, these discharges can be observed only over short ranges. For the APPJs, streamer bullets that carry their own electric potential are propagated. As they arrive at sharp objects such as pin electrodes over a short range, they can create a negative corona discharge. In such situations, the creation of secondary ionized and excited species is expected around the pin electrodes. A schematic of a corona discharge APPJ is present in Figure 1.8.

1.3 Breakdown mechanism of APPJs

The importance of APPJ sources has increased in recent years because of their ability to create reactive species at atmospheric pressure. The investigation of different electrode configurations has also been performed to improve the performance of APPJ sources according their intended application. An understanding of the generation of plasma inside a capillary tube and the propagation of plasma as jet provides valuable information for the modification of these sources for improved performance. In this section we discuss the breakdown mechanism for a single electrode, double electrode, and parallel electrode configured APPJs.

1.3.1 Single electrode configuration

Single electrode configured APPJs are suitable in terms of attempting to understand the breakdown mechanism of plasma ignition inside a capillary tube and its propagation. Figure 1.9 shows a schematic of a single electrode configured APPJ.

As shown in Figure 1. 9, the discharge generated from a single electrode can be classified into two groups, (I) downstream jet and (II) upstream jet. When

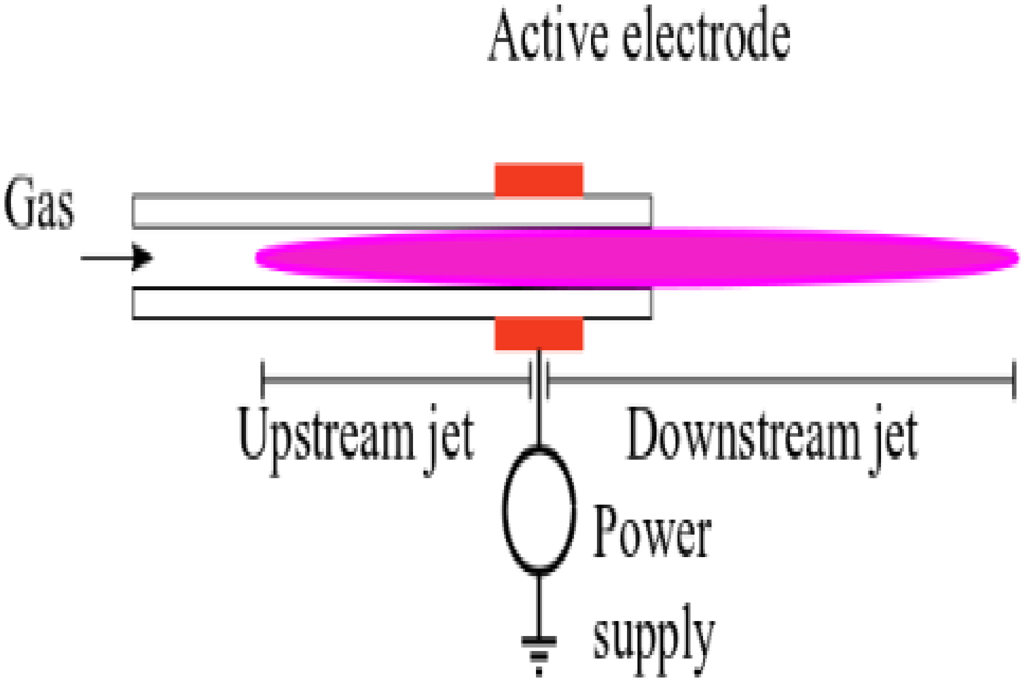

Figure 1.9: Schematic for single electrode APPJ configuration.

the applied voltage at the active electrode increases and exceeds the breakdown voltage, this creates a plasma plume in the downward and upward direction in these configurations. A further increase of the applied voltage beyond the breakdown voltage increases the jet length in the upward direction compares to the forward jet. Glow discharge occurs as the emission intensity in the forward direction decreases compared to the upward direction as the corona discharge and glow discharge further ionize the working gas inside the capillary tube, which accounts for such a mechanism [19] [31]. The jet length in these APPJs sources is strongly corelated with the applied gas flow rates, rather than the applied voltage. A single electrode configuration generates electrical discharges at the active electrode, which propagates through the gas to create a glow discharge.

1.3.2 Double electrode configuration

The inclusion of an additional grounded electrode to the single electrode configuration is defined as a double electrode configuration and its schematic is shown in figure 1.10.

In the double electrode configured APPJ, discharge can be categorized into

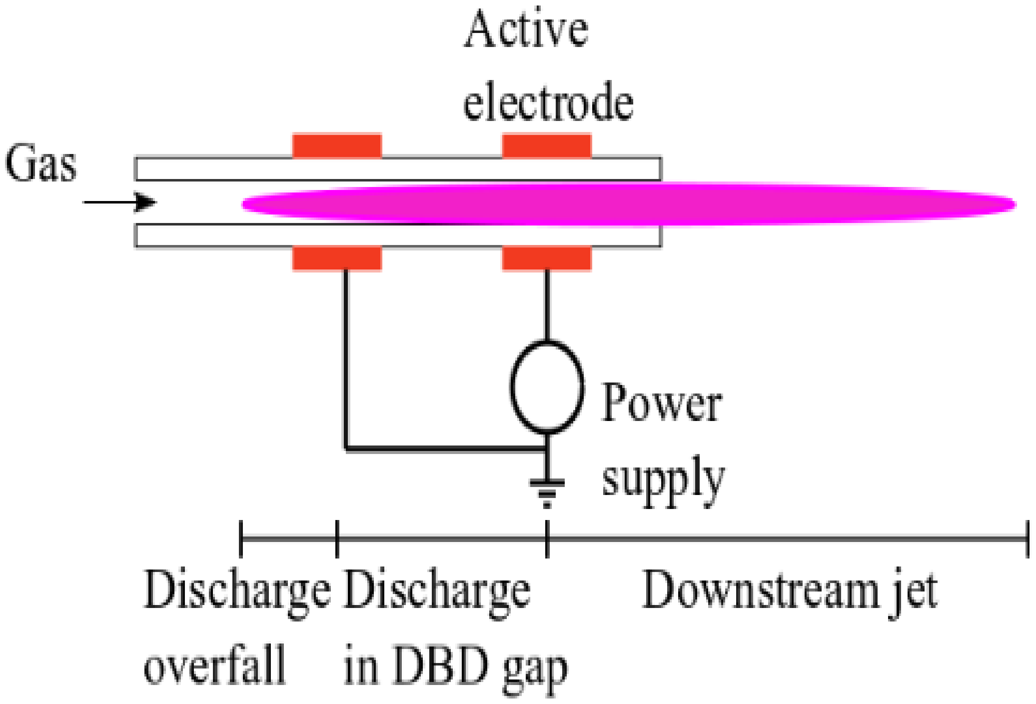

Figure 1.10: Schematic for double electrode APPJ configuration.

three groups: (I) downstream jet, (II) discharge at DBD gap, and (III) discharge overfall at upward jet. Similar to the single electrode configured APPJ, electrical discharge starts from the active electrode. Because of the attachment of the grounded electrode to the dielectric capillary tube, the behavior of the upward jet changes from the single electrode configured APPJ. Plasma discharge that occurs inside the capillary tube now experiences the ground voltage at a certain distance, compared to the virtual ground potential in the single electrode configuration. The presence of a ground potential affects the charge particles resulting in high conductivity. This causes the corona discharge at the ground electrode to glow strongly through the DBD gap. As the applied voltage is increased, the discharge that occurs at the ground electrode tends to generate discharge overfall in the upward flow direction [31].

1.3.3 Parallel electrode configuration

In this configuration, the active electrode and ground electrode are attached parallel to the dielectric capillary tube as shown in Figure 1.11.

As seen in Figure 1.11, the parallel electrode configured APPJ also has

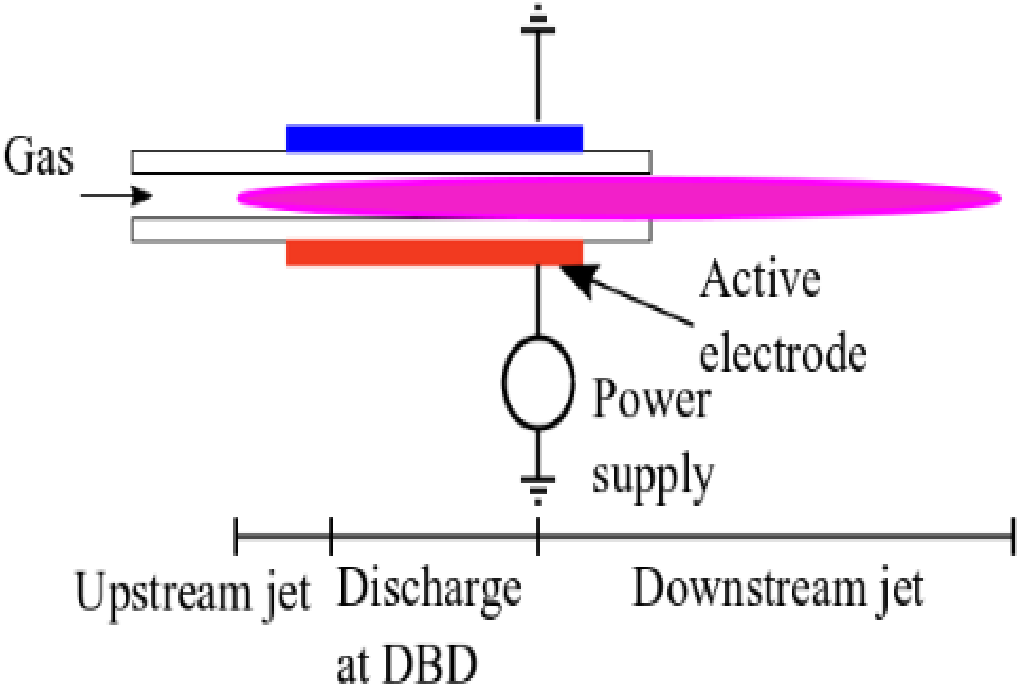

Figure 1.11: Schematic for parallel electrode APPJ configuration.

three different discharge regions; (I) downstream jet, (II) discharge at DBD, and (III) upstream jet. The length of the electrodes in the parallel electrode configuration is greater than that of the single and double electrode configurations. The attachment of electrodes parallel to each other act as a DBD plasma generator. In these sources, it is essential to use large outer diameter capillary tubes to avoid the occurrence of corona discharge between the two electrodes at the outer surface.

Similar to the previously explained breakdown mechanism, parallel electrode configuration APPJ also followed the same mechanism. Another important point to consider in these sources is maintaining a gap between the electrodes and the nozzle exit to avoid arc discharge between them.

1.3.4 Plasma jet propagation velocity and propagation phase

Many studies have investigated the properties of plasma jet and their propagation has been identified to occur as streamers or bullets [32] [33]. Images taken using high-speed CCD cameras have confirmed that plasma jets propagate as streamers [15] [18] [34]. Such propagations has also been further investigated based on the polarity of the applied voltage pulse. These studies confirm that a plasma jet can increase the streamer intensity and its propagation for a positive polarity of the applied pulse, with a decrease observed for a negative polarity. The intensity of the streamers plays a major role in the generation of radicals along the jet propagation direction along, in addition to supplying its own streamer potential.

Studies conducted by Begum *et al* [35], clearly describe the propagation of the plasma jet as being divided into three separate categories including the transition phase, propagation phase, and collapsing phase. The main feature of the transition phase is an increase of the streamer velocity to its maximum level. In addition, the study revealed that the streamer velocity is significantly affected by the applied voltage compared to the flow behavior and the pulse width.

Studies on the plasma jet properties have also identified a relationship between the streamer velocity and electric field strength [36]. These studies show that an increase of the electric field causes an increase of the streamer velocity. These experimental results indicate that there is an increase of the electric field strength on the streamers due to the applied voltage waveform or an external source causes an increase of the streamer velocity. Such an increase of the streamer velocity also increases the propagation phase [35].

Considering a physical point of view, the electric field along the plasma jet propagation direction affects the drift velocity, mobility, and mean free path. These parameters will affect in turn affect the plasma jet properties such as the plasma jet length, as well as the chemical kinetics along the plasma jet. Under the influence of an electric field, the drift of electrons can be expressed as equation 1.2 as follows.

$$v_{\mathrm{ed}} = \frac{eE}{m_{\mathrm{e}}\nu_{\mathrm{ea}}} \tag{1.2}$$

where, v_{ed} is the electron drift velocity, ν_{ea} is the collisional rate of electrons and atoms, m_{e} is the mass of the electron, e is the charge of the electron, and E is the electric field strength along the plasma jet.

The drift of the electrons can also be expressed using the mobility (μ_{e}) of the electrons as shown in the equation 1.3.

$$v_{\mathrm{ed}} = \mu_{\mathrm{e}}E \tag{1.3}$$

where mobility can be expressed using equation 1.4,

$$\mu_{\mathrm{e}} = \frac{e}{m_{\mathrm{e}}\nu_{\mathrm{ea}}} \tag{1.4}$$

According to the equation 1.4, mobility depends on ν_{ea}. The collision rate of electrons and atoms can be express using the mean free path as shown in equation 1.5.

$$\nu_{\mathrm{ea}} = \frac{\overline{v_{\mathrm{e}}}}{\lambda_{\mathrm{ea}}} \tag{1.5}$$

where, ($\overline{v_{\mathrm{e}}}$) and λ_{ea} are electron average velocity and mean free path for electron-atom collisions, respectively. In addition, the mean free path can be expressed using the cross-section (σ) and number density (n_{a}) of atoms. . Therefore, equation 1.5 can be rewritten as equation 1.6 a and equation 1.4 as equation 1.7.

$$\nu_{\mathrm{ea}} = \sigma_{\mathrm{ea}}n_{\mathrm{a}}\overline{v_{\mathrm{e}}} \tag{1.6}$$

$$\mu_{\mathrm{e}} = \frac{e}{m_{\mathrm{e}}\sigma_{\mathrm{ea}}n_{\mathrm{a}}\overline{v_{\mathrm{e}}}} \tag{1.7}$$

The behavior of the plasma is similar to the behavior of gases. The gas laws can be used to express the kinetic energies of the electrons as shown in equation

1.8.

$$\text{Kinetic energy of electron} = \frac{1}{2}m_{\mathrm{e}}\overline{v_{\mathrm{e}}}^2 = \frac{3}{2}kT_{\mathrm{e}} \tag{1.8}$$

where, k is the Boltzmann constant, and T_e is the electron temperature. Using equation 1.8, average velocity of the electrons can be expressed using thermodynamic parameters. Hence equation 1.7 can be rewrite as follows.

$$\mu_{\mathrm{e}} = \frac{e}{\sigma_{\mathrm{ea}} n_{\mathrm{a}} \sqrt{3 m_{\mathrm{e}} k T_{\mathrm{e}}}} \tag{1.9}$$

The change in the electron temperature and the number density of atoms will affect the mobility of electrons along the plasma jet. This will affect the drift velocity in a given electric field and the kinetic energy of the electrons to change the plasma jet properties.

1.4 Reactive species generation

The applied electric field acting on the carrier gas results in the generation of plasma through the ionization process inside the capillary tube or the DBD phenomenon. Electrical discharge is the main contributor to the generation of plasma and its strength depends on the type of discharge that occurs in the APP system. Processes such as photo-dissociation, heavy particle excitation, metastable excitation, and recombination of ions and electrons also result in the generation of reactive species. Different carrier gaseous requires different amount of dislocating energies to generate positive ions and electrons. Given that this study only used helium as the carrier gas, this section discusses the theoretical background of reactive species generation in plasma.

1.4.1 Excitation and ionization processes

The transfer of electrical energy to the electrons and ions increases their kinetic energy. Elastic and inelastic collisions between kinetic electrons and ions with atoms and molecules generate excited and ionized radicals. In APP, processes such as metastable excitation, charge transfer and penning ionization can also produce excited species [37].Metastable helium has a longer lifetime than the other neutral species and contribute significantly to the excitation of other neutral species [38]. The transitions that occur from the helium metastable states of 1s3p ^3P, 1s2p ^3P, and 1s2s ^3S generally have enough energy to undergo transitions of N_2(X) to a N_2(B) and/or N_2(C) levels [39].

Charge transfer reactions generally occur in helium-based APPJs. Murakami *et al* [40] listed the possible reactions of charge transfer under the positive-ion reaction category such as $He^+ + O \longrightarrow He + O^+$, $He^+ + N_2 \longrightarrow He + {N_2}^+$, and $He_2^+ + N_2 \longrightarrow He_2^* + {N_2}^+$ [40] [41] [42] [43]. Helium metastable level of 1s2s ^3S have a large amount of internal energy for its transition, thus penning ionization possible [37] [39] [40] [44] [45].

1.4.2 Dissociation processes

Electronically excited molecules can be produced through dissociation processes such as photo-dissociation, electron induced dissociation, metastable induced dissociation, and dissociative charge transfer [37]. Photo-dissociation processes are generally involve the absorption of one or more photons that separate the chemical bonding of atom or molecules. The bond energies of H_2O and H_2O_2 for OH production are on the order of 0.24 eV and 0.14 eV respectively, and the dissociation process of the bonds are significantly affected by the emission photons energy.

Electrons in the plasma have a board range of energy distribution and as they interact with the molecules, they transfers some of their kinetic energy to break chemical bonds. Murakami *et al* [40], listed possible electron induced dissociative processes related to the helium APP, such as, $e + O_2 \longrightarrow O + O + e$, $e + N_2 \longrightarrow N + N + e$, and $e + H_2O \longrightarrow H + OH + e$ [40] [46] [47] [48].

Deexcitation of the helium metastable level is associated with a large amount of energy. As it transfers its deexcitation energy to molecules, it underdoes separation of the chemical bonds to create new radicals [37]. Possible processes in helium APP are $He^* + O_3 \longrightarrow He + O + O_2^+ + e$, and $He^* + N_2 \longrightarrow He + N + N^+ + e$ [40] [49].

Another dissociation process that occurs in helium plasma is dissociative charge transfer. In this process, positive helium ions transfer their energy though via the capture of an electron from their neighboring molecule, causing it to become unstable and dissociate. Possible reactions of such a process for helium plasma include, $He^+ + O_3 \longrightarrow He + O_2 + O^+$, $He^+ + N_2 \longrightarrow He + N + N^+$, and $He^+ + OH \longrightarrow He + H + O^+$ [40] [42].

Table 1.1: Possible Penning ionization reactions that occur in helium APP

Reaction	Reference
$He^* + O_2 \longrightarrow He + O_2^+ + e$	[40] [49]
$He^* + N_2 \longrightarrow He + N_2^+ + e$	[40] [43]
$He^* + H_2O \longrightarrow He + H_2O^+ + e$	[40]
$He_2^* + O_2 \longrightarrow 2\,He + O_2^+ + e$	[40] [49]
$He_2^* + N_2 \longrightarrow 2\,He + N_2^+ + e$	[40] [50]

1.4.3 Penning ionization

The Penning ionization process can be defined as the process in which a metastable atom A collides with another atom or molecule B, to produce an ion B^+, thus deexciting A in the process [51]. For the helium plasma, metastable helium plays a major role in this process according to the following reactions listed in Table 1.1, due to Penning ionization.

Identification of these radicals through the OES provides experimental evidence that the helium plasma jet used in this study underwent Penning ionization.

The emission lines of the OH(A), and N_2 second positive system are widely using to estimate plasma temperatures. Table 1.2, 1.3, and 1.4 list the possible reactions and their corresponding rate coefficients for the generation of OH(A), N_2 second positive system, and N_2^+ first negative system.

Table 1.2: Possible reactions for the generation of OH and their corresponding rate coefficients [37]

Reaction	Rate coefficient k (m^{3}s^{-1})	Reference
Electron excitation		
$OH(\mathrm{X}) + e \longrightarrow OH(\mathrm{A}) + e$	3.2×10^{-14} - 7.5×10^{-13}	[37] [52]
Electron dissociation		
$e + H_2O \longrightarrow OH(\mathrm{X}) + H + e$	2.3×10^{-18} - 8.6×10^{-16}	[40] [53]
$e + H_2O \longrightarrow OH(\mathrm{A}) + H + e$	1.6×10^{-19} - 1.2×10^{-16}	[40] [53]
Dissociative attachment		
$e + H_2O \longrightarrow OH(\mathrm{A}) + H^-$	4.8×10^{-18} - 7.8×10^{-17}	[53]
Electron-ion dissociative recombination		
$e + H_2O^+ \longrightarrow OH(\mathrm{A/X}) + H$	$5.1 \times 10^{-14} T_e^{-1/2}$	[40] [54]
$e + H_3O^+ \longrightarrow OH(\mathrm{A/X}) + H_2$	$1.05 \times 10^{-13} T_e^{-1/2}$	[55]
Positive-negative ion recombination		
$H^- + H_3O^+ \longrightarrow OH(\mathrm{A/X}) + H_2 + H$	2.3×10^{-13}	[55]
Metastable excitation		
$N_2(\mathrm{A}) + OH(\mathrm{X}) \longrightarrow OH(\mathrm{A}) + N_2(\mathrm{X})$	10^{-17}	[56]
$He^* + H_2O \longrightarrow OH + H + He$	4.5×10^{-16}	[40]

† Excitation energy of the N_2(C) level is approximately 11 eV and energy transfer from metastable He^* is higher than the requirement. Even though, this process is not investigated through the helium plasma, experimental evidence for the metastable excitation process involving argon plasma has been studied [37] [59].

Table 1.3: Possible reactions for the generation of excited N_2 and their corresponding rate coefficients [37]

Reaction	Rate coefficient k (m^3s^{-1})	Reference
Electron excitation		
$N_2(X) + e \longrightarrow N_2(C) + e$	1.3×10^{-19} - 2.7×10^{-16}	[37] [57]
$N_2(X) + e \longrightarrow N_2(A) + e$	5.6×10^{-16} - 2.7×10^{-14}	[37] [57]
Dissociative recombination		
${N_4}^+ + e \longrightarrow N_2(C) + N_2(X)$	2.6×10^{-12}	[40] [58]
Metastable excitation		
$N_2(A) + N_2(A) \longrightarrow N_2(C) + N_2(X)$	1.5×10^{-16}	[40] [59]
$He^* + N_2(X) \longrightarrow N_2(C) + He$	—	†

Table 1.4: *Possible reactions for the generation of excited N_2^+(B) and their corresponding rate coefficients* [37]

Reaction	Rate coefficient k (m^3s^{-1})	Reference
Electron excitation		
$N_2(X) + e \longrightarrow N_2^+(B) + 2\,e$	2.4×10^{-24} - 2.9×10^{-18}	[40] [53]
$N_2^+(X) + e \longrightarrow N_2^+(B) + e$	3.4×10^{-15} - 1.9×10^{-14}	[37]
Dissociative recombination		
${N_3}^+ + N \longrightarrow {N_2}^+(B) + N_2(X)$	0.2×10^{-16}	[60]
Metastable excitation		
$He^* + N_2(X) \longrightarrow {N_2}^+(B) + He + e$	7×10^{-16}	[40]

1.5 Optical emission spectroscopy of APPJ

The important features of the APPJ are its ability to generate charged particles, excited, and reactive species at atmospheric pressure. These radicals can

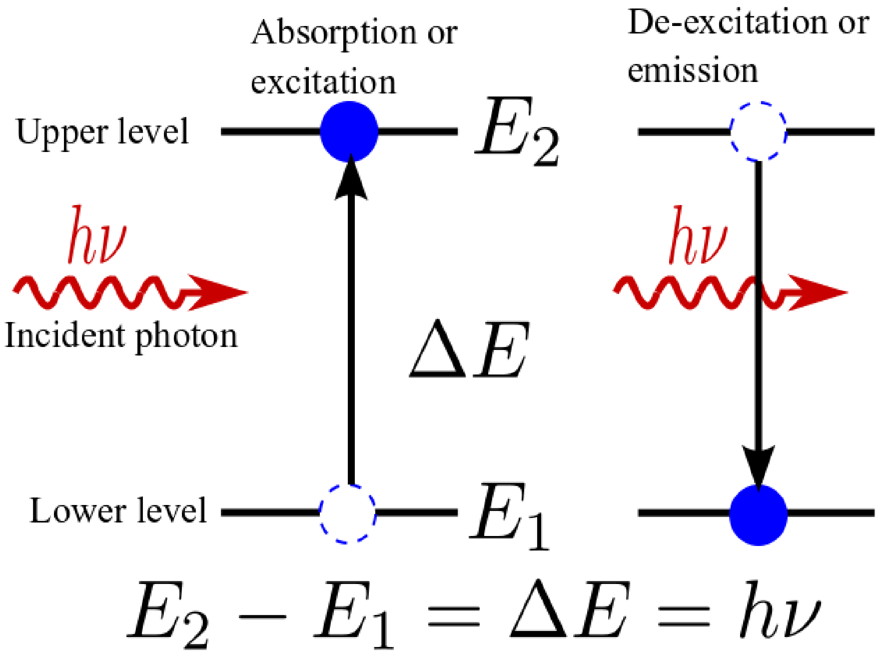

Figure 1.12: Schematic diagram for excitation and deexcitation process

be used in sterilization processes, material fabrication, and surface treatment of biomaterials [61] [62] [63] [64] [65]. The generation of plasma in an open system deviates from the local thermal equilibrium because of the imbalance in the density of ions and electrons. Such deviation results in the different thermodynamic properties. Radical generation due to discharge varies with position as the jet propagates. These parameters allow for the development of suitable APPJ devices to satisfy specific application requirements. This section focuses on the discussion of the basics of plasma temperature estimation using the optical spectra and the identification of radical generation and propagation along the plasma jet.

To analyze the thermodynamic properties and reactive species of the APPJ, optical emission spectroscopy (OES) is widely used. This technique provides a board range of information about the radicals associated with the discharge plasma. The basic physical phenomenon used in this OES technique is the determination of the intensity or the photon count associated with specific wavelengths. Transition of excited electrons from a higher energy level to a lower energy level results in the emission of a photon and due to the structure of the energy levels, the wavelengths of these transitions are discrete. The energy transported by the photon is equal to the energy difference between two energy levels as shown in Figure 1.12.

As shown in Figure 1.12, excitation can occur from the incident photon or a discharge excitation. Deexcitation processes emit photons, which carry information about the electronic structure of the atom or the molecule. The energy of the photon is equal to the energy difference between the transition energy levels. Each element has a unique emission spectrum because its electronic structure defines the information to identify the possible elements associated with the APP. In addition, the intensity of the emission spectrum depends on the half-life of the excited energy levels, which is represented as the transition probability or Einstein coefficient (A_{ij}). The relationship between the time of spontaneous transition (τ_{ij}) and the transition probability (A_{ij}) from the upper level i and lower level j can be expressed using equation 1.10.

$$\tau_{ij}[s] = \frac{1}{A_{ij}} \tag{1.10}$$

1.5.1 Plasma temperatures

The thermodynamic properties of plasma are known to be gas temperature (T_g), excitation temperature (T_{exc}), electron temperature (T_e), and electron density (n_e). Equilibrium plasma or thermal plasma in closed chambers generally occur at the local thermal equilibrium (LTE). The thermodynamic properties of these plasmas maintain equilibrium of the temperature as $T_g = T_{exc} = T_e$. Cold plasma or APP, occur at non-local thermal equilibrium (NLTE) and cause deviation of the thermodynamic properties from it equal values to $T_g < T_{exc} < T_e$ [66] [67] [68].

The gas temperature in APP has been widely estimate using rotational spectroscopy information. The NLTE ion temperature or the gas temperature has a lower value due to a higher density of neutral species compared to the LTE condition. Transition between the rotational levels of neutral atoms and molecules will be affected by the gas temperature, resulting in the generation of spectra associated with the excited levels. Therefore, fitting a temperature dependent simulated rotational spectrum to the experimental observations over a spectrum facilitates the estimation of the gas temperature. In APP studies, the second positive band of nitrogen N_2 (C-B) is widely used for this purpose where the wavelength of 337.1 nm corresponding to the transition of N_2 (C-B, 0-0) is the primary candidate [69] [70]. However, some studies used the Boltzmann energy distribution of hydroxyl (OH) to estimate the gas temperature [66] [71].

The excitation temperature provides information about the population of excited energy levels using the Boltzmann distribution [72] [73]. The optical emission lines of the excited gas are generally used to estimate T_{exc}. For this estimation, the Boltzmann plot was used based on the intensities of the observed emission lines using equation 1.11.

$$I_{ij} = \frac{A_{ij} g_i}{\lambda_{ij}} e^{\frac{-E_i}{k_B T_{exc}}} \tag{1.11}$$

where, I_{ij} and λ_{ij} are the recorded intensity and correspondence wavelength of the emission lines, respectively. A_{ij} is the Einstein coefficient for the transition from the upper level i to lower level j. The statistical weights of the upper level and its corresponding energy value are represented as g_i, and E_i respectively, while k_B is the Boltzmann constant.

The electron temperature provides information about electron behavior in the discharge plasma. Generally, T_e has been estimated based on the modeling of experimental data using a Maxwellian distribution [72] [74]. Apart from this approach, the corona balance model is used to estimate the electron temperature based on OES information for hydrogen emission lines. In this estimation, equation 1.12 is used.

$$\ln\left(\frac{I_{ij} \Sigma_{i>j} A_{ij}}{A_{ij} h v_{ij} b_{lj}}\right) = -\frac{E_{ij}}{k_B T_e} + C \tag{1.12}$$

where, $\Sigma_{i>j} A_{ij}$ is the summation of all the spontaneous radiative emissions, h is the plank constant, v_{ij} is the correspondence frequency, b_{lj} is a coefficient, and C is a constant [74].

In this dissertation, only the estimation of the excitation temperature was conducted based on experimental observations, considering the resolution of the spectrometer.

1.5.2 Detection of radicals along the helium APPJ

Plasma discharge generated reactive species plays a major role in the numerous applications including surface treatment, wound healings, thin coating, and nano particle synthesis using APPJ sources [4] [6] [15] [61]. As these radicals were created at near room temperature and propagate through the plasma jet, these sources are of particular importance in the fields of bio-engineering and biomedicine. Most of these fields can benefit from the ability of these sources to generate reactive oxygen, nitrogen, and hydroxyl (OH) radicals.

The intensity of reactive radicals created from APPJ sources depends on the diameter of the capillary tube, the applied voltage, the polarity of the electrodes, the gas flow rate, and the feeding gas. Many studies have investigated the generation of radicals from different APPJ sources using optical emission spectroscopy. In addition, there are numerous published reports on the use of numerical simulations to model the production and propagation of these radicals to understand their behavior [40] [75] [76] [77] [78] [79].

The production of radicals depends on the discharge processes, two-body or three-body reactions, radiative collisions, and penning ionization. The properties such as the radiative decay strength of the reactive species affects the intensity of the peak position along the propagation before a decrease [35] [80].

In this study, helium (He) is used as the feeding gas and identification of the radical was conducted by investigating the optical emission lines and comparing them to atomic spectra, and molecular spectra databases [39]. Table 1.5 list the impactive radicals observed using OES for the APPJ sources used in this study.

Table 1.5: Basic information on the most impactive emission lines observed using OES to study the plasma jets

Species	Wavelength (nm)	Transition
Hydroxyl (OH)	309	$A^2\Sigma^+$ - $X^2\Pi$
Oxygen ion (O_2^+)	258; 282; 297; 373	$A^2\Pi_u$ - $X^2\Pi_g$ (Second negative system)
Oxygen (O I)	777	$3p^5$P - $3s^5$S
Nitrogen (N_2)	315: 337: 357: 380	$C^3\Pi_u$ - $B^3\Pi_g$ (Second positive system)
Nitrogen ion (N_2^+)	391; 427	$B^2\Sigma_u^+$ - $X^2\Sigma_g^+$ (First negative system)
H_α	656	Balmer series
H_β	486	Balmer series
He I	471	$4s^3$S - $2p^3$P
He I	587	$3d^3$D - $2p^3$P
He I	667	$3d^1$D - $2p^1$P
He I	706	$3s^3$S - $2p^3$P
He I	728	$3s^1$S - $2p^1$P

1.6 Importance of surface treatment for bio-applications

Cell culturing on bio-material surfaces is important in drug screening, gene-editing technologies, modelling and the investigation of human diseases, and re-programming of relevant cells [81]. To grow the cell cultures, this require devices that have similar properties to cells including their microenvironment, cell-cell interactions, and cell-substrate interactions [6] [82] [83]. Devices that possess these properties are known to be bio-compatible microdevices. These devices should also be non-toxic, chemically inert, transparent, and gas permeable [82] [83] [84]. In addition, biological cells should adhere to the bio-compatible materials.

This section focuses on attempting to understand the developing mechanism of bio-compatible material for cell cultures, its properties, and ability to culture cells on devices.

1.6.1 Polydimethylsiloxane

Polydimethylsiloxane (PDMS) is one of most widely used bio-compatible material in the field of bioengineering. These materials are non-toxic, chemically inert, transparent, and gas permeable properties, which are required for viable culture cells. However, PDMS is hydrophobic, which prevents cell attachment to this substrate. Due to the empirical formula of PDMS $(C_2H_6OSi)_n$, it has the properties of a liquid (when the number of monomers repetitions "n" is low) and also a semi-solid (when n is high) [85] [86].

In this study, spin coated PDMS dishes, were used. A previously reported PDMS (Sylgard 184 Silicone Elastomer Kit, Tokyo, Japan) by Yamada *et al* [63] [64] was used in this study and is shown in Figure 1.13. To obtain thorough spread of the PDMS layer on a dish, a spin-coating method was used. For this purpose, 0.1 mL PDMS was placed on a glass base cell culture dish (35 mm Tissue culture dishes, 93040, TPP, Switzerland) using a 1 mL syringe and spin coated at 1000 rpm for 60 seconds, followed by 3000 rpm for 120 seconds (MSA-100, Mikasa Corporation, Tokyo, Japan). Then, these dishes were cured in an oven at 60 °C overnight.

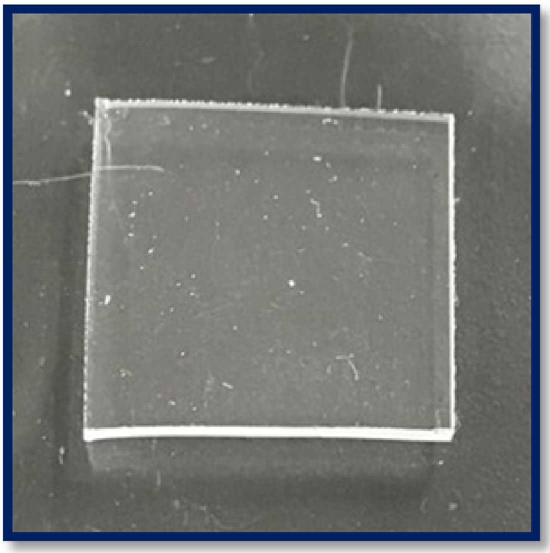

Figure 1.13: PDMS sheet

Although PDMS is a bio-friendly and compatible material, it requires a surface treatment to improve its hydrophilic properties to improve its applicability. Generally, surface treatments of these PDMS surfaces for cell culture applications are performed using low-pressure plasma irradiation with a mask [63] [64].

Plasma irradiation of PDMS oxidize its surfaces to improve its hydrophilicity. Due to the structure of PDMS, plasma irradiation is expected to change the rotation of the polymer structure. This minimized the absorption of hydrophobic and negatively charge molecules on the surface. After irradiation, as the relaxation time increases, the treated surfaces tends to change their hydrophilic properties and become hydrophobic. The cause of this transition is due to the reformation of the rotated polymer chains at the irradiation time to their initial conditions.

1.6.2 Hydrophilicity of PDMS surfaces

Low pressure plasma irradiation of PDMS surface using a mask is expected to oxidize the $\equiv \mathrm{Si}-\mathrm{CH}_3$ groups to $\equiv \mathrm{Si}-\mathrm{O}-\mathrm{Si}\equiv$ thus forming a siliceous layer on the unmasked areas as shown in Figure 1.14. Such oxidization converts the hydrophobic property to hydrophilic on PDMS to facilitate the adhesion of cells.

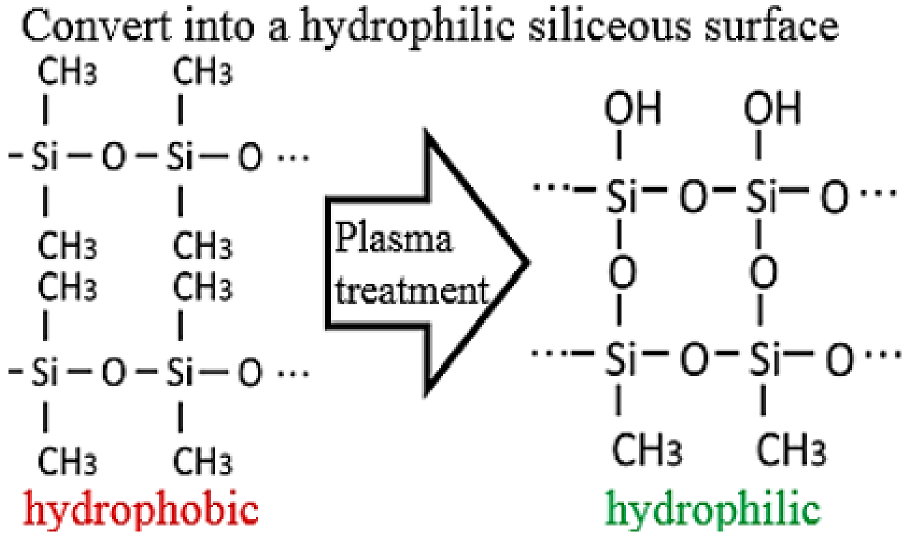

Figure 1.14: Oxidization of PDMS surface due to plasma irradiation

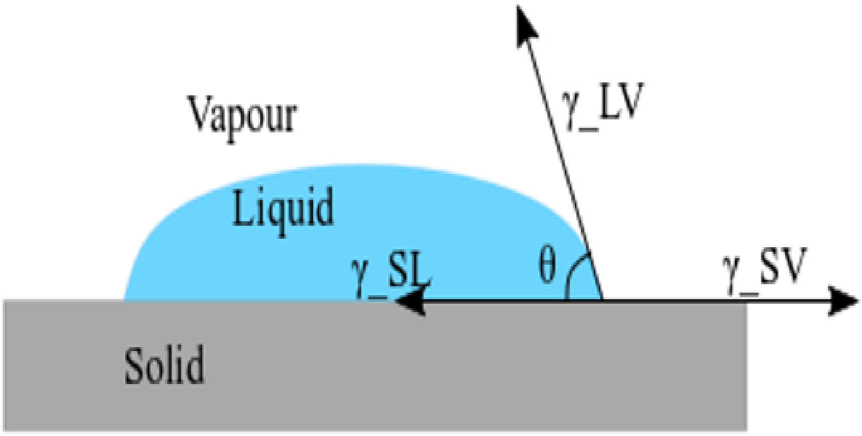

Figure 1.15: Schematic of a water droplet on a flat surface with surface tension forces and contact angle

The simplest technique to study wettability (hydrophilic condition) on a surface is the use of the contact angle estimation method. Estimation of the contact angle on a surface was suggested by Young, using three separate surface tension forces between a solid and a liquid interface. These three tension force are γ_{SL} (at the interface of the solid and liquid), γ_{LV} (at the interface between the liquid and vapor), and γ_{SV} (at the interface of the solid and vapor). The water contact angle θ is the angle measured through the liquid where the liquid-vapor interface meets a solid surface as shown in Figure 1.15. Combining these three surface tension forces, Young expressed the estimation of wettability using equation 1.13.

$$\gamma_{SL} + \gamma_{LV} \cos\theta - \gamma_{SV} = 0 \tag{1.13}$$

The contact angle θ used to determine the hydrophilicity of the surface as $0^\circ < \theta < 90^\circ$indicates hydrophilicity and $90^\circ < \theta < 180^\circ$indicates hydrophobicity. To estimate the contact angle, the water droplet sessile method was used and the experimental details are provided in Chapter 3 and 4.

1.7 Plasma patterning

To develop iPSCs in laboratory conditions, this requires a microdevice such as PDMS. Treating the PDMS surfaces using plasma can improve the hydrophilicity and cell culture of these devices. To obtain cell clusters in a certain area, plasma treatments were carried out using the mask on PDMS surfaces.

Recent studies have investigated the fabrication of surfaces such as PET, PVC, Silicon, and organic materials using APPJ sources without a mask [87] [88] [89]. However, the use of APPJ for plasma patterning on bio-compatible materials has not been investigated. This section discusses the techniques used in plasma patterning on PDMS surfaces using low-pressure plasma with a mask and APPJ without a mask.

1.7.1 Mask plasma patterning

The use of sealed cascades to generate low-pressure plasma spreads the plasma throughout the chamber. To achieve plasma patterning using these plasma sources, the use of masks is required for bio-compatible materials. Cell culture and culture facilitating serum mediums were investigated on low-pressure plasma-treated PDMS surfaces [63] [64]. To obtain the desire results for cell cultures in microdevices, it is necessary to use a mask to reduce the plasma treated area. Figure 1.16 shows the patterning of hiPSCs on PDMS surfaces using a low-pressure plasma with a mask [64].

Although, low-pressure plasma with a mask are used in applications involving iPSCs cell culture and property investigation, this technique cannot be used to change the pattern size as a function of the plasma parameters, except to change the mask size. Reduction of the mask or the pattern size using low-pressure plasma irradiation can be achieved up to certain extent because of mask charging and the generation of a plasma sheath. In addition, a study by Yamada *et al* [63] [64] demonstrated that the wettability or contact angle of the fabricated surface is the same for different irradiation times.

The plasma sheath that occurs in the mask patterning will be affected by the diffusion process. The strength of the plasma sheath and the diffusion process due to the plasma irradiation condition is expected to affect the plasma patterning size under mask patterning conditions.

1.7.2 Mask-free plasma patterning

Similar to the low-pressure plasma, APPJ also generates reactive and excited species such as O, which are expected to oxidize the surfaces of PDMS. Operating under atmospheric pressure APPJs provide non-equilibrium plasma that is suitable for temperature sensitive bio-compatible surface modification. The distin-

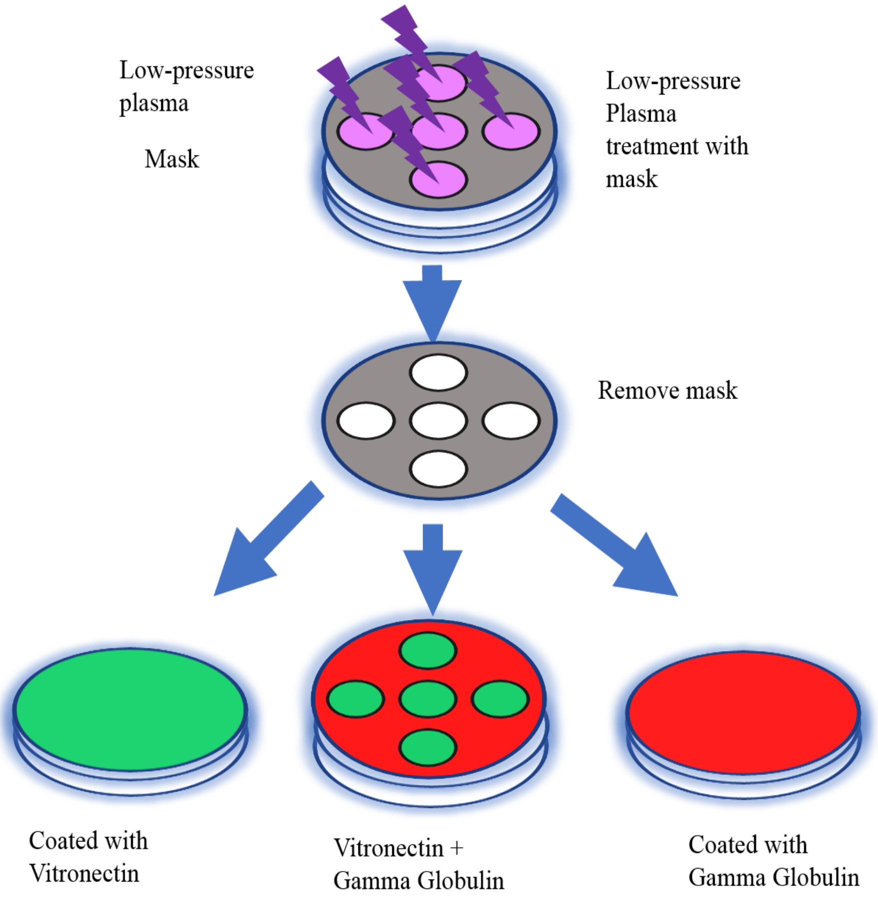

Figure 1.16: Fabricating PDMS surface using low-pressure plasma with mask to facilitate serum coatings for patterned hiPSCs cell culture [64]

guishing feature of the use of an APPJ source in plasma patterning is that a mask is unnecessary for treating surfaces. The jet property of a cone shape can be focused to the desired treated area when using these sources.

Many studies have investigated use of APPJ sources to generate arrays of patterns without a mask for bio-medicine applications [90] [91]. Compared to the low-pressure plasma source, APPJ does not spread throughout a large volume and the properties of APPJ can be changed by varying the parameters as discussed in chapter 2. A summary of mask-free plasma patterning using APPJ is shown in Figure 1.17.

The plasma patterning size for mask-free plasma patterning condition is dependent on the diffusion process. Diffusion of excited species along with the reactive species on the treated surface will determine the pattern size.

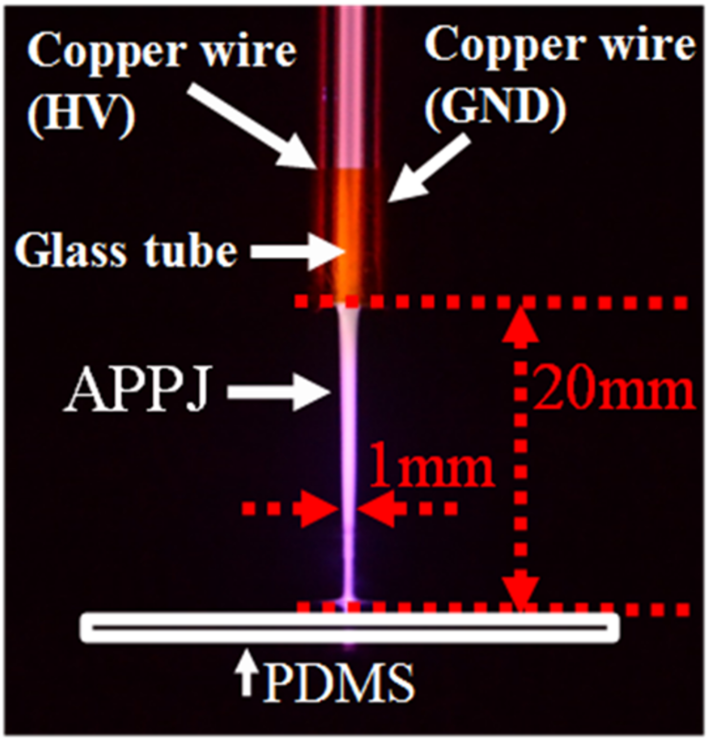

Figure 1.17: Camera image of APPJ for mask-free plasma patterning [6]

1.7.3 Plasma sheath and diffusion process

As the electrons and positive ions move towards the sample surface, they tend to generate separate regions of ions when they interact with neutral atoms. These regions push more of the opposite charge ions for diffuse through plasma irradiation [92] [93]. This concept is known as the plasma sheath or Debye sheath in plasma technology. The length of the plasma sheath or the Debye length can be expressed using the equation 1.14.

$$\lambda_D = (\frac{\epsilon_0 k_B T_e}{n_e e^2})^{\frac{1}{2}} \tag{1.14}$$

where, λ_D is the Debye length, ϵ_0 is the permittivity of the free space, k_B is the Boltzmann constant, T_e is the electron temperature, n_e is the electron density, and e is the electron charge. According to equation 1.14, the Debye length or the plasma sheath depends on the electron temperature and the electron density. Its relation is express in the figure 1.18.

As illustrated in figure 1.18, the Debye length or the plasma sheath mainly depends on the density of electrons and the electron temperature. An increase of the

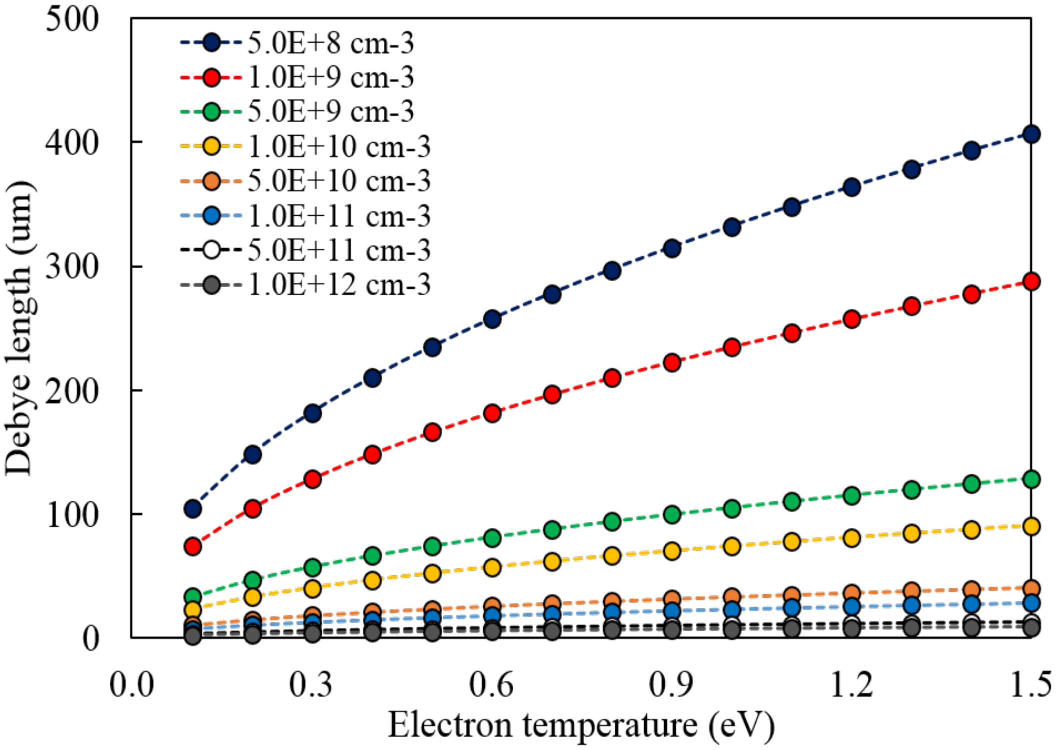

Figure 1.18: Debye length as a function against electron temperature for different electron density in (cm^{-3}).

electron temperature causes an increase of the plasma sheath. An increase in the electron density will decrease the plasma sheath and its dependence on the electron temperature becomes invalid on and beyond electron densities of $10^{12} cm^{-3}$. Such a mechanism is expected to affect the plasma patterning size, especially in the case of mask patterning.

In addition to the effect of the plasma sheath on mask patterning, another important process that affects plasma patterning with and without mask patterning is the diffusion process. As the reactive and excited species interact with the sample surfaces, diffusion processes affect the diffusion regions. The diffusion area (diameter ϕ of diffusion area) is expected to be affected by the irradiation time (t) and the diffusion coefficient (α) and its relation is expressed by equation 1.15 as follows.

$$\phi \propto 4\sqrt{\alpha t} \tag{1.15}$$

Equation 1.15 also can be expanding as equation 1.16 as follows.

$$\ln \phi \cong \frac{1}{2} \ln t + \ln 4\sqrt{\alpha} \tag{1.16}$$

1.8 Motivation

The APPJ provides a wide area of applicability and due to its thermal properties near atmospheric conditions, it is better suited for use in the field of biotechnology. The production of energetic charged particles such as electrons, and reactive species can modify the wetting property of bio-compatible materials. This study focused on the investigation of a novel approach involving the use APPJ in mask free plasma patterning as an alternative to conventional low-pressure plasma patterning using a mask.

The use of low-pressure plasma for fabricating bio-compatible material requires expensive equipment such as vacuum pumps and closed chambers. In addition, these sources require the use of a mask to achieve plasma patterning, and difficulty is encountered in controlling the pattern as a function of the irradiation time. Mask charging and plasma sheath on the mask occurred on the scale of a few tens of microns, thus, these sources are not best suited for plasma patterning of cell cluster size.

As APPJ is used as an alternative approach to plasma patterning for bio-compatible materials, it is necessary to identify the parameters such as the inner tube diameter, electrode configuration, irradiation time, and mask effect to determine the optimum conditions to produce the required plasma patterning size. Considering the theoretical approach for APPJ plasma patterning as a function of the aforementioned e parameters, the following hypotheses are proposed;

Hypothesis I: APPJ can facilitate mask-free plasma patterning for cell cultures.

Hypothesis II: The inclusion of an additional pin grounded electrode at the bottom of the plasma jet is able to reduce the plasma pattern size.

Hypothesis III: A decrease in the tube diameter will decrease the radius of the plasma jet and its effective treatment area will decrease the plasma patterning size.

Hypothesis IV: The use of a mask during APPJ irradiation will not affect the plasma patterning size for different irradiation times.

The investigations of these hypothesizes were conducted using the APPJ sources and varying its parameters. The experimental evidence and evaluation of the hypotheses will be discussed in Chapters 3 and 4.

1.9 Scope and outline of the dissertation

The APP sources such as APPJ and their breakdown mechanisms and properties have been well-studied. In addition, the wettability of biocompatible materials and the modification of these materials using plasma sources were studied to identify suitable environments for cell culture. The ability to generate the excited radicals and reactive species at the atmospheric condition render these sources as suitable for bio-applications. The generation of radicals and their propagation varied according to the electrode configuration of the APPJ and its discharge type. Modification of biocompatible materials using APPJ irradiation improves the wettability.

The aim of this study is to investigate the properties of APPJ such as jet length, radical generation, and propagation along the jet for different parameters. The know parameters of gas flow rate, electrode configurations, polarities of electrodes, applied voltage, and diameter of the capillary tube were investigated to identify the properties of APPJ. The ability to use APPJ sources in plasma patterning without a mask was also investigated with pattern size controlling parameters.

This thesis includes five chapters which begin with an introduction of atmospheric pressure plasma sources. Discharge of plasma inside a capillary tube and its breakdown mechanism for different electrode configurations are discussed. In addition, the spectroscopy results for the detection of reactive species and their propagation are discussed for APPJ surface treatment.

In chapter 2, the investigation of APPJ properties as a function of the effective parameters is discussed. APPJ configurations and their behavior for different parameters are examined based on experimental results.

Chapter 3 focuses on the investigation of the use of APPJ for mask free plasma patterning and cell cultures on treated surfaces without a mask. This novel approach successfully achieved plasma patterning without a mask, compared to conventional low-pressure plasma patterning with a mask.

In chapter 4, investigation of the parameters that affect the control of the wetting size using the APPJ is discussed. Parameters such as the electrode configuration, irradiation time, tube diameter, and mask effect are considered as a function of the irradiation time to identify the controlling parameters. Experimental evidence is presented expressed to evaluate the effects of the parameters on the wetting size.

Finally, an overall summary of the properties of APPJ devices and their effective parameters is presented. The ability of plasma patterning and the control of the patterning size is discussed in chapter 5.

Chapter 2

Investigation of APPJ properties using radical generation and propagation against effective parameters

The aim of this chapter is to investigate the parameters that affect the properties of the atmospheric pressure plasma jets along with the generation and propagation of radicals. The investigation considered the effect of the electrode configuration, an additional floating pin electrode at the bottom of the plasma jet, the polarity of the electrodes, gas flow rate, capillary diameter, and the applied voltage. The theoretical background of these parameters with respect to the APPJ properties are discussed in addition to the experimental evidence used to differentiate between the possible mechanisms.

2.1 Introduction

Interest in atmospheric pressure plasma sources has increased significantly over the last few decades because of their ability to operate at room temperature and ease of use [17] [94] [95]. These sources have numerous uses including nano particle synthesis [4] [5], mask-free plasma patterning [6], sterilization [95] [96] [97], wound healing [98] [99] [100] [101], surface treatment [87] [88] [102] [103], and other medical applications [104] [105] [106]. One of the best known APP source is atmospheric pressure plasma jet (APPJ). Many configurations of APPJs have been investigated for different AC, DC, and pulse waveforms for frequencies ranging from the kHz to GHz scale to generate plasma jets [107] [108] [109] [110].

The applicability of APPJs depends on their jet properties. Properties such as the jet length, cone shape, and glow discharge throughout propagation are important parameters for the use of APPJs in localized plasma treatments and plasma patterning. APPJs with a short jet length tend to generate arc discharges when the effective gap between the electrodes and the plasma that exit from the nozzle is small. This can negatively impact the operational conditions and create hazard situations. To overcome these disadvantages, it is necessary to generate longer plasma jets. Increasing the gas flow and applied voltage can lead to an increase of the plasma jet length [31]. However, an increase of the flow rate deforms the plasma jets as the flow regime change from laminar to turbulent [31] [111]. To maintain laminar plasma flow at high gas flow rates, it is necessary to increase the inner diameter of the capillary tube [73] [111] [112]. The increase of the tube diameter causes an increase of the gap between the electrodes and the discharge inside the capillary tube, [12] [13] [14] in addition to an increase in the plasma jet diameter. As such, it is necessary to investigate APPJs and their parameters to generate plasma jets that are suitable for specific applications.

An in-depth understanding of the breakdown mechanism of these sources is important to the application of plasma jet to specific situations, based on their properties. The parallel and double electrodes configured APPJs used in this study have different plasma properties due to their breakdown mechanism, as is explained in section 1.3.

The importance of APPJ sources is based on their ability to generate and propagate excited and reactive species. The improvement of these sources has been investigated to satisfy application specific requirements by analyzing the properties of generated species. Optical emission spectroscopy and mass spectroscopy are widely used techniques for the identification of radicals from APPJ sources [15] [80] [113] [114]. Due to the complex behavior of the radical generation process and the difficulty in obtaining experimental evidence from APPJ sources, numerical simulation modelling is widely used to estimate the generation and propagation of possible excited and reactive species [15] [40] [76] [77] [78] [115] [116] [117].

Although numerical modelling has the advantage of facilitating the estimation of the densities of the entire set of reactive species, experimental investigation will provide more reliable information. The radical distribution along the plasma jet has been investigated in numerous studies, however, the behavior of the distribution varies according to the experimental condition [35] [80] [110] [118] [119]. Differences in the electrode configuration alignment affect the properties of the APPJ. Thus, changes the in APPJ properties also affect the generation of radicals, their propagation, and their thermodynamic properties.

In this study, experimental data was acquired on the plasma jet properties along with the generation and propagation of radicals for APPJs with parallel electrodes, double electrodes, and double electrodes with and without a grounded floating pin electrode at the bottom of the jet configuration. Parameters such as the applied voltage, electrode configuration, additional pin electrode at the bottom of the plasma jet, polarity of the electrode, gas flow rate, and tube diameter were considered to determine their effect on the plasma jet properties. Experimental data were evaluated to investigate the properties of plasma jet and to determine the optimal conditions of APPJs that are suitable for mask and mask-free plasma patterning, for cell cultures.

2.2 Parameters that define the plasma jet properties

To investigate the optimal APPJs for plasma patterning, it is necessary to identify the effect of different parameters on the plasma jet. For this purpose, this section discusses the influence of parameters on the APPJ.

2.2.1 Electrode configuration and the addition of a pin electrode at the bottom of the plasma jet

Two glow discharge APPJ configurations known as the parallel and double electrode configurations were considered in this study to investigate the properties of plasma jets. The fundamental aspects of the breakdown mechanism of these two plasma jet types were explained in chapter 1.3. This section presents an in-depth discussion of the effect of the electrode configuration with an additional pin electrode at the bottom of the plasma jet on the properties of the jet.

The attachment of electrodes parallel to the capillary tube generate strong electric fields. The applied electric field in this configuration is perpendicular to the plasma flow direction. The strong electric field cause the ions in the plasma to flow to the electrodes instead of propagating through the atmosphere. This results in a low self-contain electric field for plasma bullets. The mobility and the drift velocity of the electrons and ions are thus affected by this electric field and cause a decrease of the plasma propagation velocity at the nozzle exit. This leads to a decrease of the propagation phase of the plasma jet and its length. Even though these charged particles propagate through the atmosphere, weak electric potential lines from the electrodes tend to scatter into the atmosphere, thereby reducing the strength of the plasma jet. In addition, if the end of the parallel electrodes close to the nozzle exit generates strong electric field lines, this can cause the charge particles to generate a reverse cathode fall discharge and inhibit the plasma jet propagation.

In the case of the double electrode configured APPJ, the active and ground electrodes generate a potential gradient in the same plane as the plasma flow direction. Such an electrode configuration allows the charged particles to propagate through atmosphere as a jet due to the pressure gradient. Therefore, the plasma bullets have a higher electric potential compared to parallel electrode configured APPJs. This causes an increase of the mobility and the drift velocity of the electrons and charge ions, as explained in section 1.3.4. Moreover, this leads to an increase of the plasma bullet velocity and the propagation phase is comparable to that of the parallel electrode configured plasma jet. The polarity of the electrodes also affects the plasma jet in this configuration. Placing the active electrode near the nozzle exit causes the plasma jet to flow equally for the upstream and downstream directions, as discussed in the breakdown mechanism for a single electrode APPJ [31]. As the upstream plasma jet reaches the ground electrode, it undergoes cathode fall discharge to generate a glow inside the capillary tube [31]. A downstream plasma jet propagates through air without undergoing cathode fall discharge. However, changing the polarity of the electrode at the nozzle exit to the ground voltage affects the properties of the plasma jet [31] [35]. As the discharge occur in the active electrode and flows equally in the upstream and downstream directions, the ground voltage of the electrode near the nozzle exit causes the charge ions to undergo cathode fall glow discharge. In this situation, the plasma jet is expected to undergo discharge overfall at the ground electrode to form a plasma jet with a short jet length because the plasma bullets are affected by the lower electric potential. Placing an active electrode near the nozzle exit can cause fall back of the charge ions resulting in reverse glow discharge at the nozzle exit, thereby reducing the plasma jet length.

In this study, the effect of an additional pin ground electrode at the bottom of the plasma jet in the double electrode configuration was also investigated. The application of a potential to the additional pin electrode produces additional potential lines at the bottom of the plasma jet. This modification to the double electrode configuration APPJ is expected to increase the electric field strength along the plasma jet propagation direction and the propagation velocity. Moreover, the propagation phase of the plasma jet causes an increase of the jet length [35] [119] [120]. In addition, the plasma jet is expected to undergo a cathode fall discharge at the additional pin electrode to generate secondary radicals at the bottom of the plasma jet. Similar to the streamer triggered discharge at the grounded electrode for the double electrode configuration as described by Jiang *et al* [31], it is expected that the bottom of the plasma jet will undergo a streamer triggered discharge in this study. This will affect the density of the radicals at the additional pin electrode. The polarity of the electrode also plays an important role in defining the plasma jet properties. The additional pin electrode without a grounded or voltage connection will be considered to be the floating pin electrode throughout the study unless otherwise noted. Placing a floating pin electrode at the bottom of the plasma jet is expected to be analogous to the APPJ without an additional pin electrode at the bottom of the plasma jet. However, it is expected to have a slight effect on the plasma jet characteristics due to the metallic properties of the pin electrode. However, this situation is not the subject of this study.

Given that the experimental investigation of these APPJs as a function of the electrode configuration is incomplete, one of the objectives of this investigation is to obtain experimental evidence to justify the breakdown and propagation mechanism expressed in this section.

2.2.2 Polarity of the electrodes

The polarity of the electrodes play a critical role in defining plasma jet properties, especially for the double electrode configured APPJ. As explained in section 2.2.1, a change in the polarity of the electrodes affects the breakdown and discharge propagation of the plasma jet. This section will examine the possible effects associated with the alignment of polarities to the double electrode configuration with an additional pin electrode at the bottom of the plasma jet.

The inclusion of an additional pin electrode with a ground or potential connection will cause an increase of the electric field, thereby changing the plasma jet properties. In this case, the electric field strength along the plasma jet propagation is the main factor that determines the plasma jet length. If the polarity between the electrode near the nozzle exit and the additional pin electrode is the same, it is expected that a zero potential gradient will be maintained along the jet propagation. This will lead to a diminished electric field strength and a reduction of the propagation velocity of the plasma along with propagation phase, which will almost eliminate the plasma jet.

The application of opposite polarities between the electrode at the nozzle exit and the additional pin electrode is expected to increase the electric field strength along the jet propagation direction. Such an increase in electric field is expected to result in an increase of the propagation velocity of the plasma, along with propagation phase, leading to an increase of the jet length. For opposite polarity configurations, an active electrode near the nozzle exit and a grounded connection at the additional pin electrode will lead to an increase of the plasma jet length compared to the floating pin electrode configuration.

Moreover, changing the polarities of the two electrodes to the grounded voltage at the electrode near the nozzle exit and the high-voltage waveform at the additional pin electrode can generate an electric field along the plasma jet propagation direction. This is expected to increase the electric field along the plasma jet propagation direction, thereby increasing the plasma jet length. Given that the additional pin electrode acts as the active electrode at the bottom of the plasma jet, the streamers with excited radicals are expected to undergo a discharge in the atmosphere. Therefore, in this study, it is expected that the plasma jet length will be increased using this polarity configuration.

Such changes in the electrode polarity in the double electrode configuration with an additional pin electrode is also expected to change the generation and propagation of the radicals along the plasma jet. However, since plasma patterning is investigated using the APPJ in this study, the application of a high voltage at the bottom can create hazardous conditions in addition to damaging the treated samples. Therefore, an investigation of the properties of plasma as a function of polarity will be conducted to determine the effect of the plasma jet length.

2.2.3 Diameter of capillary

The reduction of the plasma patterning size can benefit from the use of micro plasma jets. To achieve micro-scale APPJ, it is necessary to reduce the diameter of the capillary tube. A study conducted by Wu *et al* [120], revealed that a decrease of the tube diameter causes a decrease of the plasma jet length. Moreover, the electric field of the streamers tends to decrease rapidly along the direction of the plasma jet propagation as the tube inner diameter decreases. However, there is a limit to the decrease of the diameter of the capillary tube due to the Debye length (λ_D). To generate and propagate plasma from the nozzle exit, it is necessary to maintain a larger capillary diameter compared to the Debye length. The electron density (n_e) and the electron temperature (T_e) are the most important parameters that affect the Debye length as shown in equation 1.13.

A decrease of the tube diameter reduces the rate of gas flow to the system and causes a decrease of the plasma jet length. A study conducted by Cheng *et* *al* [121] demonstrated that a decrease of the tube diameter results in a decrease of the electron density of the streamers and causes a decrease of the reaction along the plasma jet propagation direction. This causes a decrease of the plasma jet length. In addition, it causes a larger deviation in the thermodynamic behavior as the DBD gap is reduced [6] [73]. In numerous prior studies, this variation has been investigated based on experimental and theoretical work [15] [31] [75] [76] [77] [78] [113] [115] [122] [123] [124]. A decrease of the tube diameter causes a reduction of the electron density and this is expected to decrease the density of radicals generated along the plasma jet. In this study, the effect of the tube diameter will be investigated based on experimental observations to confirm these concepts.

2.2.4 Flow behavior

Sustainability of plasma discharge inside the capillary tube depends on the applied gas flow rate (GFR). If the GFR is too low or too high, this can cause a decrease of the plasma jet length and lead to damage of the DBD capillary walls due to the thermodynamic and discharge properties.

The gas and plasma flow are governed by fluid dynamics. Therefore, the behavior of plasma jets needs to be considered when defining a suitable APPJ for specific applications. In fluid dynamics, the definition of the laminar flow and turbulent flow regimes considers flow behavior. Several studies have demonstrated that the APPJ length increase as the GFR increase in the laminar regime, whereas the jet length decreases as the GFR increases in turbulent regime [73] [111] [112] [125].

Generally, regime classification was performed based on estimation of the Reynolds number. The Reynolds number (Re) was estimated using equation 2.1 as follows [73] [125].

$$Re = \frac{\rho_{gas} D_{tube} V_{flow}}{\mu_{gas}} \tag{2.1}$$

where, ρ_{gas} is the density of the gas, which depends on the temperature, V_{flow} is the flow velocity, D_{tube} is the capillary diameter, and μ_{gas} is the dynamic viscosity of the gas, which, depends on the temperature. The flow velocity was calculated using the balance of the input and output volume per second, as shown in equation 2.2;

$$V_{flow} = \frac{GFR}{\frac{\pi D_{tube}^2}{4}} \tag{2.2}$$

As shown in equation 2.1 and 2.2, an increase in GFR increases the linear flow velocity and causes Reynolds number to increase.

The electrode configuration and the type of gas defined the limit of the Reynolds number to classify the different regimes [126]. For the helium plasma jet with a double electrode configuration, a Reynolds number of 200 is expected as the benchmark for classification of the regimes [73] [125]. Therefore, in this study, the investigation of the flow behavior for APPJs with $Re < 200$ is consider to be in the laminar flow regime and $Re \geq 200$ to be in turbulent flow regime [125].

The flow velocity of the feeding gas and the diameter of the capillary affect the plasma flow behavior according to the estimated Reynolds number. Many studies have investigated APPJ propagation as plasma or streamer bullets [95] [119] [120] [127]. Propagating plasma bullets have three phases known as the transition phase, propagation phase, and collapsing phase [35]. The transition phase starts from the nozzle. The bullet accelerates until it reaches the maximum velocity, then continues to propagate at this velocity in the propagation phase. Subsequently, the velocity decrease rapidly during the collapsing phase.

An increase of the feeding gas flow velocity does not affect the jet velocity during the transition phase. However, an increase of GFR causes an increase of the propagation length of the plasma streamers due to an increase plasma jet velocity in the propagation phase before the collapse of the streamer. The density of the electron, positive ions, and excited species of the plasma streamers is expected to increase with the increase of GFR. Therefore, an increase in the propagation length and density of the streamer heads is expected to cause an increase of the intensity of the reaction of plasma and atmospheric molecules as the jet propagates. An increase of the GFR also causes an increase of the flow velocity. This is expected to shift the intensity of the emission lines along the plasma jet, considering their emission lifetimes.

A decrease of the tube diameter results in a reduction of the jet length, which causes a decrease of the length of the bullet propagation [120]. The admixture of air molecules increases with plasma as the feeding gas flow increases, causing a change of the reaction and decay rates of the emission. These changes affect the intensity of the radicals along the plasma jet.

2.2.5 Application of voltage

The application of high-voltage waveforms using the electrodes facilitate the generation of electrical discharge to produce plasma. Several studies have investigated the generation of APPJs using different waveforms such as pulsed low frequency DC [95] [98] [107], low frequency AC [18] [128] [129] [130], radio frequency driven [21] [131] [132], and microwave driven [133] [134] voltage pulses.

In this study, the generation of APPJ using low frequency AC waveforms is investigated. Generally, the breakdown of rare gaseous molecules occurs at high voltages (in kilovolts). To obtain a high-voltage waveform with a low frequency in the kilovolt range, an inverter transformer connected to the primary DC or AC source was considered.

The working gas for the APPJ configuration requires a specific breakdown voltage to generate glow discharge, as explained in sections 1.1 and 1.2. An applied voltage higher than the breakdown voltage will cause an increase of the electric field to break down the working gas to form a discharge plasma in the DBD capillary. The behavior of the discharge plasma can be understood by observing and analyzing the discharge current waveform. For the APPJs generated in the capillary DBDs, the discharge current waveforms can be estimated using a method proposed by Oh *et al* [114]. In this method, the discharge current was estimated using the difference between the displacement current waveforms for the plasma on and off conditions.

There are several important features of the applied voltage waveform used to generate plasma including; (I) provides a peak voltage that is larger than the plasma ignite voltage, and (II) maintains the duty cycle with frequency change to sustain the plasma in the capillary. These properties of the applied voltage waveform are expected to influence the type of discharge in addition to the plasma jet properties. An increase in the peak-to-peak voltage is expected to cause an increase of the electric field of the streamers, thereby increasing the propagation velocity. It has been shown in several studies that an increase of the applied voltage causes an increase of the plasma jet length [31] [35] [111] [135]. In this study, one of the objectives is to investigate this phenomenon to determine its impact on APPJ.

Based on the results of several studies on the impact of the applied voltage on the plasma jet, it has been determined that this parameter affects the propagation of plasma bullets and the radical distribution [35] [110] [135]. An increase of the applied voltage causes an increase of the plasma bullet velocity and its propagation length, which causes an increase of the jet length [31]. An increase of the jet length and the propagation phase of the plasma bullets results in an improvement of the reactions that occur along the plasma jet, leading to an increase of the intensity of the radicals. Moreover, a study conducted by Xiong *et al* [110] demonstrated that an increase of the applied voltage causes an increase of the discharge current. This will cause an increase of the density of radicals along the plasma jet. A temporal investigation of the spectra revealed that an increase in the applied voltage causes a shift in the intensity peak to lower time values, and an increase of the intensity [110] [135].

An increase of the pulse width causes a decrease of the jet velocities and a shift of the peak of the temporal distribution to a larger time value [135]. Further investigation on the spatial distribution of the jet velocity also revealed that an increase in the pulse width results in a decrease of the peak values of the jet velocity, in addition to an increase of the propagation length. The frequency of the waveform pulse also affected the jet velocity distribution in temporal studies. Specifically, an increase in the frequency caused a decrease in the time at which the peak occurred. However, this does not affect the peak value of the jet velocity and the distribution length. The spatial evaluation of the jet velocity distribution in terms of frequency variance is similar for all frequencies [135].

Considering the parameters that affect radical propagation, this study will investigate the spatial distribution of radicals along the double electrode plasma jet as a function of the feeding gas flow rate and applied voltage.

2.3 Properties of reactive species generated in helium plasma

Electric discharge occurred in the capillary tube, whereby energy was transferred to helium to generate excited and ionized helium, in addition to electrons. As the plasma jet propagates it goes through a different process, causing the generation of reactive and excited species. The generation of species along the plasma jet can be classified into two different phases according to the radical generation mechanisms as, (I) inside the capillary, and (II) at the atmosphere.

In phase (I), the discharge process causes the generation of helium ions, excited helium, in addition to electrons. Propagation of these radicals along the electric field cause a collision reaction process that increases their density. In phase (II), the streamer contains excited helium, helium ions, and electrons that propagate through via an interaction with ambient air. This results in chemical and collision reactions to generate different set of radicals containing nitrogen, hydroxyl (OH), and oxygen atoms [40]. These reactions affect the generation of reactive and excited species along the plasma jet.

Helium plasma jets generally contain helium ions, electrons, excited helium, and neutral helium inside the capillary tube [66] [110]. These energetic helium ions, electrons, and excited helium interact with the atmosphere to generate reactive species of hydroxyl (OH), nitrogen, and oxygen, which are notable in the emission spectra of the helium plasma jets shown in Figure 2.1.

As shown in this figure, the optical emission spectra of the excited transitions were recorded in the UV-visible-near IR range (200 – 900 nm). The emission

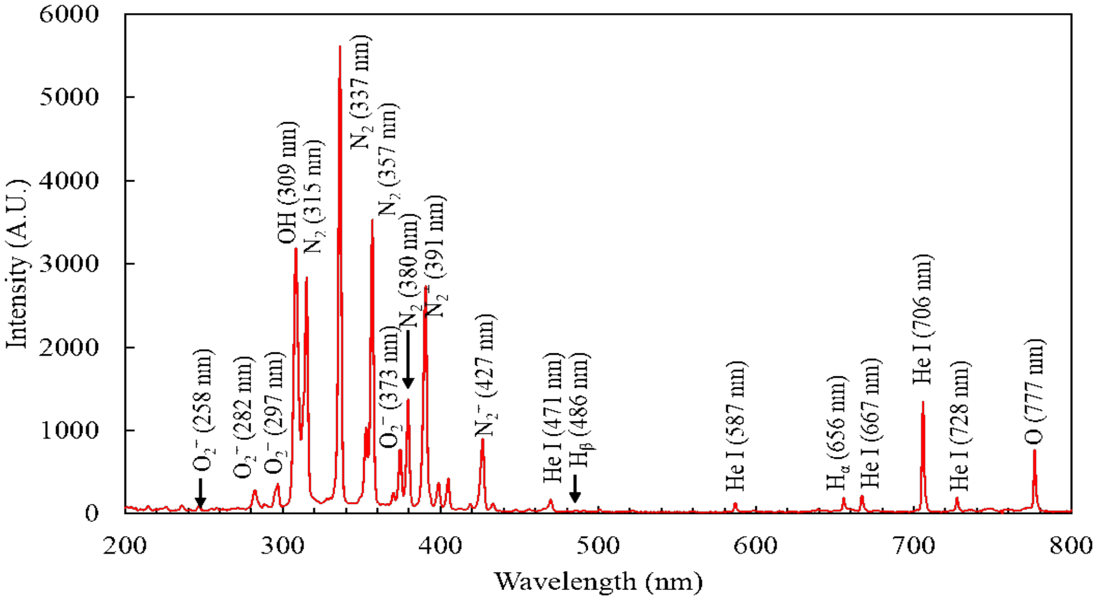

Figure 2.1: Helium APPJ spectroscopy for the range of 200 – 900 nm

lines are associated with the nitrogen second positive system (SPS), OH (A-X), N_2^+ first negative system (FNS), O_2^+ second negative system (SNS) and several He I and O I lines indicate their strong presence.

2.3.1 Helium

Studies on the properties of helium have revealed that it exhibits both orthohelium (triplet) and parahelium (singlet) arrangements, resulting in two separate series of emission lines [38] [136]. The first state of orthohelium is obtained at 19.8196 eV and has the configuration of 1s2s ^{3}S, whereas parahelium at 20.6158 eV has the configuration of 1s2s ^{1}S [39]. The emission transition between the orthohelium levels of 389, 471, 587, and 706 nm exhibits a strong intensity compared to the 667 nm and 728 nm parahelium lines in the helium spectrum. In addition, the first excited level of helium of 1s2s ^{3}S has an energy of 19.81 eV and a lifetime of 7862 s, making it the longest-lived metastable level for neutral atomic species [38] [39] [136]. The transfer of energy from the long-lived energy levels of helium affects the breaking of the molecular bonding of water, nitrogen, and oxygen to generate excited molecules, and to separate the molecules as well as molecule ions. As a result of these properties, excited helium serves as an important source for the storage of energy for discharge plasma. Table 2.1 summarize the first 10 levels of helium and its properties.

As shown in Table 2.1, the orthohelium states tend to have a longer lifetime compared to the parahelium states. As a result, a higher density of excited helium is maintained in these states compared to the orthohelium states. Therefore, the deexcitation process from these states tends to result in the emission of high intensity lines. The most intense helium emission lines also depend on the lifetime of the upper level and transition. The properties of these lines in the helium APPJ are also summarized in Table 2.2 [39].

Table 2.1: First 10 helium excited levels and their properties

Configuration of Energy level	Energy (eV) [39]	Wavelength (nm) of transition to ground state	Einstein A coefficient A_{ij} ($\frac{1}{s}$) [39]	Lifetime
1s2s ^{3}S	19.8196	62.56	1.272E-4	7862 s
1s2s ^{1}S	20.6158			
1s2p ^{3}P	20.9641	59.14	1.764E+2	5.66 ms
1s2p ^{1}P	21.218	58.43	1.80E+9	55.6 ps
1s3s ^{3}S	22.7185			
1s3s ^{1}S	22.9203			
1s3p ^{3}P	23.0071	53.89	1.21E-1	8.26 s
1s3d ^{3}D	23.0737			
1s3d ^{1}D	23.0741	53.73	1.30E+3	0.7 ms
1s3p ^{1}P	23.087	53.70	5.66E+8	1.77 ns

Table 2.2: Summary of the properties of the most intense helium emission lines in APPJ

Wavelength (nm)	Configuration [39]		Energy (eV) [39]		Einstein A coefficient A_{ij} (1/s) [39]	Lifetime
	Upper level	Lower level	Upper level	Lower level		
389	1s3p ^{3}P	1s2s ^{3}S	23.0071	19.8196	9.47E+6	106 ns
471	1s4s ^{3}S	1s2p ^{3}P	23.5939	20.9641	3.17E+6	315 ns
587	1s3d ^{3}D	1s2p ^{3}P	23.0737	20.9641	4.20E+7	23 ns
667	1s3d ^{1}D	1s2p ^{1}P	23.0741	21.2180	2.12E+7	47 ns
706	1s3s ^{3}S	1s2p ^{3}P	22.7185	20.9641	9.28E+6	108 ns
728	1s3s ^{1}S	1s2p ^{1}P	22.9203	21.2180	1.83E+7	54 ns

Transition between energy levels in the orthohelium (triplet states) also tends to have a longer lifetime compared to parahelium (singlet states) transitions as shown in Table 2.1. A longer lifetime in the upper levels of emission transitions and its 1s2s ^{3}S metastable level means that helium can improve the penning ionization on radicals of oxygen and nitrogen along the plasma propagation.

2.3.2 Hydroxyl (OH)

The hydroxyl (OH) radicals are generated in the helium APP via dissociation processes. The emission lines of OH ($A^2\Sigma^+$ - $X^2\Pi_i$), that appear approximately at 309 nm in APP are due to water vapor in the atmosphere. Due to the lower bonding energies of 0.24 and 0.14 eV for H_2O and H_2O_2 respectively, dissociation processes such as photo-dissociation or photo-ionization cause the generation of OH radicals. However, the excitation process of OH (X-A) require energies of 4.01 eV or higher. The kinetic energy of the electron distribution is large at the nozzle exit, causing the generation of a vast amount of excited OH (A) [37] [46]. Along the jet propagation direction, the decrease in the electron energy distribution function (EEDF) and the increase in the air fraction cause a decrease in the production OH (A) [46].

The rotational band energy levels in the excited and ground state energy bands utilize with the OH emission lines to estimate the gas temperature using high resolution spectroscopy. In addition, the effective lifetime of the OH (A-X) transitions decrease at approximately 1 ns, causing a vast decrease in the OH (A) population along the propagation direction.

2.3.3 Nitrogen

The nitrogen second positive system (SPS) $N_2(C^3\Pi_u - B^3\Pi_g)$, often exhibit strong emission in APP because of the presence of N2 in the atmosphere and the emission lines of this system are in the range of 268 nm to 546 nm. Direct electron impact excitation, metastable excitation, and dissociative recombination cause the generation of the nitrogen SPS system. The systematic alignment of the energy levels of nitrogen tends to contain rotational energy structures [137]. In many studies, the emission lines of the nitrogen SPS system were used to estimate the gas temperature using the band head (0,0), vibrational transition at 337 nm, and (0,2) vibrational transition at 380 nm, because of their symmetrical rotational levels in the transition bands [37] [73].

Penning ionization is a dominant process in helium plasma because of the energies of the metastable states. Nitrogen in air affects the penning ionization process and generates a vast amount of ionized nitrogen molecules (N_2^+). The energies associated with the ionized nitrogen account for the emission lines observed in many spectra of nitrogen. The first negative system (FNS) of nitrogen $N_2^+(B^2\Sigma_u^+ - X^2\Sigma_g^+)$ is often observed in such spectra, with the dominant band head of 391 nm associated with the transition between the 0,0 vibrational levels.

2.3.4 Oxygen

Reactive oxygen species (ROS) play a major role in development of APPJ sources for plasma medicine because they can be used for sterilization purposes, including inactivation or the killing of cancer cells. Dissociation of O_2 molecules in air generates ROS. The density of the atomic oxygen produced from helium plasma is affected by the admixture of molecule of O_2 [15]. Murakami *et al* [40] observed that the generation of ROS involved negative ions, positive ions, and the recombination of electron-positive ions. The optical spectra of ROS are dominated by the emission line at 777 nm, which is due to the transition from the upper level 3p ^{5}P (10.74 eV) to lower level 3s ^{5}S (9.14 eV) [39] [80].

2.4 Experimental conditions

The investigation of the parameters that determined the APPJ properties was experimentally conducted. In this section we present the experimental procedures.

2.4.1 Low-frequency AC voltage sources

Since low-frequency AC waveforms were used to drive the APPJ in this study, we investigated two types of voltage sources. For both sources, we used an inverter transformer to amplify the primary input voltage to obtain a secondary voltage waveform, which was used to generate plasma discharge inside capillary tubes.

The primary AC source used in this study was a household voltage source with 100 V operated at a frequency of 50 Hz. The primary DC source (AK400W-SV-110) was powered using a household AC source to obtain a DC pulse. These sources were connected to a neon inverter transformer (NEON M-5) to obtain high-voltage waveforms. Variance in the peak-to-peak voltage was achieved from the primary AC source using a high-voltage controller connected at the output. However, the DC

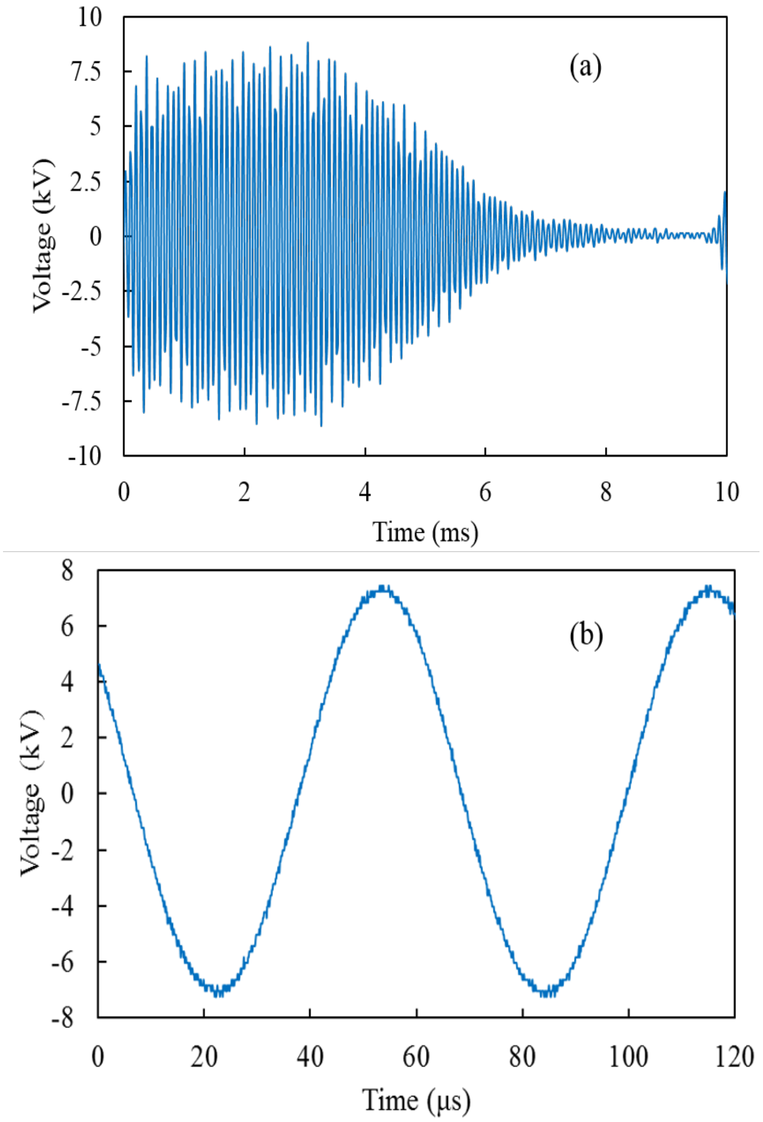

Figure 2.2: Output high-voltage waveform from neon transformer connected to; (a) primary AC source, and (b) primary DC source

power supply source facilitated the variation of the amplitude of the DC pulse to vary the amplitude of the peak-to-peak voltage. Examples of the output waveform of these two sources are shown in Figure 2.2.

As shown in Figure 2.2 (a), the primary AC source generates a high-voltage pulse with amplitude varying pulses at two different frequencies. The envelop of the pulse waveform at 100 Hz contains a high-voltage waveform at 11 kHz. As shown in Figure 2.2 (b), the connection of a DC source to the neon transformer generates a sinusoidal high-voltage waveform at 16 kHz.

A comparison between the parallel electrode and the double electrode APPJs, and mask free plasma patterning (in chapter 3) was conducted using the power source shown in Figure 2.2 (a). A modified double electrode APPJ with an additional pin electrode that facilitated controllable plasma wetting (in chapter 4) was used in combination with the power source shown in Figure 2.2 (b).

2.4.2 Parallel electrode configuration

A schematic of the parallel electrode APPJ set up is shown in Figure 2.3. Two copper wires of length 60 mm each were insulated and connected parallel to the quartz capillary tube. The ends of the electrodes were placed 2 mm above the nozzle exit to avoid arc discharge. The inner diameter of the capillary tube was 2 mm, and the outer diameter was 4 mm. Helium with a purity of 99 % was used as the carrier gas because of its low breakdown voltage.

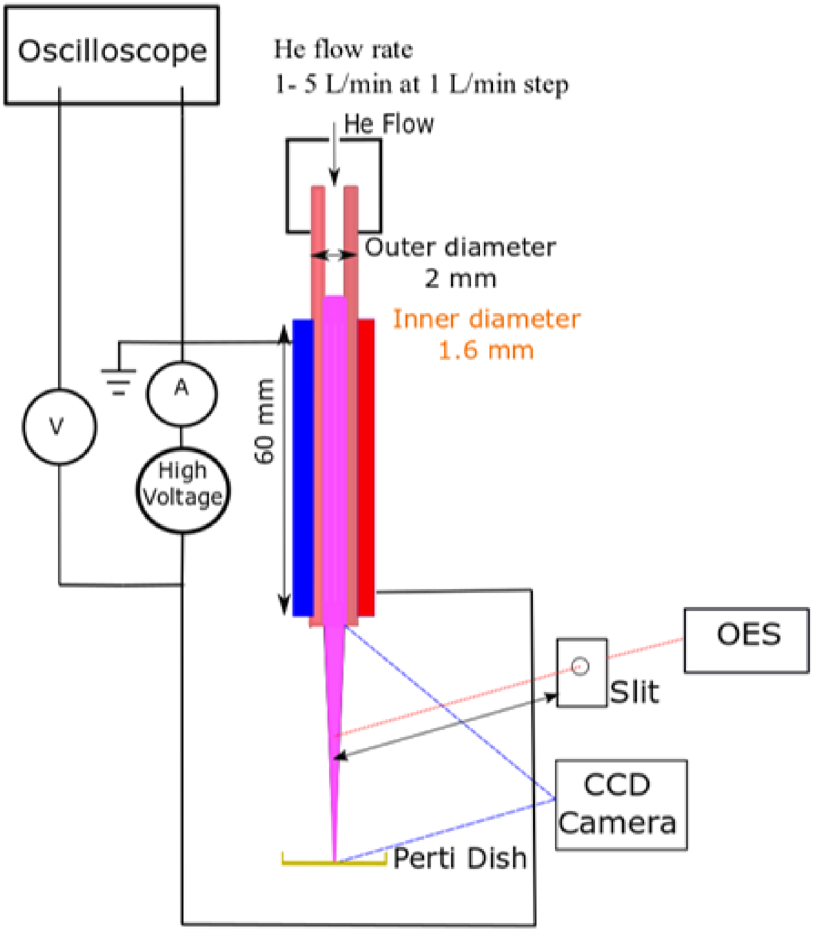

Figure 2.3: Schematic diagram of parallel electrode experimental setup

The low-frequency, high-voltage waveform obtained for the power source shown in Figure 2.2 (a) was applied to one of the electrodes and the other electrode was grounded. Using a manual mass flow meter, (YR-90) helium was allowed to flow to the capillary tube and the GFR was varied between 1 L/min to 5 L/min in 1 L/min steps. Images of the APPJs were collected using a digital camera (Nikon D3100, with Micro-Nikkor-lens and 2x multiplier) to analyze the APPJ properties.

2.4.3 Double electrode configuration

A schematic diagram of the double electrode APPJ configuration is shown in Figure 2.4. Two copper foils with a width of 10 mm and a thickness of 2 mm were attached to the capillary tube with a gap distance of 60 mm. Low-frequency, high-voltage waveforms from the power sources shown in Figure 2.2 (a) and 2.2 (b) were applied to active electrode, and the other electrode was grounded.

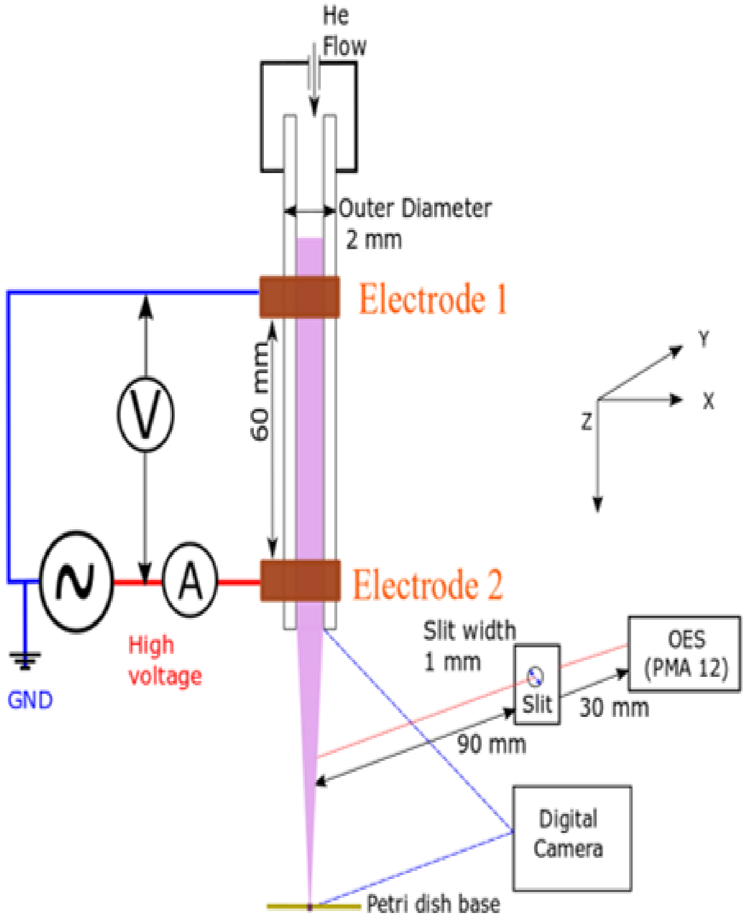

Figure 2.4: Schematic diagram of double electrode experimental setup

Capillary tubes with a tube inner diameter of 2.0 mm and an outer diameter 4.0 mm were used to generate the APPJ for comparison with the parallel electrode configured APPJ. Using a manual mass flow meter (YR-90), helium with a purity of 99 % was allowed to flow to the capillary tube and the GFR was varied between 1 L/min to 5 L/min in 1 L/min steps. Images of the APPJs were collected using a digital camera (Nikon D3100, with Micro-Nikkor-lens and 2x multiplier) to analyze their properties.

2.4.4 Double electrode configuration with an additional floating pin electrode

To investigate the properties of APPJ as a function of the electrode configuration, polarity, and tube diameter, the double electrode configuration was modified to include an additional floating pin electrode at the bottom of the plasma jet as shown in Figure 2.5. Plasma discharge was obtained in this experimental set up using the low-frequency high-voltage waveform presented in Figure 2.2 (b).

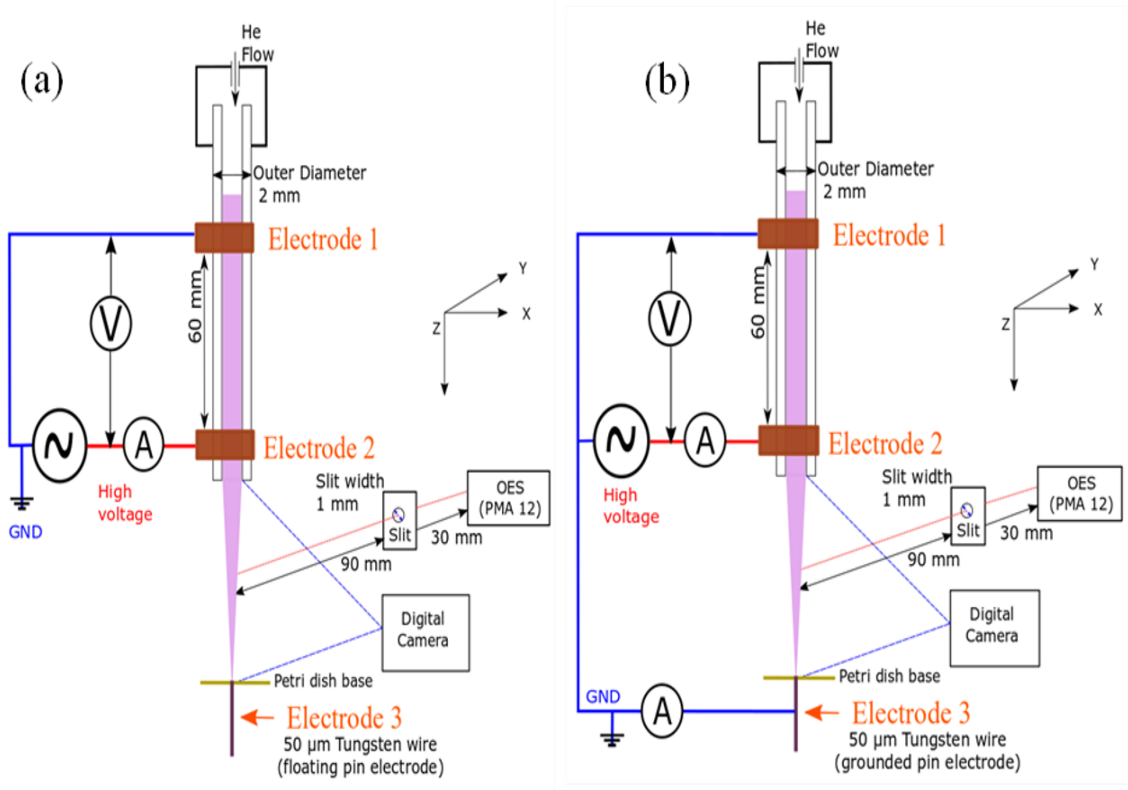

Figure 2.5: Schematic of the experimental setup for the double electrode APPJ; (a) with a floating pin electrode, and (b) with an additional grounded pin electrode at the bottom of plasma jet

To investigate the effect of the additional pin electrode, tube diameter, gas flow, applied voltage, and polarity with respect to the properties of the APPJ, capillary tubes with an outer diameter of 2.0 mm and inner diameters of 1.4 mm and 1.0 mm, and inhouse produced capillary tubes with nozzle exit inner diameters of 120 μm, and 60 μm, respectively, were used. To produce the inhouse capillary tubes, one end of a capillary tube with an outer diameter of 2.0 mm and an inner diameter of 1.0 mm was gradually tapered to form a capillary tip. These capillary tubes with micro-scale inner diameters were similar in shape to those used by Kim *et al* [90] without an angled nozzle tip.

Tungsten wire with a diameter of 50 μm was attached to the bottom of the APPJ as the additional pin electrode, through a Petri dish. The additional pin electrode with (grounded pin electrode) and without (floating pin electrode) ground connections was used for all the experimental conditions except for the investigations on polarity.

The capillary tubes with inner diameters of 1.4 mm and 1.0 mm were fed with 99 %pure Helium using a manual (YR-90) gas flow meter ranging from 1 – 5 slm in 1 slm steps. In comparison, the micro-capillaries with inner tube diameters of 120 μm and 60 μm were fed at 100 – 350 sccm in 50 sccm steps using a digital flow meter (SEC-E40). These flow rates were used to study the behavior of APPJ during the transition from the laminar to turbulent regime, in addition to the tube diameter.

The length of the plasma jets was estimated using a binarization method by converting the images acquired using a digital camera (Nikon D3100, with Micro-Nikkor-lens and 2x multiplier) into a data.

2.4.5 Procedure for APPJ parameter evaluation

To estimate the APPJ length, the captured digital images were converted into a binary format using an inhouse program. The parameters of the program were adjusted until the estimated inner diameter based on the binary image was closed to the actual size of the capillary tube. The estimated diameter and jet length were then used to analyze the APPJ parameters. The procedure for determining the APPJ length and its diameter is shown in Figure 2.6.

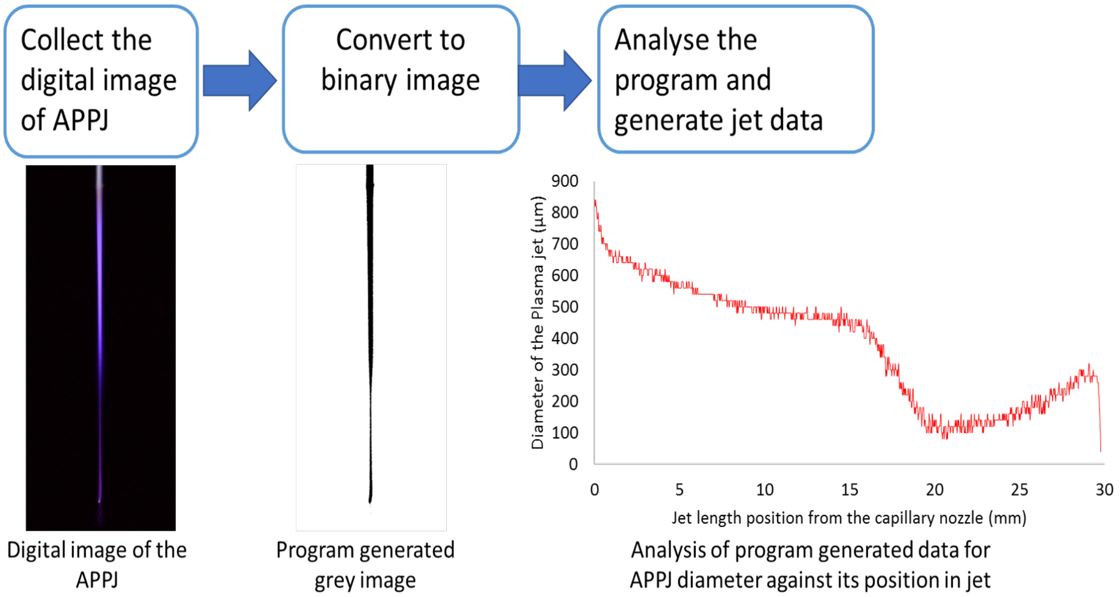

Figure 2.6: Procedure for determining APPJ length and its diameter

2.4.6 Optical emission spectroscopy system

A spectrometer (HAMMAMATSU: PMA12) with spectral resolution $\Delta\lambda$ $\sim$ of 0.7 nm was used in this study to collect the spectra of the APPJs in the region of 200 – 800 nm. To obtain localized spectra along the plasma jet, a single slit with a diameter of 1.0 mm was placed between the plasma jet and the optical sensor (ϕ = 1.0 mm) at distances of 90 mm and 30 mm. A schematic of the spectral system is shown in Figure 2.7.

As shown in Figure 2.7, a single slit was used to obtain the localized spectra. The width of these spectra was estimated using equations 2.3 and 2.4 as follows:

$$\tan\theta = \frac{y_1}{x_1} = \frac{y_2}{x_2} \tag{2.3}$$

$$y_1 = \frac{y_2}{x_2} x_1 =\sim 3mm \tag{2.4}$$

The optical emission spectra for the APPJ configurations used in this study were obtained by placing a single slit between the plasma jet and the optical sensor to obtain localized spectra.

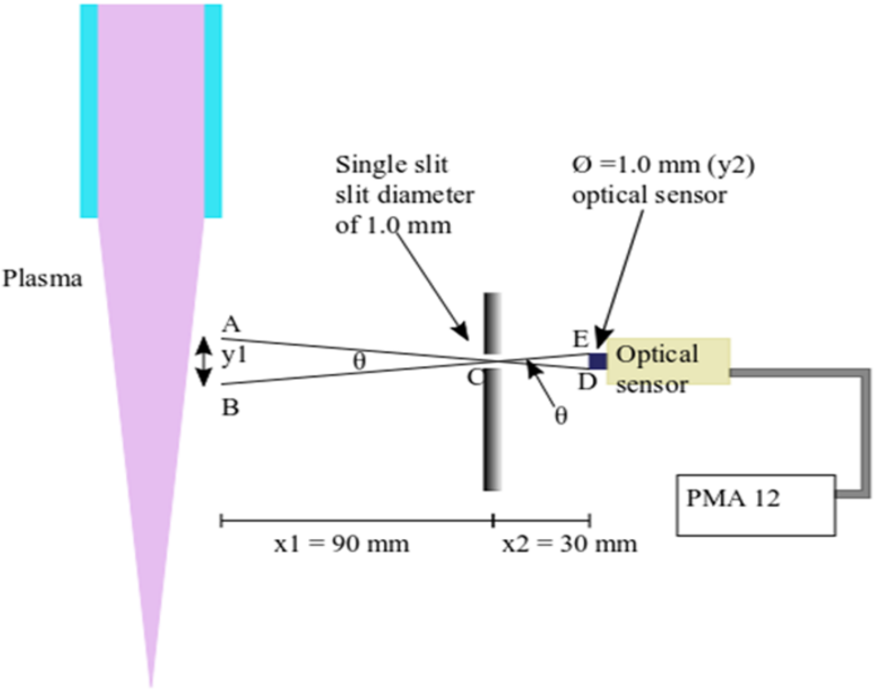

Figure 2.7: Schematic of localized spectra acquisition OES system

2.5 Results and discussion

The acquired experimental data discussed in section 2.4 were evaluated to analyze and determine the impact of the different parameters on the properties of APPJ. In this section, the experimental results are discussed in addition to the theoretical background, in terms of the effects of the different parameters on the properties of APPJ.

2.5.1 Comparison between parallel electrode and double electrode configurations

Figure 2.8 shows digital images of the APPJ for parallel and double electrode configurations. A capillary tube with inner and outer diameters of 2.0 mm and 4.0 mm respectively, was used for both APPJ configurations.

As shown in Figure 2.8, the plasma discharge inside the capillary tube had a low intensity violet color for the parallel electrode configuration and a high intensity near-white color for the double electrode configuration. In addition, APPJ in the

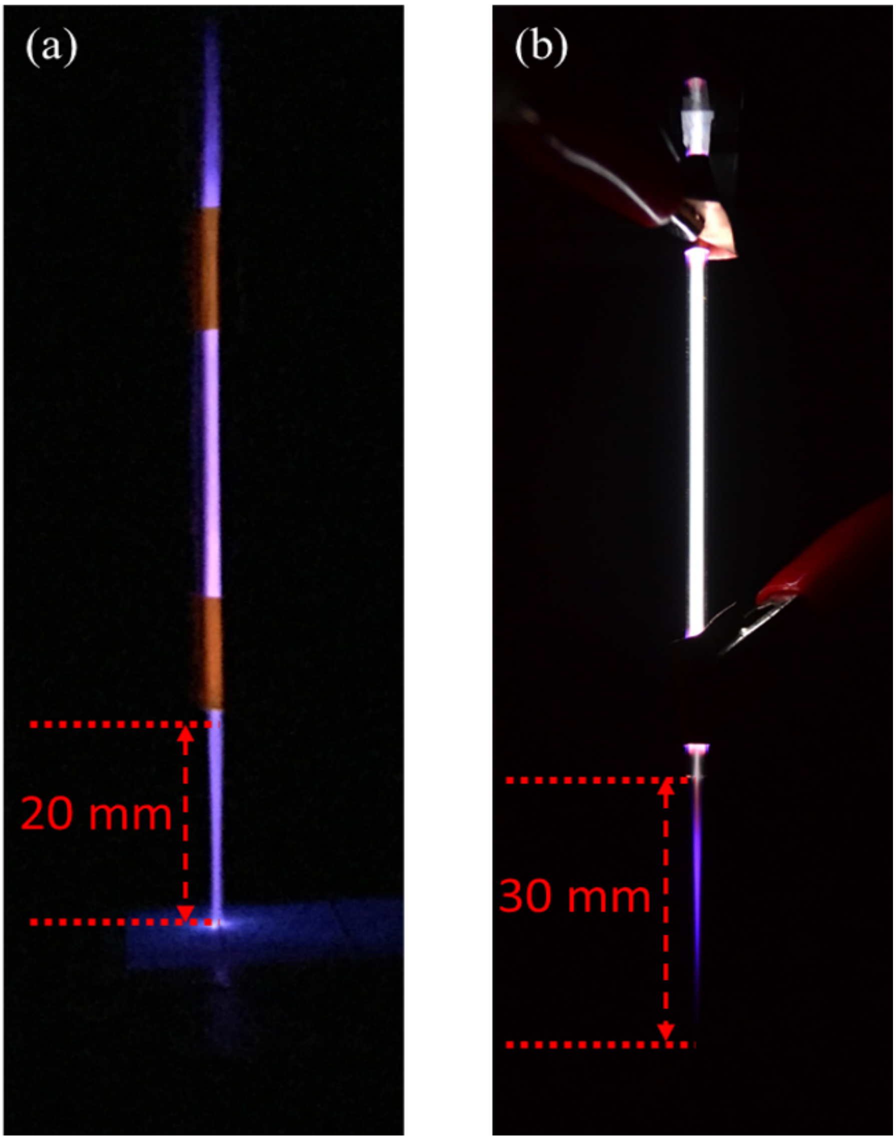

Figure 2.8: Digital image of the APPJ; (a) parallel electrode configuration, and (b) double electrode configuration

atmosphere also exhibited a high intensity color for the double electrode compared to the parallel electrode configuration. As discussed in chapter 1.3 and section 2.2.1, the electric field in the plasma jet propagation direction affects the plasma bullet velocity. Moreover, in the double electrode configuration, the upstream plasma jet undergoes a cathode fall discharge to increase the intensity of glow discharge inside the capillary tube compared to the parallel electrode configured APPJ.

Considering the images acquired for the APPJs for different gas flow rates for both electrode configurations, the jet length was estimated using the procedure described in section 2.3.4. These estimated jet length values are plotted against the flow rate in Figure 2.9.

As shown in Figure 2.9, the double electrode APPJ generated a longer plasma jet than the parallel electrode configuration for the same applied voltage, gas flow, and tube diameter. The larger variance of the jet length is due to the effect of the electric field direction, which caused an increase in the drift velocity and the mobility of the plasma bullets. The strength of the external electric field due to plasma bullet propagation was low for the parallel electrode configuration, and decreased the propagation phase of the plasma jet. This behavior affects the reaction of the plasma plume with ambient air, thereby reducing the intensity of the emission lines of excited and reactive species. In contrast, for the double electrode configuration, the external electric field strength was high and caused an increase in the energy of electrons and charge ions. This increase in energy caused an increase in the cross-section of the reactions and the intensity of the emission lines of excited and reactive species. Therefore, the variance of the electrode configuration affects the plasma jet length due to the strength of the external electric field in the plasma jet propagation direction.

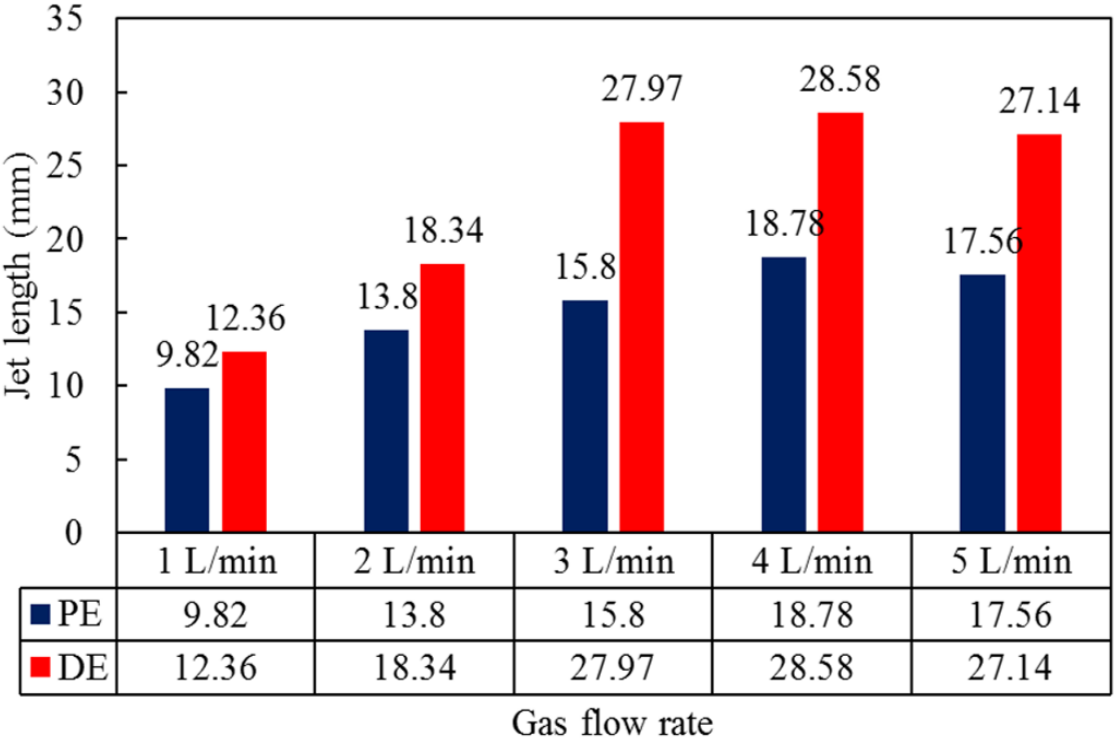

	1 L/min	2 L/min	3 L/min	4 L/min	5 L/min
■ PE	9.82	13.8	15.8	18.78	17.56
■ DE	12.36	18.34	27.97	28.58	27.14

Figure 2.9: Jet length comparison between parallel electrode and double electrode configurations

2.5.2 Effect of an additional floating pin electrode in the double electrode APPJ

A double electrode configured APPJ generates a longer jet length due to its electrode alignment. To investigate the impact of the electrode configuration, an additional floating pin electrode was attached to the bottom of the plasma jet and digital images were acquired with and without a grounded additional pin electrode as shown in Figure 2.10.

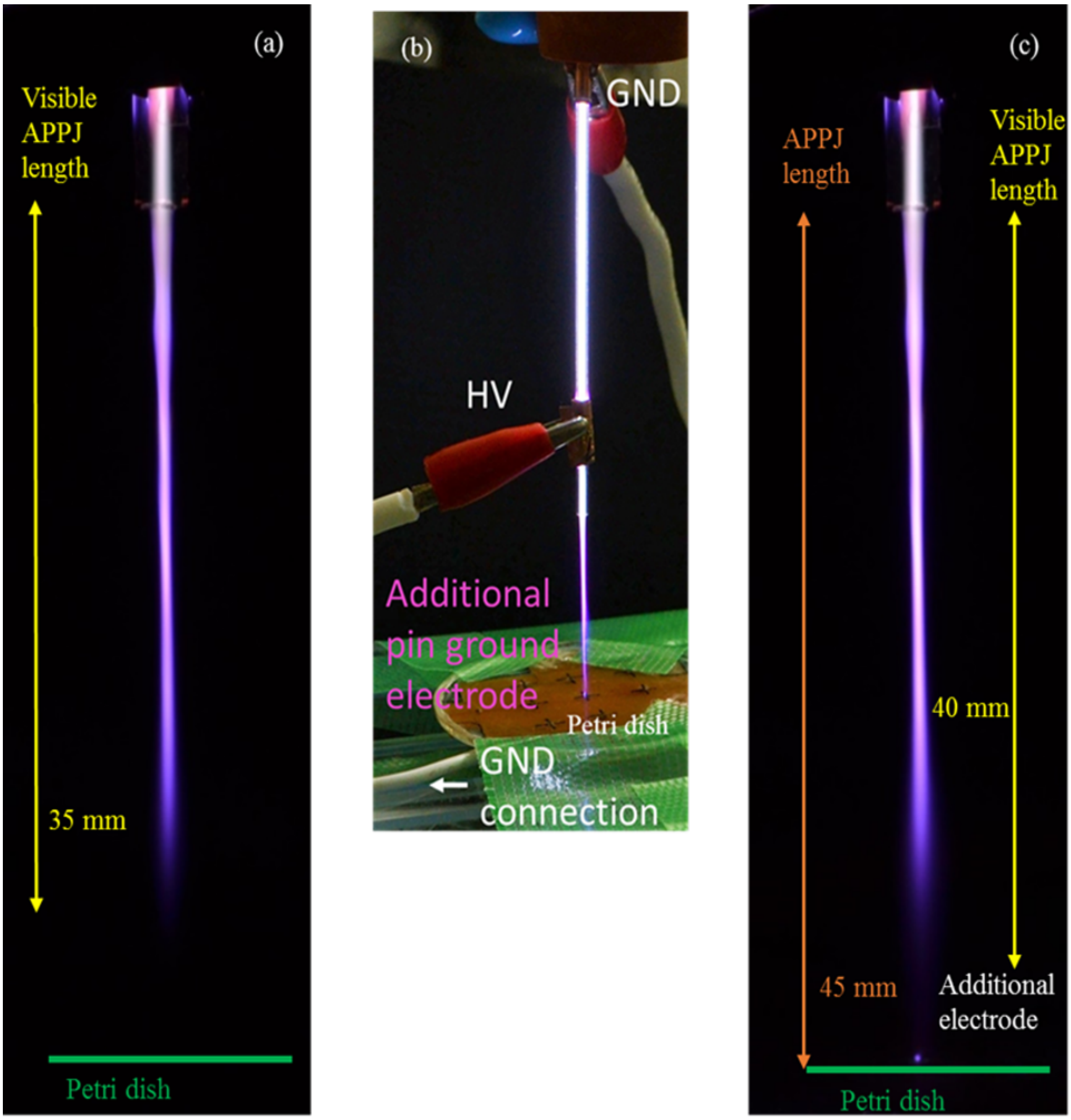

Figure 2.10: Digital images of the double electrode APPJ; (a) with the additional floating pin electrode, (b), and (c) with the additional grounded pin electrode

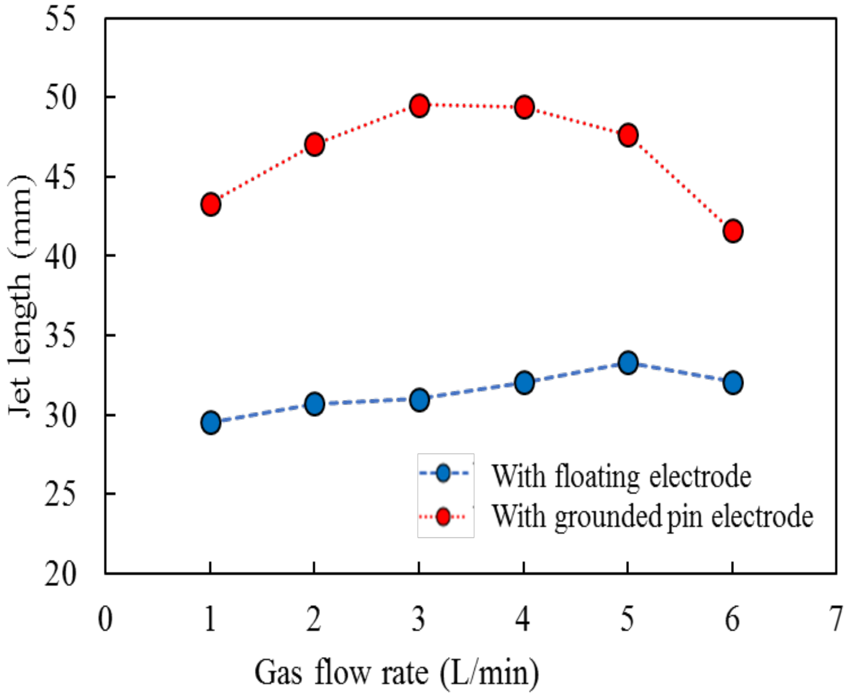

Figure 2.11: Comparison of jet length between APPJ with and without an additional floating pin ground electrode

The impact of the additional floating pin electrode on the APPJ length was analyzed using the digital images and compared to the double electrode configured APPJ without the additional floating pin electrode, as shown in Figure 2.11.

As shown in Figure 2.11, the additional pin electrode connected to the ground voltage increased the jet length compared to the floating electrode configuration. Given that the streamers experience the effect of the higher electric field strength at the bottom of the plasma jet, this causes an increase of the propagation velocity and propagation phase. As such, there is an increase of the plasma jet length for the additional grounded pin electrode configuration. Moreover, the plasma jet undergoes discharge at the additional grounded pin electrode, as shown in 2.10. To confirm this discharge, a discharge current waveform at the additional grounded pin electrode was obtained and is shown in Figure 2.12.

As shown in Figure 2.12 (c), there is a triggered discharge at the additional grounded pin electrode. Similar to the cathode fall discharge at the grounded electrode in the double electrode configuration presented in the chapter 1.3, a discharge is expected at the additional grounded pin electrode.

Triggered discharge at the additional grounded electrode is expected to

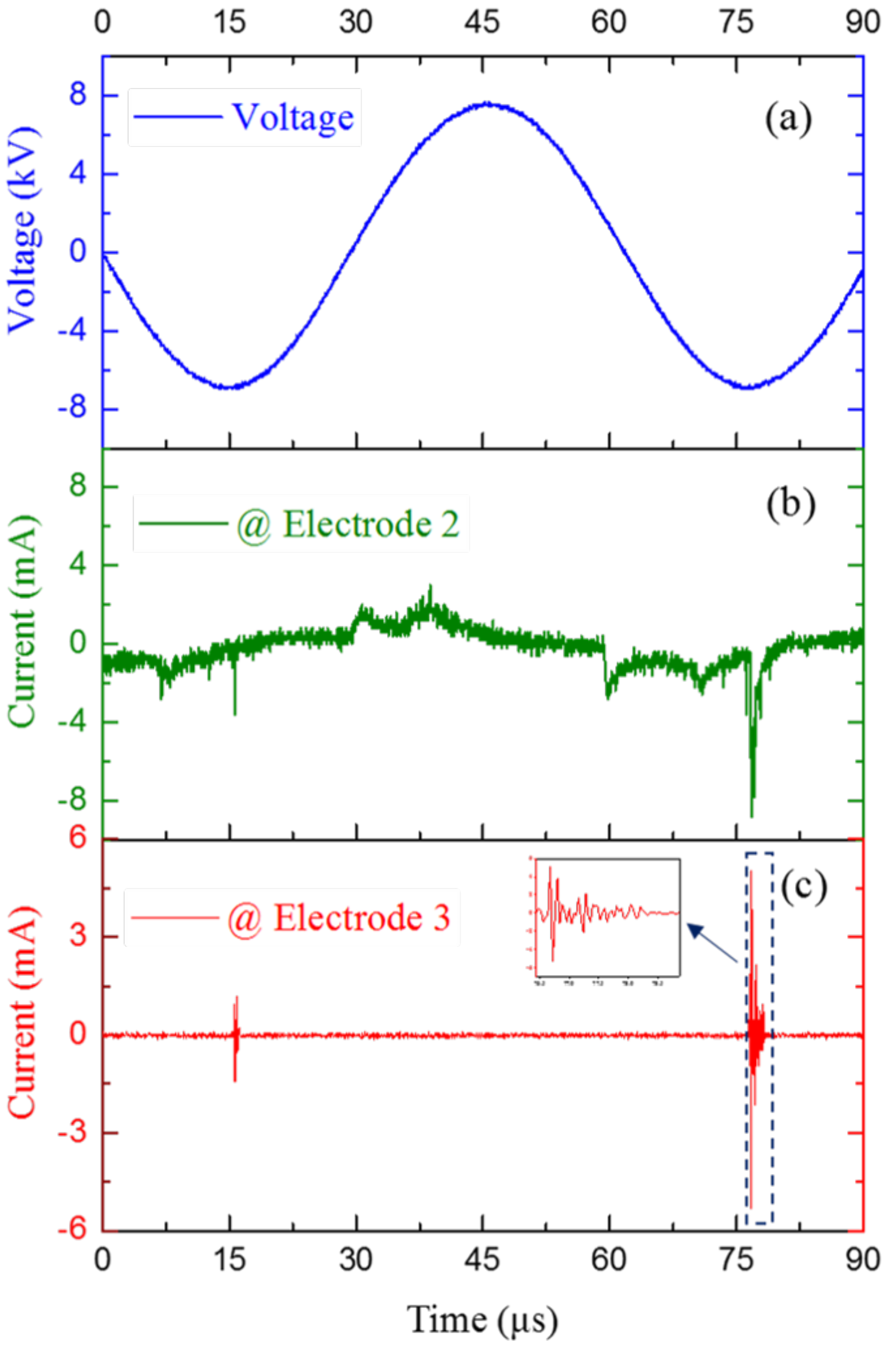

Figure 2.12: (a) Applied high voltage (blue) at a frequency of 16 kHz, (b) discharge current waveform at active electrode/electrode 2 (green), and (c) discharge current waveform for an additional floating pin grounded electrode/electrode 3 (red)

undergo secondary radical generation at the bottom of the plasma jet [138]. To confirm this phenomenon, localized OES was collected in the vicinity of the additional grounded pin electrode as shown in Figure 2.13.

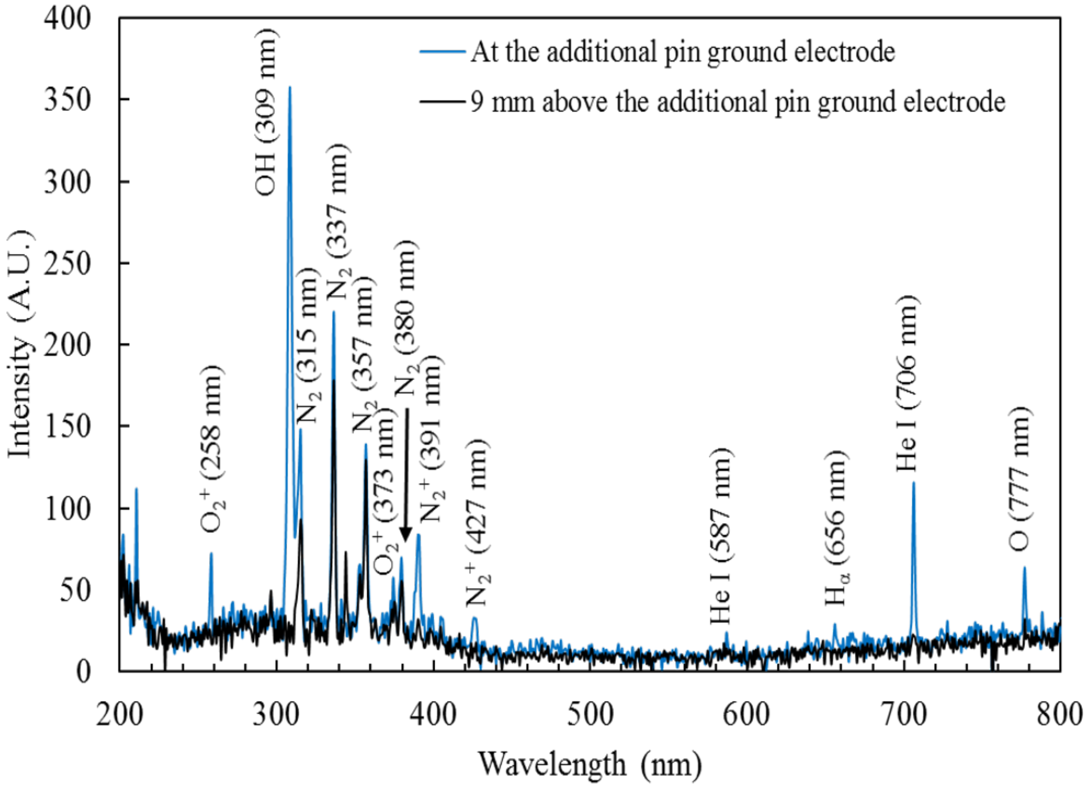

Figure 2.13: OES of the APPJ at the additional grounded pin electrode and 9 mm above

The optical spectra shown in Figure 2.13 confirm that the intensity of the emission lines of nitrogen radicals along with OH, oxygen, and helium are enhanced at the additional grounded pin electrode. These results confirm the prediction that the plasma jet undergoes a triggered glow discharge to produce secondary radicals at the bottom of the jet. The secondary radical generation is expected to undergo collision ionization, and photoionization at the additional grounded pin electrode when triggered glow discharge occurs.

The water molecules in air are expected to undergo a photoionization process to increase the density of OH radicals at the additional grounded pin electrode. The bond energies of H_2O and H_2O_2 for OH generation are 0.24 eV and 0.14 eV respectively, and it is expected that they will be affected by the energy of the emission lines of excited He, nitrogen, and oxygen, to increase the OH density.

Optical emission spectra were collected for the three different electrode configurations of APPJs discussed in this study. The identification of radicals and their intensities are shown in Figure 2.14 for the same conditions used to generate the plasma jet.

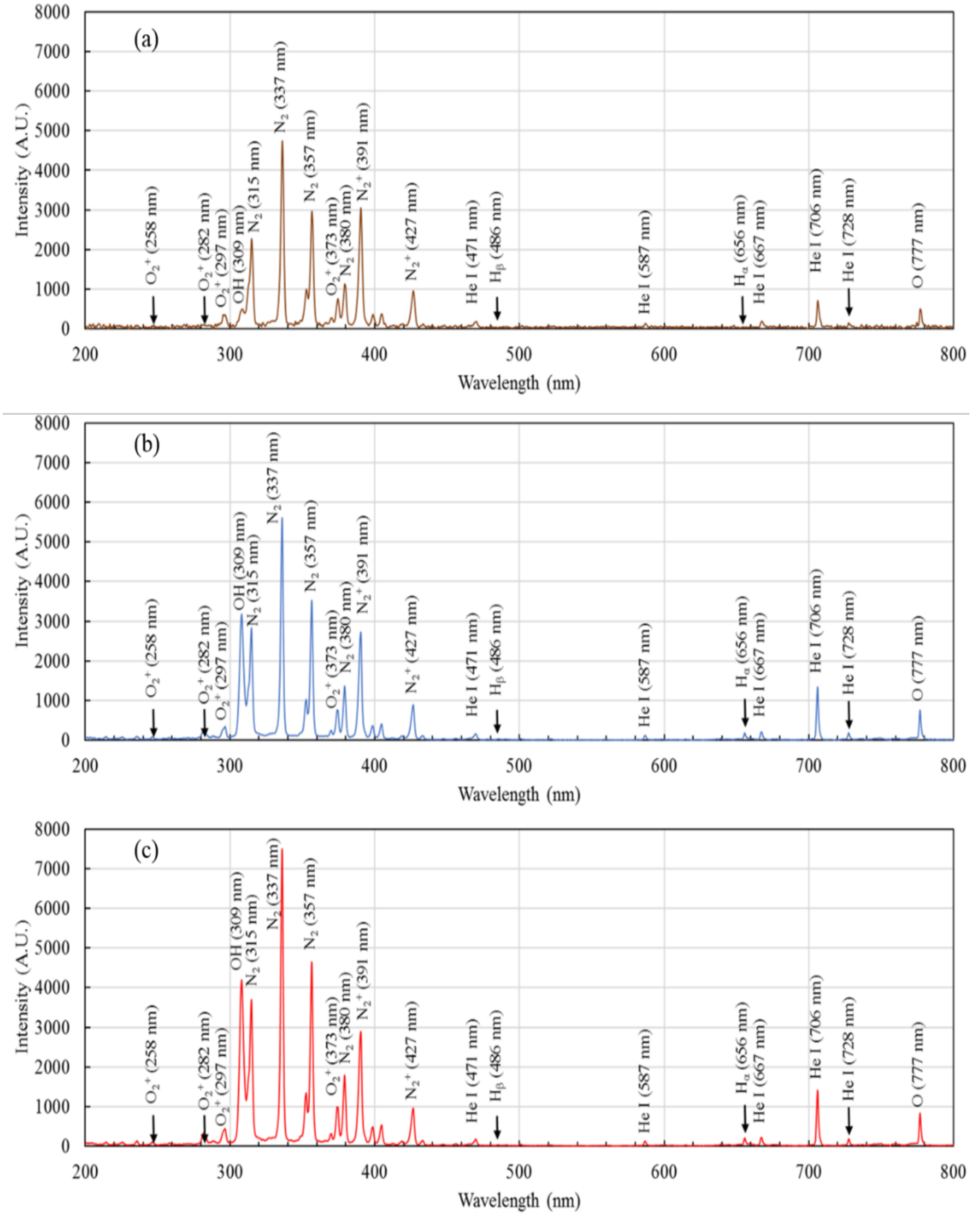

Figure 2.14: Optical emission spectra for the (a) parallel electrode, (b) double electrode with additional floating pin electrode, and (c) double electrode with additional grounded pin electrode configured helium APPJ at 3 mm below the nozzle exit for a capillary with a tube diameter of 2.0 mm and a flow rate of 3 L/min

As shown in Figure 2.14, all three types of electrode configured helium APPJs indicate the presence of excited helium, oxygen, nitrogen, and hydroxyls. Comparing the parallel electrode and double electrode configurations, the intensity of the emission lines is higher for the double electrode configured APPJ relative to the parallel electrode configuration. These results confirm that the increase in electric field strength along the propagation direction causes an increase of the cross-section of the reactions and the intensity of the emission lines. The most notable differences in the spectra presented in Figures 2.14 (a) and (b) are the increase of OH (A-X) and the emission lines of penning ionization.

These results confirm the assertion regarding the increase of discharge using the double electrode configuration at a high electric potential via the streamers and the increase in the production of radicals due to the increase in the density of excited and charged species.

Considering Figures 2.14 (b) and (c), the additional grounded pin electrode configuration resulted in an improvement of the properties of the APPJ and an increase of the intensity of the emission lines. The additional grounded pin electrode caused an increase of the propagation velocity and the propagation phase because the high electric field strength is expected to result in an increase in radical production. As the additional grounded pin electrode undergoes a triggered discharge, the production of secondary radicals will affect the upstream direction of the plasma jet in air, similar to the breakdown mechanism of APPJs discussed in chapter 1.3. This is expected to increase the collision and photoionization processes along the plasma jet, thereby increasing the intensity of the helium lines.

Experimental observations confirms that a change in the electrode configuration affects the plasma jet properties.

2.5.3 Effect of electrode polarity

The polarity of the electrodes is expected to have a significant effect on the properties of the plasma jet. Changes of the polarity are ineffective in the parallel electrode configuration because both electrodes are parallel to each DBD capillary. As discussed in chapter 1.3, in the double electrode configuration, discharge occurs at the active electrode (connect to HV waveform). A change in the polarity will change the position of the active electrode, and thereby affect the discharge process at the capillary tube. The properties of the plasma jet at the ground electrode at the nozzle exit was discussed for the double electrode configuration in a study by Begum *et al* [35],In a separate study, the position of the active electrode near the nozzle exit was discussed by Jiang *et al* [31]. Therefore, the effect of polarity on the APPJ with double electrode configurations without an additional pin electrode will not be investigated in this study.

To examine the overall coverage, the polarity of the electrodes was investigated for APPJs with an additional pin electrode for a grounded or high voltage waveform. Figure 2.15 shows the electrodes polarities and the digital images of the APPJs. The parameters involved in the investigation of the APPJ properties were kept the same for all the setups except for the investigation of the polarity of the electrodes.

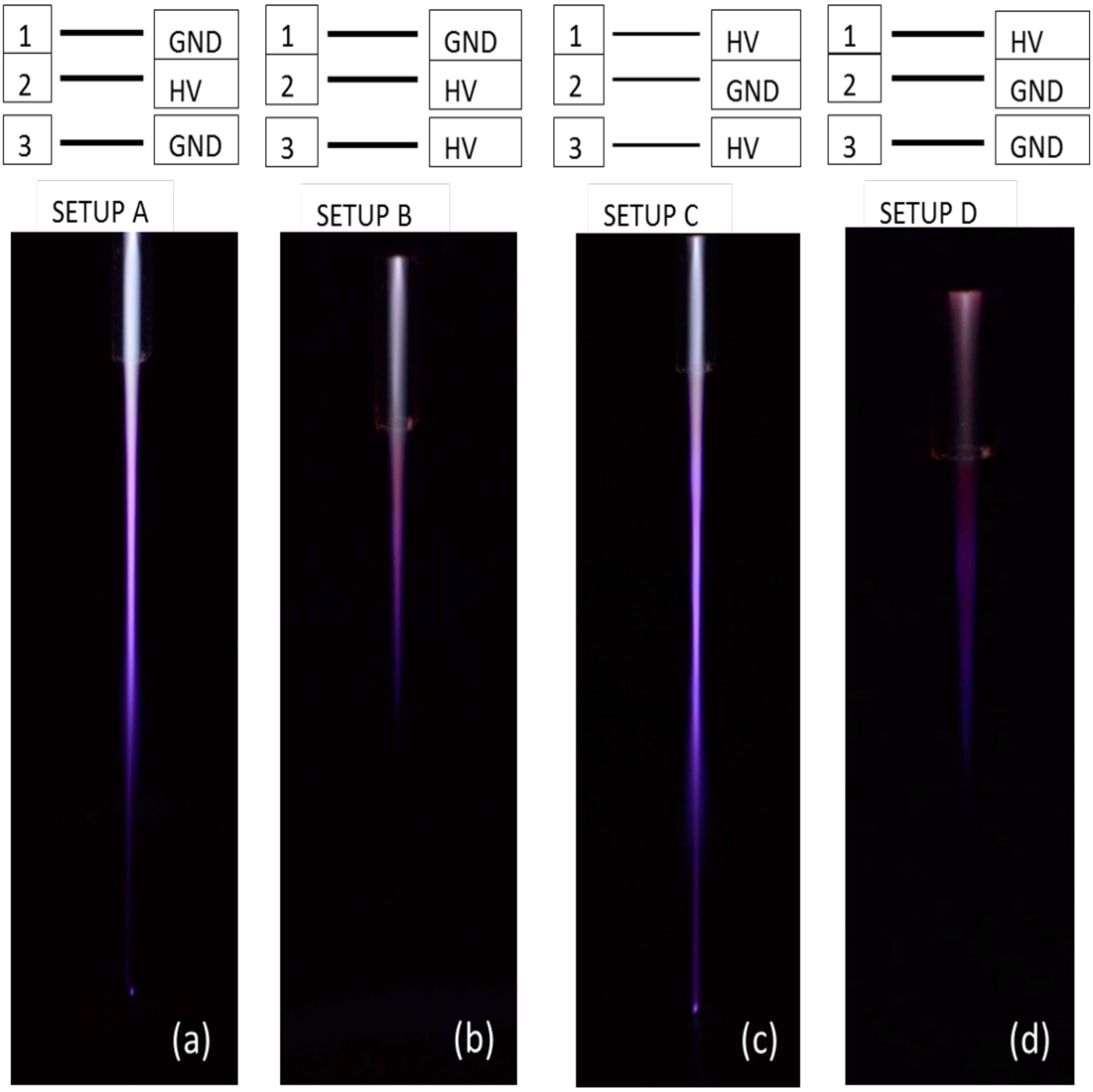

Figure 2.15: Digital images of the APPJ for different polarities of electrode configurations: (a) Setup A, (b) Setup B, (c) Setup C, and (d) Setup D (Electrode 1, 2, and 3 in Figure 2.4 (b) identified as 1, 2, and 3 respectively)

As shown in Figure 2.15, APPJs occurred in setups A, and C in which electrodes have opposite polarities along the jet propagation. Comparing setup, A and C, the observed APPJs are similar. However, this study did not consider in-depth observation of the plasma jet by reducing the imaging exposure time. Therefore, it was difficult to identify significant differences between these two setups.

Although, the investigation did not involve the collection of data to differentiate between these two conditions, it is expected that they will be affected by the electron density generated at the active electrodes of the plasma jet. Reverse cathode fall glow discharge in setup C from the setup A can also be considered to have an impact on the plasma jet properties.

For the similar electrode polarity at electrodes 2 and 3 in setup B and D, there was a decrease of the APPJ length at short distances based on the experimental data. Compared to setup B, the visible intensity and length of the APPJ obtained using setup D is smaller. In setup B and D, the presence of an active electrode and a grounded electrode near the nozzle exit affects the discharge in the upstream and downstream jet. In setup D, charged ions go through a cathode overfall at the grounded electrode, which is expected to reduce the intensity of the energetic electrons, thereby affecting the plasma jet properties compared to setup B. It is expected that this will decrease the plasma jet length and its visible intensity. As the plasma jet propagates in air, the strength of the electric field is expected to be reduced because the polarity at the additional pin electrode and that near the nozzle exit is the same. Based on studies to investigate the relationship between the electric field strength and the propagation velocity, a decrease in the former causes a decrease of the latter. It is possible to reduce the propagation phase of the APPJ to decrease the plasma jet length.

2.5.4 Effect of the capillary tube diameter and flow behavior on APPJ

A change of the flow behavior from the laminar to turbulent regime affects the plasma jet length as discussed in the section 2.2.3 and 2.2.4. To investigate this phenomenon, a capillary tube with an inner diameter of 1.0 mm and outer diameter of 2.0 mm was used to generate the APPJ for the additional floating pin electrode and the grounded additional pin electrode configurations,. Figure 2.16 shows the digital images of the APPJs as a function of the flow rate, for which the other parameters are of the same order.

As shown in Figure 2.16, an increase in the GFR affects the behavior of the plasma jet. Figure 2.16 (a), and (b) show the APPJs in the laminar regime and Figures 2.16 (c), (d), and (e) present results for the turbulent regime according to

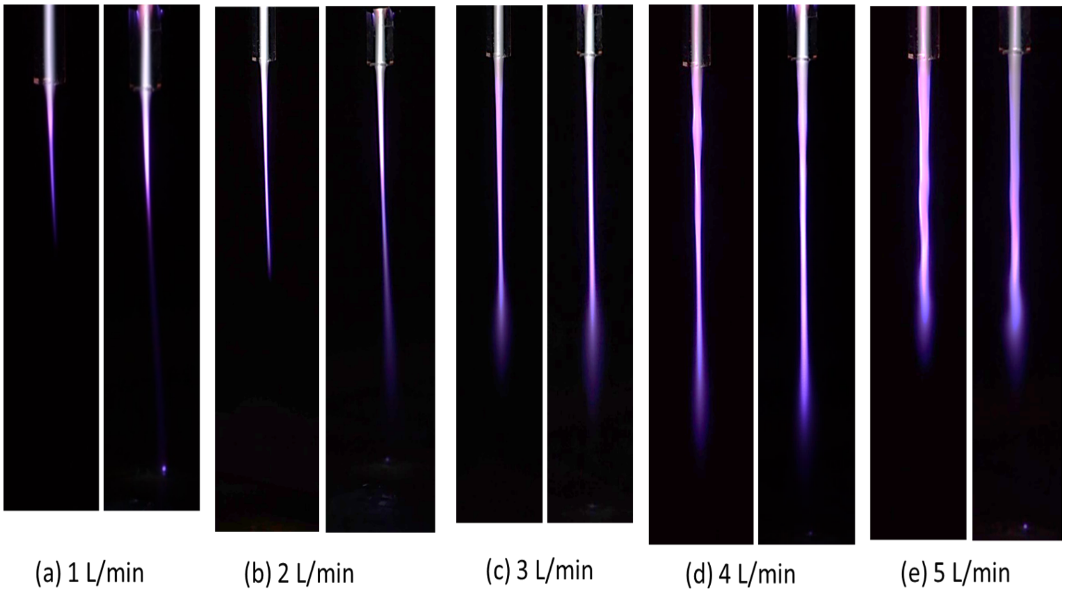

Figure 2.16: Digital images of the APPJ without an additional grounded electrode (left) and with an additional grounded electrode (right) for gas flow rates of (a) 1 L/min, (b) 2 L/min, (c) 3 L/min, (d) 4 L/min, and (e) 5 L/min

estimated Reynolds number. The increase of the GFR in the laminar regime caused an increase of the APPJ length while maintaining the cone shape of the plasma jet. However, as the flow regime shifted from laminar to turbulent, the APPJs exhibit instability and an increase of the GFR in the turbulent regime led to a reduction of the plasma jet length [31] [111] [139].

Given that the occurrence of a smooth and stable plasma jet depends on the flow behavior, it was observed that the flow behavior depends on the inner diameter of the capillary tube and the GFR. In this study, the highest APPJ occurred in the laminar region for mask free plasma patterning.

To understand the effect of the capillary tube diameter, different capillary tubes were used in this study is indicated in section 2.3.4. Figures 2.17 and 2.18 show the APPJ length for different inner diameters of the capillary tubes and the GFR. As shown in Figures 2.17 and 2.18, the jet length varied as a function of the GFR, irrespective of the additional floating pin electrode connection that was used. In addition, the jet length exhibited an increase up to a specific GFR, then subsequently decreased with a further increase of the GFR. Therefore, to establish the flow regime shift as the cause of this deviation, an estimation of the Reynold number was performed using equation 2.1 for each of the capillary tubes as a function of their feeder GFR. A summary of the results is shown in Table 2.3.

As shown in the Table 2.3, the flow rates identified in red have the highest

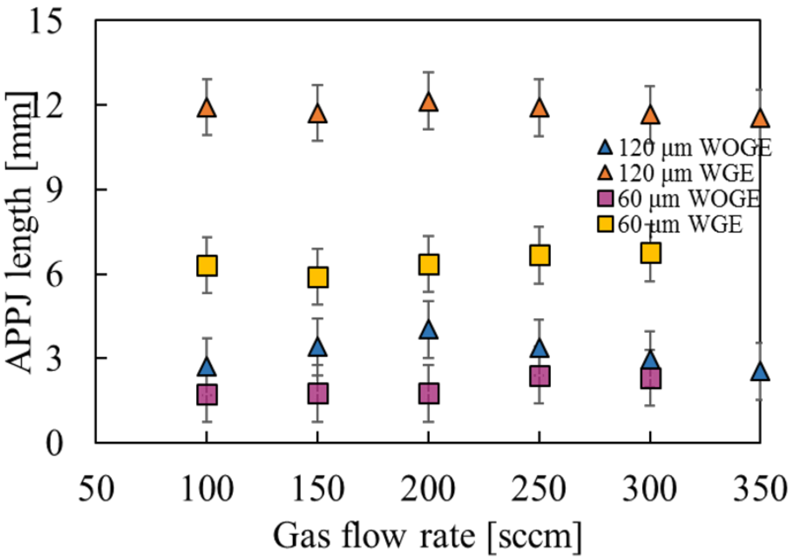

Figure 2.17: APPJ length for 120 μm, and 60 μm inner diameter capillary tube as a function of the gas flow rate for an additional grounded pin electrode identified as WGE, and with an additional floating pin electrode identified as WOGE at 16 kV$_{(p-p)}$ waveform

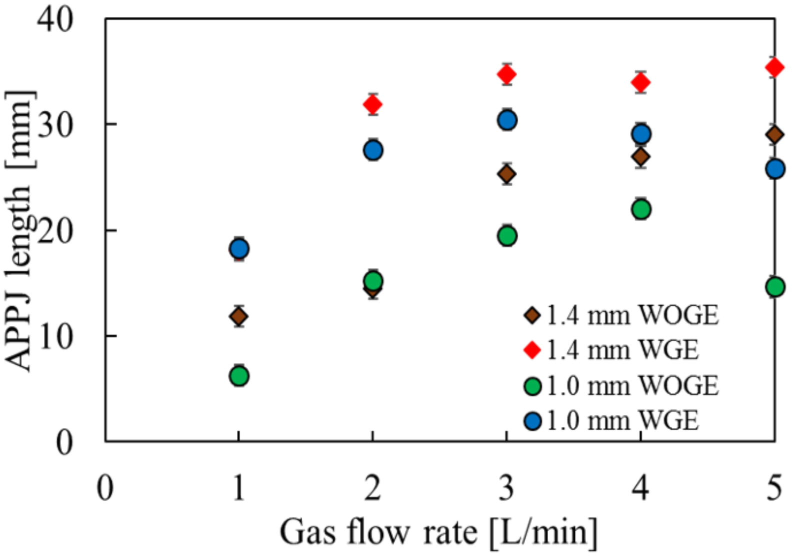

Figure 2.18: APPJ length for 1.4 mm and 1.0 mm inner diameter capillary tube as a function of the gas flow rate for an additional grounded pin electrode identified as WGE, and an additional floating pin electrode identified as WOGE at 16 kV$_{(p-p)}$ waveform

APPJ in the laminar regime. Estimation of flow behavior and the observed APPJ exhibit coincidence, thereby confirming that the APPJ length is affected by GFR

Table 2.3: Summary of the Reynold number estimation using equation 2.1 for different inner diameters of the capillary tubes as a function of the feeder GFR

Tube diameter (μm)	Gas flow rate (L/min)	Reynolds number
1400	1	72.75
	2	145.51
	3	218.26
	4	291.02
	5	363.78
1000	1	101.85
	2	203.71
	3	305.57
	4	407.43
	5	509.29
120	50	42.44
	100	84.88
	150	127.32
	200	169.76
	250	212.20
	300	254.64
	350	297.08
	5	363.78
60	50	84.88
	100	169.76
	150	254.64
	200	339.53
	250	424.41
	300	509.29
	350	594.17

and inner diameter of the capillary tube. These experimental results confirm that the double electrode helium APPJ is consisted with the theoretical Reynolds number of 200, as the benchmark for the classification of flow regimes.

Emission spectra of the plasma were collected using the OES system at the nozzle exit to analyze the production of radicals. Figure 2.19 shows the optical emission spectra for the double electrode configured APPJ with an additional grounded pin electrode for different capillary tubes.

As shown in Figure 2.19, the optical emission spectra for all the capillary configurations have a similar shape, but exhibit a decrease in intensity of the excited radicals at the nozzle exit as the tube diameter decreases. This occurs because a reduction of the inner tube diameter results in a decrease of the electron density of

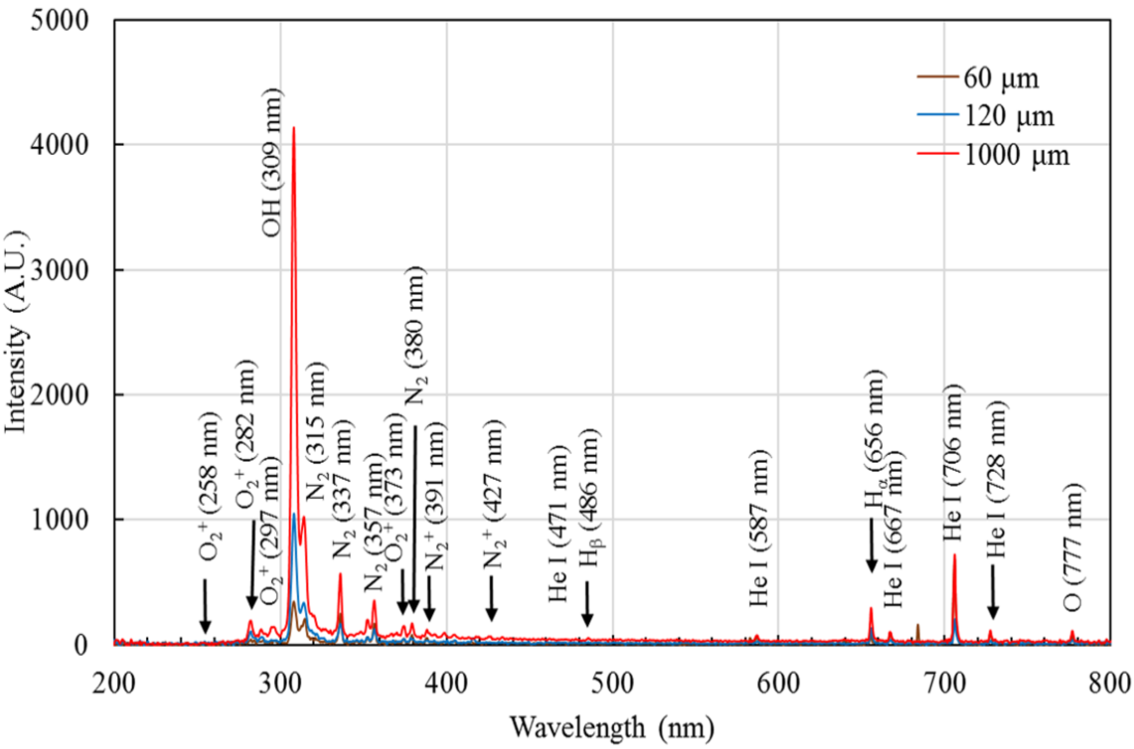

Figure 2.19: Optical emission spectra for the double electrode with an additional grounded pin electrode configured helium APPJ at nozzle exit for capillary tubes with diameters of 1000 μm, 120 μm, and 60 μm

the plasma jet [121], leading to a decrease of the cross-section of the reactions.

As expected, the highest emission intensity was observed for the OH (A-X) line. The low dissociation energy of water vapor tends to generate a high density of excited OH (A) and due to its lifetime of 1 ns, the emission intensity of OH (A-X) is highest at the nozzle exit. Notably, the information in Figure 2.19 is low or missing for parahelium energy state transitions.

The lifetime of the excited levels and the jet velocities define the emission intensity of the radicals along the plasma jet. Figure 2.20 shows the distribution of radicals at 0, 3, and 6 mm from the nozzle exit for the double electrode APPJ with a grounded additional floating pin electrode configuration and a tube diameter 1.0 mm.

Based on the optical spectra shown in Figure 2. 20, the optical emission intensity of the radicals varies with position. The OH and He I lines have the highest intensity at the nozzle exit and tend to decrease with jet propagation. Near the active electrode, the breakdown of helium gas, which is electropositive, favors the formation of electron avalanches [31] [140]. Similarly, water vapor is electronegative and favors

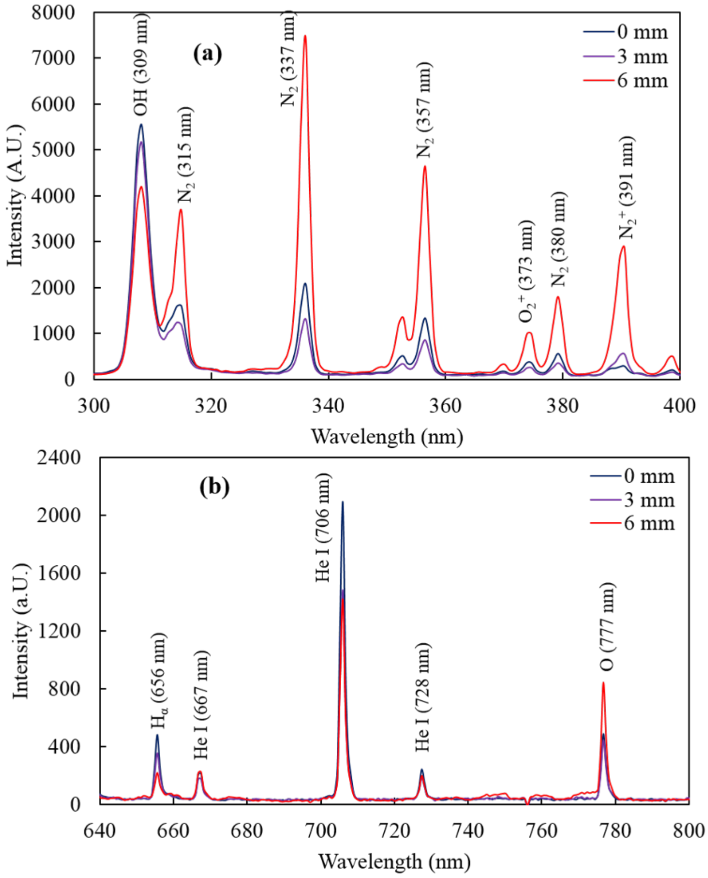

Figure 2.20: OES of the APPJ with an additional grounded pin electrode at 0 mm, 3 mm, and 6 mm from the nozzle exit along the jet propagation direction: (a) for the wavelength range 300–400 nm, and (b) for the wavelength range 640–800 nm

the addition of an electron. Thus, at the nozzle exit, accelerated electrons tends undergo the reaction $e + H_2O \longrightarrow H + OH + e$ and generate a large concentration of excited OH due to the low bond energy of e water vapor [40]. The lifetime of the half-life of the OH (A-X) transitions are on the order of 1 ns and the addition of air to the plasma changes the shape of jet via interdiffusion processes that occur along the jet, resulting in a rapid decrease in the emission intensity of OH in the propagation direction. The half-lives of the upper-state of $3s^3S$ (∼80 ns) and the lower-state $2p^3P$ (8000 s) of He I (706 nm) are higher compared to other He I transitions, in addition to their population densities, Thus, their emission are the most intense according to the spectra shown in Figure 2.20(b) [38] [39].

As the plasma jet propagates through the atmosphere, it reacts with more N_2 and O_2 to generate excited and reactive species of nitrogen and oxygen. However, the N2 second positive transition decay life of the upper level and lower level (C-B) are 36 ns and 8 μs, respectively [137]. As a result, a large emission of excited nitrogen is generated as the jet propagates. Studies from Lukas *et al* [141] and Paris *et al* [142] have revealed that at the start of the interaction of N_2 with the plasma jet, the maximum lifetime tends to decrease with time, resulting in an increase of the peak intensity of the emission lines at different positions along the plasma jet. Similar to nitrogen, the non-radiative decay of oxygen singlet states tends to have a longer life-time, resulting in large intensities along the jet propagation direction [143].

Several studies have shown that the gas flow rate is important for maintaining a stable plasma jet. However, there is limited experimental evidence for radical generation and propagation along the plasma jet as a function of variation of the gas flow for the double electrode configuration. Variations of the gas flow rates cause the plasma jet to vary its flow from laminar to turbulent, and the estimated Reynolds number can characterize this behavior based on theoretical and experimental investigations [111] [112] [125] [144]. According to the Reynolds number estimation method in reference [125], flow rates of 1.0, 1.5, and 2.0 L/min are laminar whereas 2.5 L/min, and 3.0 L/min were turbulent for the helium double electrode plasma jet.

Flow behavior is also expected to affect the spatial distribution of the plasma jet. In this respect, we investigated the distribution of the emission lines of radicals for He I ($3s^3S$ – $2p^3P$) at 706 nm, OH (A-X) at 309 nm, N_2 (C-B, 0-0) at 337 nm, and O ($3p^5P$ – $3s^5S$) at 777 nm along the plasma jet for flow rates in the range of 1.0 – 3.0 L/min in steps of 0.5 L/min. The APPJ with and without grounded additional pin electrode configurations and its distributions are presented in Figure 2.21.

The radical distribution shape along the plasma jet (Figs. 2.21 (a) and (b)) is similar for the both configurations. However, the emission intensity of the radicals is high for the plasma jet with the grounded pin electrode configuration in the laminar regime. As the flow regime changes from laminar to turbulent, the instability of the plasma affects the radical distribution and this is evident in the emission lines of OH and N_2. Considering the distributions of OH and helium along the plasma jet as shown in Figures 2.21 (I) and (II) respectively, their intensities tend to be the highest at the nozzle exit in the laminar regime. In this regime, the excited He has a stable thermal equilibrium for generating higher population densities at the nozzle exit, which decreases spontaneous emission as the jet propagates for both configurations. For OH, the generated hydroxyl radicals have a higher intensity at the nozzle exit for three reasons: (I) the low energy required to generate OH, (II) the increase of electron avalanche at the nozzle exit due to helium and the propensity of water vapor for electron attachment, and (III) a half-life of 1 ns. As such, there is a decrease of the density of OH as the jet propagates. However, when the flow regime changes from laminar to turbulent, the intensity of the excited He and OH decrease from the nozzle exit and peak at approximately 3 mm away,

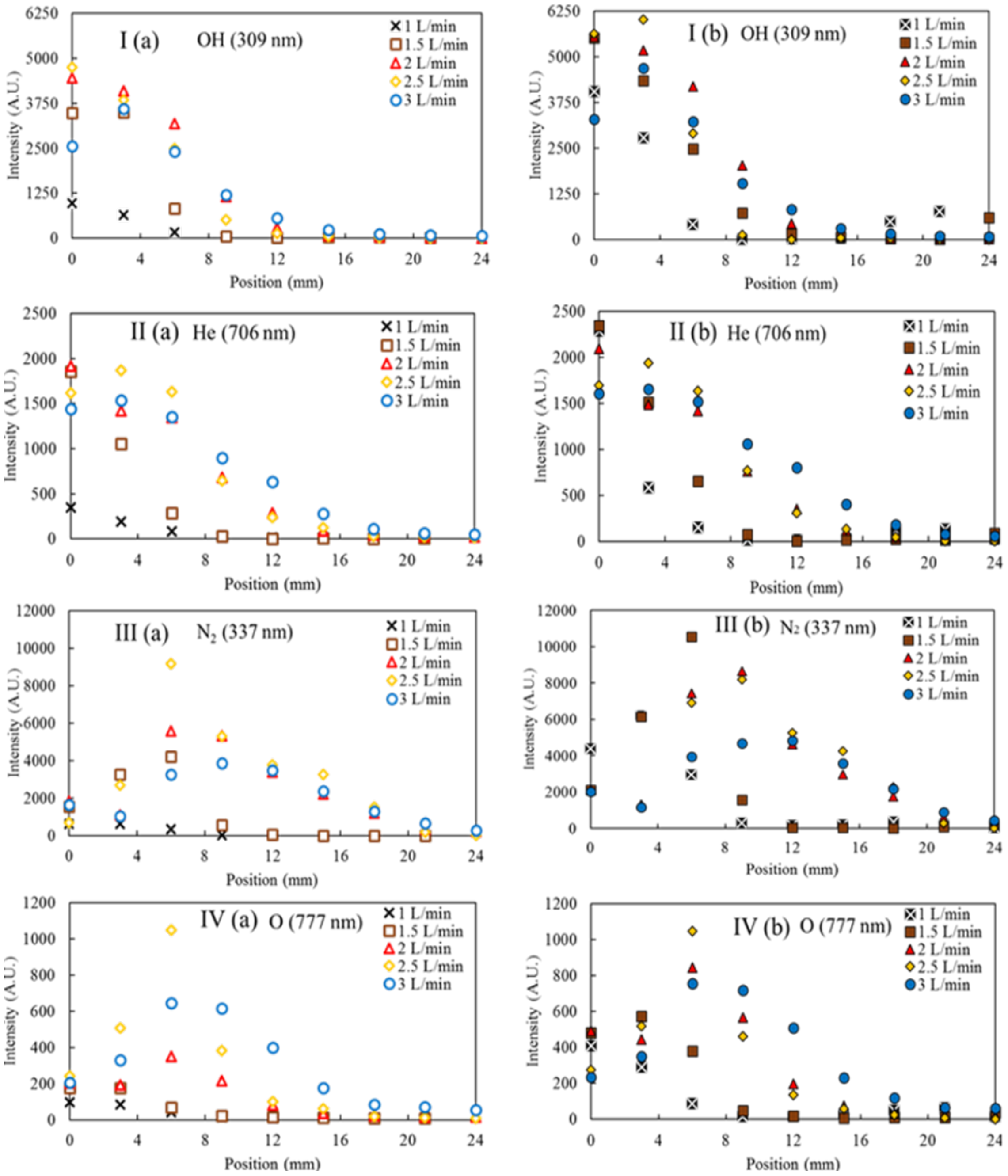

Figure 2.21: Distribution of I: OH (309 nm), II: He I (706 nm), III: N_2 (337 nm), and IV: O (777 nm) along the plasma jet for different gas flow rates (a) with floating electrode, and (b) with grounded pin electrode configuration. 1.0, 1.5, 2.0 L/min flow rates are in the laminar regime whereas 2.5 L/min and 3.0 L/min gas flow rates are in the turbulent regime according to estimated Reynold number

again exhibiting a decrease. Several studies have investigated APPJ propagation as streamer bullets [31] [35] [135], and it has been shown that flow regime variance from laminar to turbulent incorporates air into the streamer bullets, leading to instability in plasma propagation [18] [31].This instability of streamer bullets at the nozzle exit is expected to reform as it propagates through air, causing a shift of the position of the peak intensities at the nozzle exit.

The distribution of excited N_2 and O along the jet propagation in this study is similar to that reported by Uchida *et al* [80], and Begum *et al* [35]. The intensity of the peak position increases as the flow velocity increases in the laminar regime, as shown in Figures. 2.20 (III) and (IV). The peak position also shifts along the jet propagation direction, and it is evident that the additional grounded pin electrode configuration shifts this peak position more in the plasma propagation direction compared to the floating electrode configuration. As observed in the earlier referenced studies [35] [137], the plasma jet velocity is a maximum near the transition phase and also increases as the electric field strength increases [36]. This study assumes a similar framework for the peak position of the radicals and the shifting of their position along the plasma jet.

The excitation and deexcitation lifetimes of the N_2 $B^2\Sigma_u^+$ level is approximately 8 ms, causing the streamer bullets to emit a large amount of photon flux away from the nozzle exit. Figure 8 (III) shows that the peak position of the second positive system of N2 (C-B,0-0) tends to shift from 3 mm to 9 mm in the laminar regime, whereas there is an increase of the intensity of the peak position for the grounded pin electrode configuration. However, as the flow regime changes from laminar to turbulent, the intensity of the peak position decreases because of the instability of the plasma bullet and the admixture of nitrogen, causing a decrease in the nitrogen density [15]. In the case of oxygen, the propagation of the plasma jet through air causes an increase of the O_2 admixture. Such a variance is effective at a peak concentration of O, i.e., for 0.6 % O_2, before decreasing with an increase of the admixture percentage [15].

2.5.5 Effect of applied voltage

Several studies have shown that an increase in the applied voltage increases the length of the APPJ [76] [111] [145] [146]. Figures 2.22 and 2.23, show the variation of the jet length with the GFR and applied voltage for the double electrode configuration with an additional floating pin electrode and a grounded additional pin electrode configurations, respectively.

As shown in Figures 2.22 and 2.23, the jet length increases with the applied voltage only in the laminar regime. In addition, the effect of the applied voltage on the length of APPJ is limited during the transition from laminar to turbulent regime.

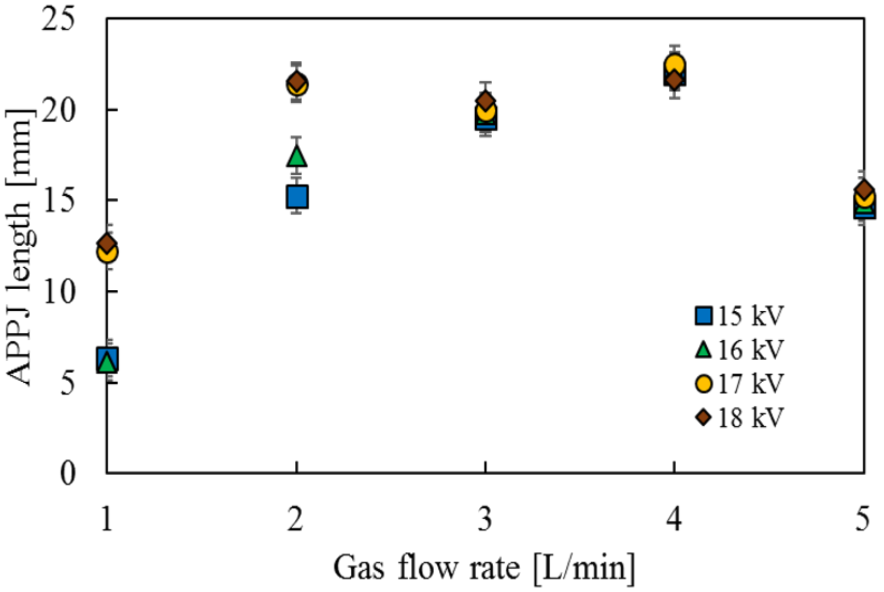

Figure 2.22: APPJ length versus gas flow rate and applied peak-to-peak voltage for 1.0 mm inner diameter capillary tube with an additional floating pin electrode configuration

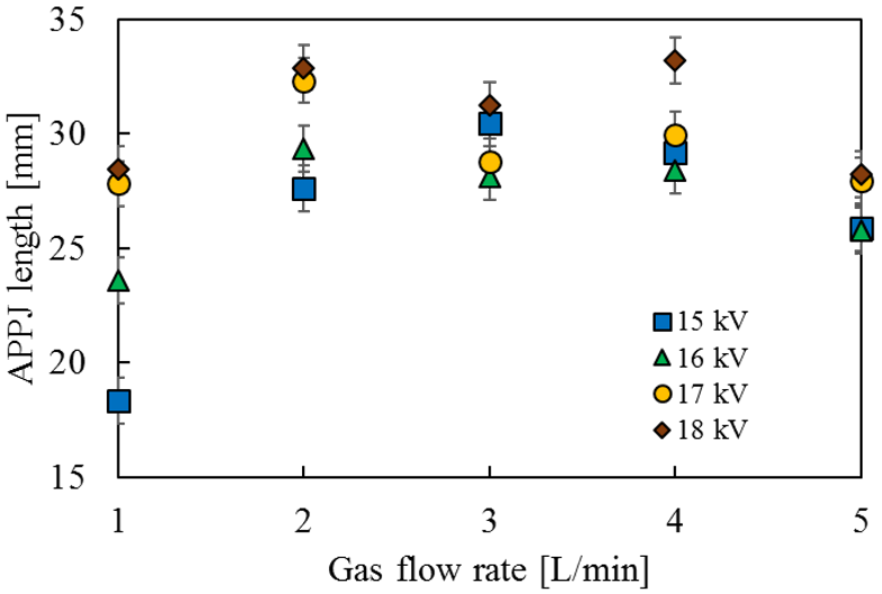

Figure 2.23: APPJ length versus gas flow rate and applied peak-to-peak voltage for 1.0 mm inner diameter capillary tube with grounded additional pin electrode configuration

The applied voltage waveform has an effect on radical propagation. The distribution of the jet velocity is affected by the applied voltage but does not result in a shift of the peak position of the radicals along the propagation direction. A study conducted by Xiong *et al* [135] revealed that an increase of the applied voltage causes a shift of the temporal evolution of the radical distribution to lower time values, while increasing the emission line intensity. Moreover, the propagation velocity also increased with the increase of the applied voltage, causing the plasma jet to travel further. These two conditions are expected to maintain similar patterns of spatial evaluation of radical distribution along the plasma jet with an increase in intensity.

To confirm this effect for the double electrode configured helium APPJ, the propagation of the emission lines of the radicals of He I ($3s^3S - 2p^3P$) at 706 nm, OH (A-X) at 309 nm, N_2 (C-B, 0-0) at 337 nm, and O ($3p^5P - 3s^5S$) at 777 nm were investigated along the plasma jet for applied voltages of 15 – 18 kV in steps of 1 kV, as shown in Figure 2.24. The capillary tube with an inner diameter 1.0 mm was used for a flow rate of 2 L/min.

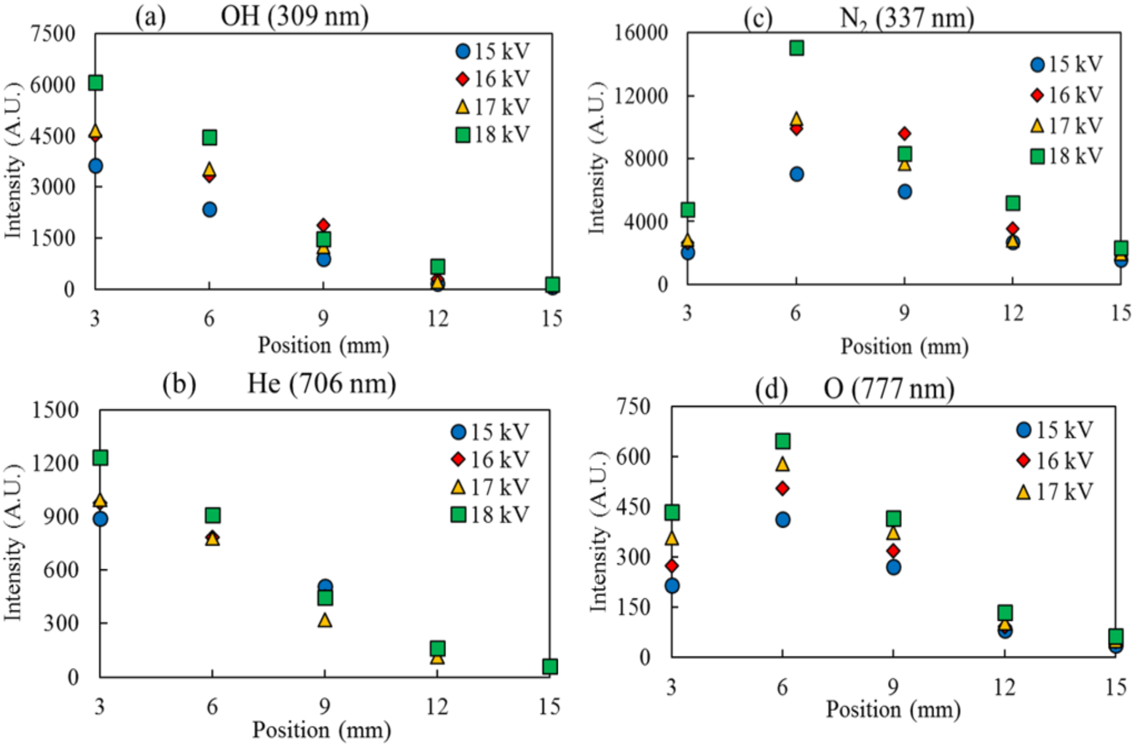

Figure 2.24: Distribution of (a) OH (309 nm), (b) He I (706 nm), (c) N_2 (337 nm), and (d) O (777 nm) along the plasma jet for different applied voltages in the range 15 kV to 18 kV for APPJs with a grounded pin electrode configuration, a tube diameter of 1.0 mm, and a gas flow rate of 2 L/min

As shown in Figure 2.24, the intensity of all the radicals emission lines increases as the applied voltage increases. However, the peak position of the radicals does not shift along the jet propagation direction as the applied voltage increases. These observations confirm that the double electrode configured APPJ is affected by the applied voltage during the increase of the production of radicals along the plasma jet.

2.5.6 Propagation of excitation temperature along the jet

The population density of the excitation levels of the working gases determine the intensity of the emission lines. Identification of these emission lines and the determination of their intensities can be performed using low-resolution spectroscopy systems. The resolution of the OES system used in this study was low. Therefore, the use of this system for the estimation of thermodynamic properties is limited. However, the estimation of the excitation temperature using experimental readings acquired from the OES system is possible, as stated earlier.

Therefore, in this study, the aim was to estimate the excitation temperature using the helium emission lines obtained for the excited levels shown in Table 2.1. The helium emission lines were used for the observed wavelengths and intensities to obtain the Boltzmann distribution plot of $\ln(I_{ij}\lambda_{ij}/A_{ij}g_i)$ versus the energy (eV) of the upper level i of the transmission. The parameters I_{ij} and λ_{ij} represent the optically obtained intensity and wavelength respectively, for helium transition from the upper level i to the lower level j. The Einstein coefficient A_{ij} and statistical weight g_i were obtained from the NIST database for the respective helium emission lines. Figure 2.25 shows the distribution of the excitation temperature along the jet propagation direction for different configurations of helium APPJ based on three different diameters of the capillary tubes for two different electrode configurations.

As shown in Figure 2.25, the helium excitation temperature T_{exc} inside the capillary between electrode 1 and electrode 2 is the same for all the inner diameter configurations. As the plasma jet propagates in the direction of the exit nozzle from electrode 2, T_{exc} exhibited a sudden decrease and the values changed depending on the diameter of the inner tube, and the effect of the additional grounded pin electrode. An increase of orthohelium transitions at the nozzle exit causes a change in the distribution of the excited helium levels, and a decrease of the excitation temperature.

In addition, APPJs with an additional grounded pin electrode configurations caused an increase of T_{exc} when compared to APPJ with an additional floating pin electrode as soon as the plasma interacted with the atmosphere molecules at the nozzle exit. As the plasma jet propagates from the exit nozzle, the He excitation

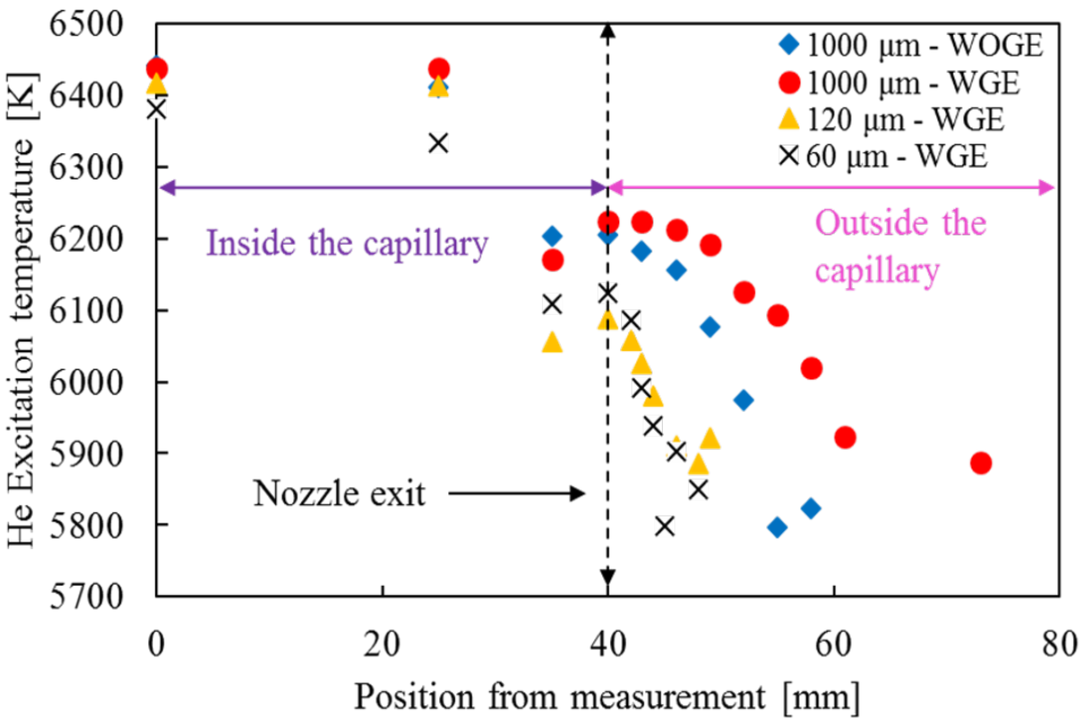

Figure 2.25: Distribution of the excitation temperature estimated based on the Boltzmann plot at various positions of the plasma jet for different configurations. Measurements were acquired for maximum APPJ in the laminar regime and for 0 mm and 20 mm below the electrode 1: (WGE: additional grounded pin electrode and WOGE: additional floating pin electrode configuration)

temperature T_{exc} decreased for all APPJ configurations. The additional grounded pin ground electrode caused T_{exc} to increase compared to the additional floating pin electrode configuration.

2.6 Conclusion

In this chapter, the effect of different parameters on the properties of APPJ was investigated, in addition to radical generation and distribution. These parameters including the electrode configuration, additional pin electrode at the bottom of the plasma jet, polarity of electrodes, gas flow rate, diameter of the capillary tube, and the applied voltage were investigated to better understand their effect on the properties of APPJ. The theoretical basis of these parameters was also considered in the investigation of the effect of the parameters, in addition to experimental data.

In the parallel electrode configuration, the strength of the external electric field in the propagation direction is lower than that of the double electrode configuration. This affects the drift velocity and the mobility of the plasma bullets. In addition, the reaction cross-sections of the electrons and charge ions with neutral species are also affected. Moreover, the electron density of the streamers or the plasma bullets is affected, causing a change in the electric potential along the propagation phase. The propagation velocity is expected to be affected by the electric potential of the streamers, resulting in an increase of the propagation phase of the plasma jet for the double electrode configuration compared to the parallel electrode configuration. Experimental results for the visible plasma jets confirmed that the plasma jet length was affected by the electrode configuration. Although experimental data on the electron density distribution and propagation velocity along the plasma jets were not acquired in this study, it was expected that these two aspects would also be affected by the interaction between the direction of the applied electric field and the flow. An increase in the reaction cross-section due to the electrode configuration affected the reactions, and the spectroscopic experimental results confirmed that the intensity of the emission lines increased for the double electrode configuration compared to the parallel electrode configuration. These results indirectly suggest that a change in the electrode configuration affects the electron density of the plasma bullets.

The inclusion of the additional grounded pin electrode to double electrode configuration at the bottom of the plasma jet provided a physical potential at a fixed distance from the plasma jet. This modification was expected to increase the electric field strength along the plasma jet and to increase the propagation velocity and propagation phase. Digital images of the plasma jets confirm that APPJ with an additional grounded pin electrode increased the plasma jet length compared to the additional floating pin electrode configuration. The discharge current obtained at the additional grounded pin electrode confirmed that the plasma jet undergoes a triggered streamer glow discharge at the bottom of the jet. This is expected to generate secondary radicals at the bottom of the plasma jet. Optical emission spectra obtained at the bottom of the plasma jet for the configuration with additional grounded pin electrodes confirmed that the secondary generation of radicals enhanced the intensities of the emission lines. Moreover, the additional grounded pin electrode was expected to increase the electron density and the reaction cross-sections along the plasma jet compared to the additional floating pin electrode configuration. The experimental emission spectra confirmed that the intensity of the emission lines was enhanced for the electrode configuration with an additional grounded pin electrode compared to the floating pin electrode.

Flow dynamics clearly affect the APPJ properties. This was confirmed by the experimental results obtained for this study. In the laminar flow regime, APPJ tends to have a smoother and longer plasma jet length compared to the APPJs in turbulent regime. The capillary diameter and the flow rate defined the flow behavior, as the jet length in the laminar flow regime increased as the flow rate increased. The change from the laminar regime to the turbulent regime caused the generation of scattered APPJs before decreasing as the flow rate was further increased.

A decrease of the tube diameter was expected to cause a decrease of the electron density of the plasma jet. Experimentally obtained optical spectra confirmed the decrease of the tube diameter resulted in a decrease of the intensity of the emission lines due to a reduction of the reaction cross-sections, even though the shape of the spectra are similar to each other. In addition, it was expected that a decrease in the flow rate would cause an increase of the time of the peak in the temporal distribution, while decreasing the intensity value of the peak emission. Experimental observation confirmed that these two phenomena can lead to a decrease of the intensity of the emission lines as the tube diameter is decreased.

Helium exhibits strong triplet transitions compared to singlet transitions due to its energy level alignment. Experimental results for helium plasma confirmed that the parahelium emission line of He I at 706 nm has the highest intensity among all the helium transitions in this study. It was also expected that the lifetime and energy levels of the excited levels would affect this behavior in helium APPJs. The visual distribution of helium based APPJs as a function of the tube diameter exhibited a similar pattern, but the intensity of the plasma jet and the length of propagation decreased as the tube diameter decreased. The experimental data collected for all the helium APPJs revealed that the excited radicals are associated with helium, oxygen, nitrogen and hydroxyls (OH).

As demonstrated in numerous studies, the APPJ properties were affected by the applied voltage. Moreover, the two APPJ configurations used in this study followed the same path. However, the inclusion of an additional grounded pin electrode caused a greater increase of the plasma jet length compared to the applied voltage, as shown in Figure 2.26.

As shown in Figure 2.26, the use of an additional floating pin electrode with the ground voltage connection can further enhance the properties compared to the applied voltage.

Propagation of the excited species depends mainly on the applied voltage and the gas flow rate as determined by the experimental results The flow behavior of the plasma jet is critical to the propagation of the excited species as the jet velocity depends on the flow rate and flow behavior. The intensity of the excited species and their peak position depend on the spatial distribution of the jet velocity in the laminar regime. The shift of the flow behavior from the laminar regime to the turbulent regime affects the admixture of nitrogen and oxygen in the reaction, causing a decrease in the intensity of the emission lines associated with the excited species. An increase of the applied voltage caused an increase of the peak position of the jet velocity but a similar shape was maintained throughout the propagation,

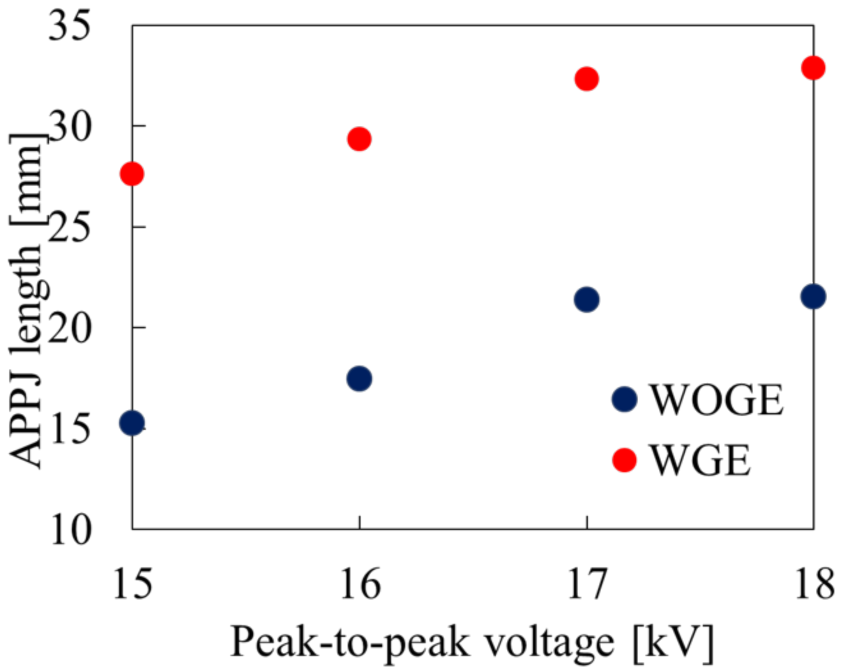

Figure 2.26: APPJs length versus the peak-to-peak voltages for 2 L/min gas flow rate for the double electrode configuration with floating pin electrode identified as WOGE and an additional grounded pin electrode identified as WGE

thereby causing an increase of the intensity of emission lines. However, a similar shape was maintained as shown in the experimental results.

As discussed in this chapter, low resolution spectroscopy can be used to estimate the excitation temperature based on the emission lines of the feeding gas. The estimated excitation temperature distribution along the plasma jet had a similar shape for all the APPJ configurations. However, a decrease of the tube diameter caused a decrease of the excitation temperature along the propagation direction. This behavior occurred because a decrease of the tube diameter caused a decrease of the jet length of the APPJ.

Experimental data on the parameters that affect the properties of APPJ revealed that carrier gases should exhibit laminar flow to obtain smooth, stable, and long plasma jet, considering the diameter of the capillary tube. The addition of an additional grounded pin electrode at the bottom of the plasma jet improved the jet properties and radical generation along the jet propagation direction. These results confirm that the double electrode configured APPJ with an additional grounded pin electrode at the bottom of the plasma jet is suitable for plasma patterning.

Chapter 3

Mask-free plasma patterning using APPJ

In this chapter, the use of atmospheric pressure plasma jet was investigated without a mask for plasma patterning and cell cultivation on the surface of treated polydimethylsiloxane as an alternative approach to conventional plasma patterning using low-pressure plasma with a mask. The contact angle was used to determine the change of the hydrophilicity of the treated surfaces. The diameter of the mask-free plasma patterned areas was investigated as a function of the irradiation time and the gas flow rate. Cell culturing was also performed on the mask-free plasma patterned areas.

3.1 Introduction

In recent decades, the field of bio-medicine has attracted increasing attention in the area of animal and human cell culturing [82] [83] [147]. The ability to grow cells on bio-compatible materials provides several advantages and has proven to be important in regenerative medicine, modelling and investigation of diseases, drug screening, and the development of gene-editing technology [81] [148] [149]. The materials used in cell culturing should possess similar properties to cells including the microenvironment, spatiotemporal distribution of soluble factors, cell-cell interaction, and cell-substrate interactions [82] [83].

Bio-compatible materials such as polydimethylsiloxane (PDMS) that is used in microdevices, are suitable for cell culturing applications [82] [83]. The properties of PDMS materials were discussed in the chapter 1 (1.7.1). Although PDMS is a suitable bio-compatible material for cell cultures, it is hydrophobic, which limits the cell-substrate interaction. Surface modification or PDMS was conducted using a plasma treatment to improve the hydrophilicity to facilitate cell-substrate interactions for cell culturing applications [91] [150]. Plasma treatments are used on the surface of PDMS for various purposes such as cleaning, improved PDMS-PDMS and PDMS-glass bonding, and to facilitate the coating of surfaces for cell-adhesion [65] [150] [151] [152].

Low-pressure plasma treatment of the surface of PDMS using a mask was conducted to modify the property from hydrophobic to hydrophilic for selected areas [63] [64] [149] to promote cell culture. Plasma treatment of this surface using low-pressure plasma to oxidize the surface to form siliceous layers for cell adhesion was discussed in chapter 1.7.2 [63] [64] [153]. Although the use of low-pressure plasma and a mask facilitates treatment of the surface, it has several disadvantages. For example, low-pressure plasma sources require special conditions such as, vacuum equipment, sealed cascades, and a significant preparation time is required before and after plasma treatment to maintain chemical equilibrium [62] [153] [154].

To address these limitations associated with plasma patterning using a mask and employing low-pressure plasma, this study investigated the use of an atmospheric pressure plasma jet without a mask. Operation occurred under non-equilibrium conditions, resulting in the generation of excited species that induce surface modification. Moreover, the necessary equipment can be easily assembled under laboratory conditions, and the properties of APPJ can provide a platform for surface treatment on PDMS surfaces without a mask.

Considering the advantages of APPJ over low-pressure plasma, the hypothesis of this study is that mask-free plasma patterning and cell culture on treated PDMS surfaces can be achieved using APPJ. In this chapter, the properties of cell cultures, and microdevices are investigated. In addition, the possibility of mask-free plasma pattering for cell culture applications using a novel approach for the generation of low-pressure plasma is examined.

3.1.1 Induced pluripotent stem cells (iPSCs)

John Gurdon discovered that differentiated somatic cells can be reprogrammed to generate pluripotent stem cells (PSCs) to generate new organisms [81] [155] [156]. The development of this concept and the associated techniques in the late 20th and early 21st centuries, facilitated the preparation of PSCs in a laboratory environment [81] [157] [158] [159] [160]. Yamanaka *et al* [147] [161] discovered that mouse and human somatic cells under pluripotent conditions can be externally reprogrammed to generate induced pluripotent stem cells (iPSCs).

Such innovative research was able to redefine the field of bio-medicine via applications such as drug screening, and genetic modification of stem cell for disease treatment [162]. Figure 3.1 shows the scientific concept of using iPSCs in the field of biomedicine [81].

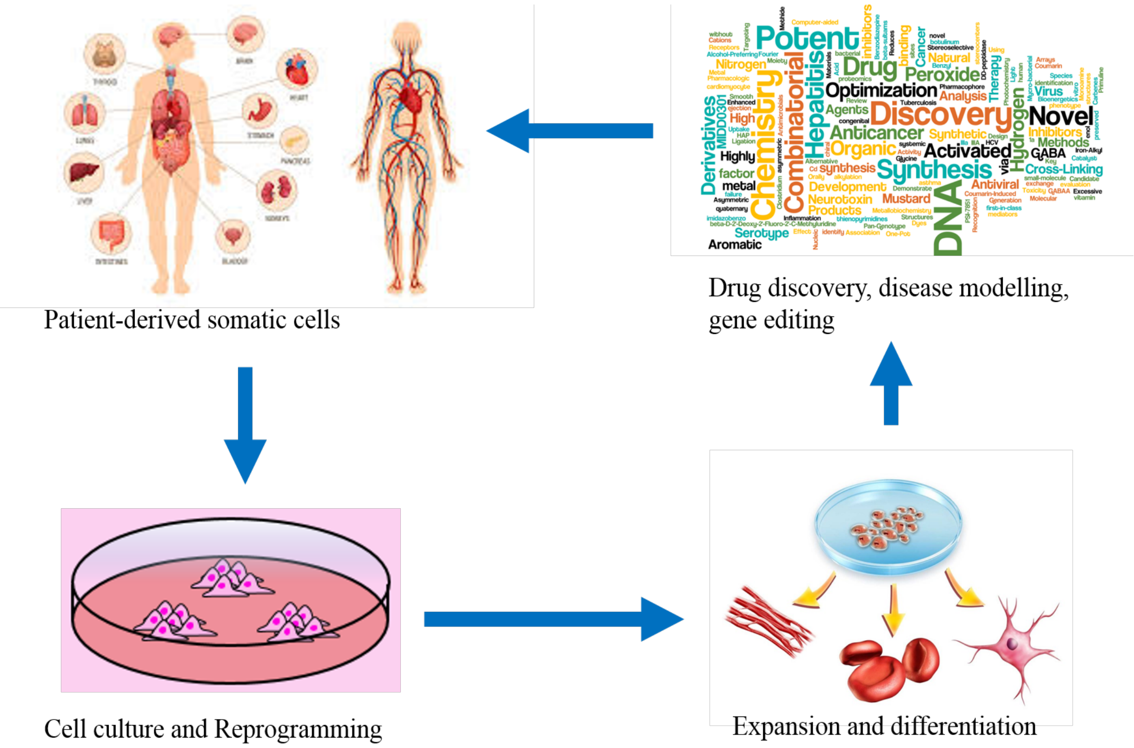

Figure 3.1: Scientific concept associated with human induced pluripotent stem cell (hiPSCs)-based treatments

3.2 Experimental conditions

The ability to use APPJ sources without a mask as an alternative approach for low-pressure plasma with a mask for plasma patterning and cell culturing was investigated in this study. The condition of the APPJ source used in this study, methods used to determine the wettability of treated PDMS surfaces, and hiPSCs cultivation on treated surface is discussed in this section.

3.2.1 Experimental setup

A parallel electrode atmospheric pressure plasma jet was used. Two copper wires with a length of 60 mm each were attached parallel to a quartz capillary tube. The inner and outer diameters of the capillary tube were 2 mm and 4 mm, respectively. A schematic of the experimental setup is shown in Figure 3.2.

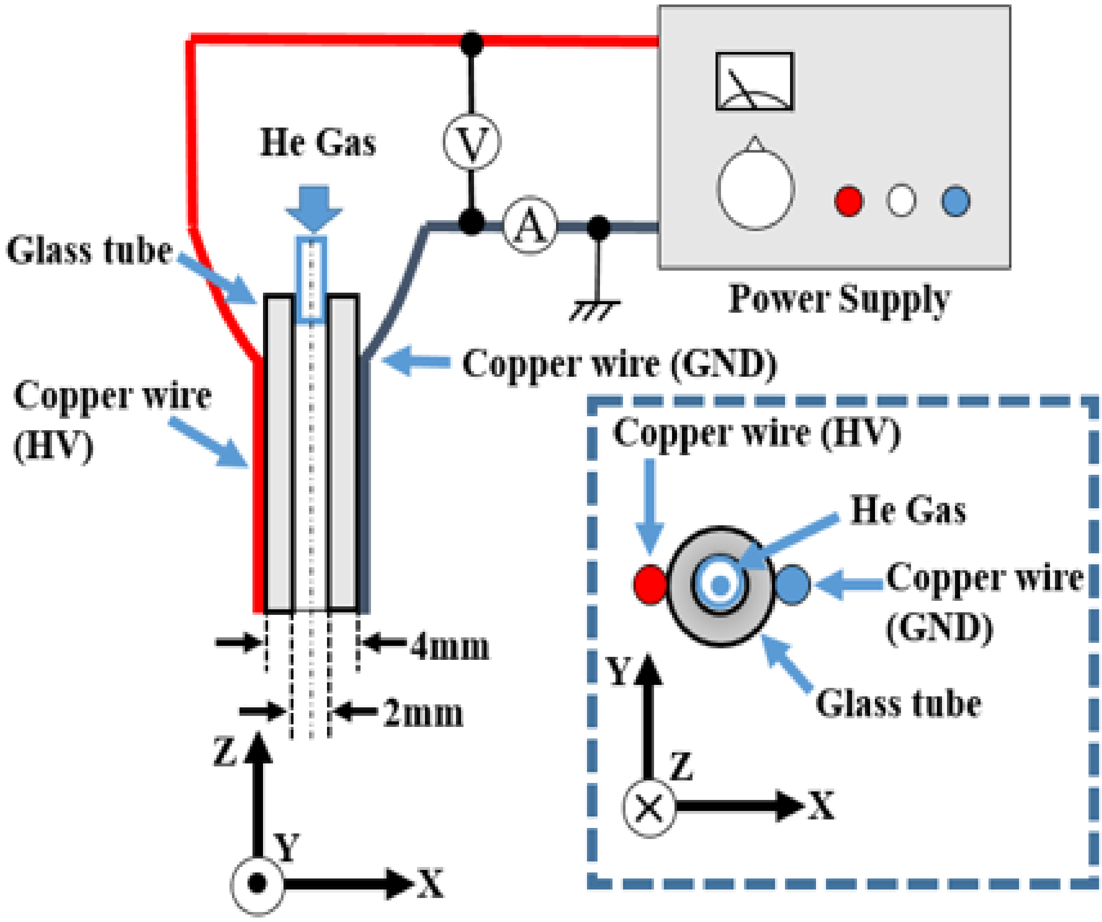

Figure 3.2: Schematic of the experimental setup [6]

This configuration allowed for a uniform parallel electric field along the tube axis and perpendicular to the feeding gas direction. The two copper wires were insulated, and the ends were kept approximately 1 mm above the tube nozzle exit to avoid a corona discharge from the nozzle to the electrodes. Helium gas was chosen as the carrier gas because of its low breakdown voltage and its ability to provide a homogeneous, uniform plasma.

A purpose-built high-voltage and low-frequency power source was used to generate the plasma. The voltage applied to generate the APPJ was kept at 20 $kV_{p\text{-}p}$ with a frequency of 11 kHz. Using a mass flow controller, the gas flow rate was varied between 1 L/min to 5 L/min in 1 L/min increments to generate the APPJ.

3.2.2 Contact angle estimation

The hydrophilicity of the surface can be determined using the wettability parameters. Attraction of a liquid to a surface can be used to quantify this property. In this study, the contact angle was used as an indicator to determine the wettability as a function of the irradiation time and gas flow rate. The adhesion of proteins such as iPSCs to bio-compatible materials depends on the wettability condition and this can be expressed as the contact angle as a function of different parameters [9] [91]. . The changes in wettability after APPJ irradiation were analyzed by measuring the contact angle in air using the sessile drop method as shown in Figure 3.3.

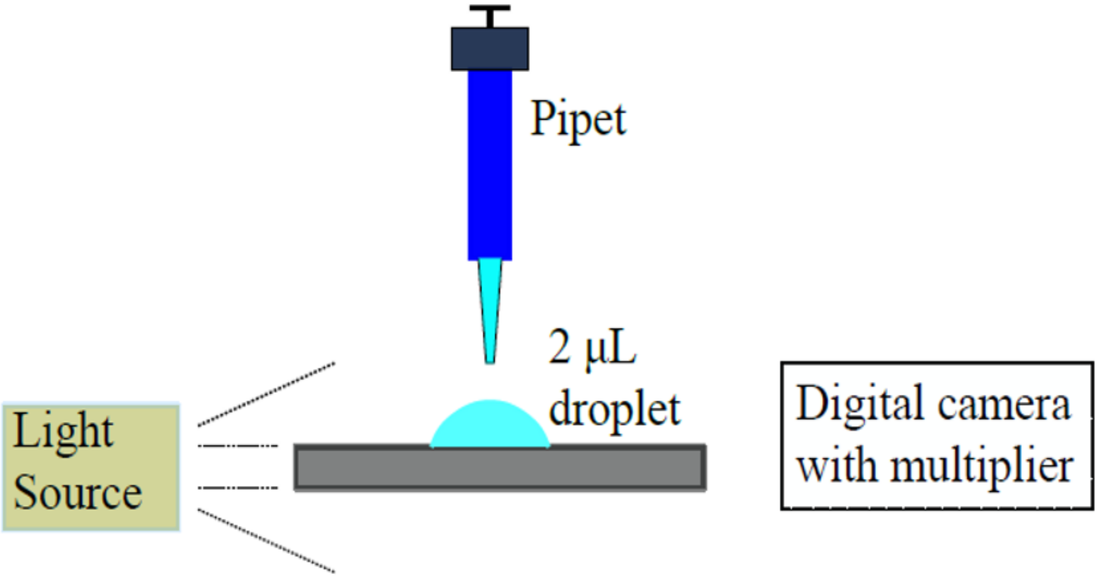

Figure 3.3: Schematic of contact angle measurement setup

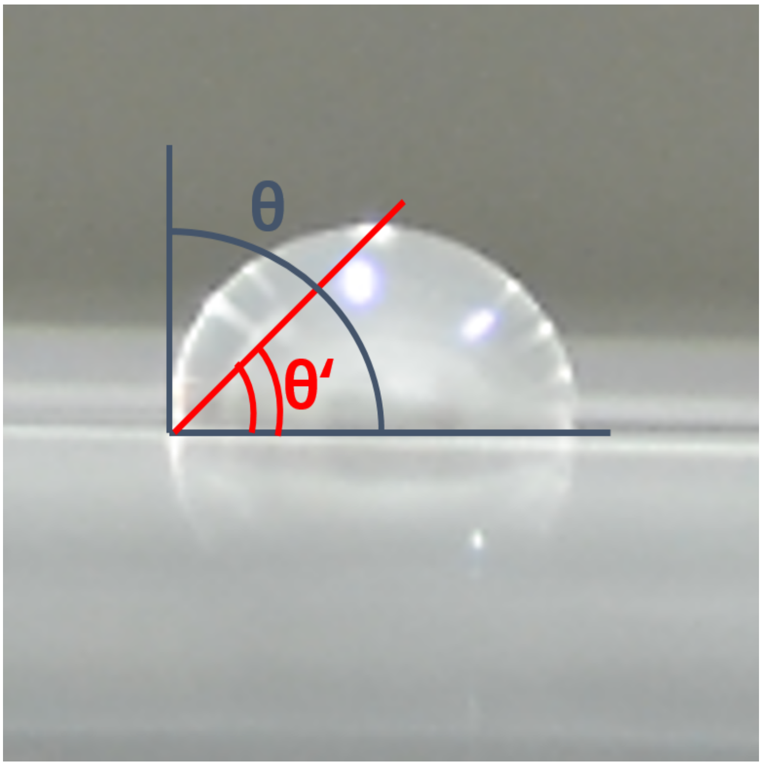

Figure 3.4: Manual estimation of contact angle using a digital image

As shown in Figure 3.3, 2.0 μL of distilled water was deposited onto the plasma treated PDMS surface. Droplets were formed on the PDMS surface and they were imaged using a digital camera. The angles were then estimated manually using the acquired digital image, as shown in Figure 3.4.

As shown in Figure 3.4, the contact angle was defined using the simple expression shown in equation 3.1;

$$Contact\ angle = \theta = 2\theta^{'} \tag{3.1}$$

where Θ is the contact angle and $\Theta^{'}$ is the angle between the vertical plane and the maximum point in the horizontal plane for the contact point of a water droplet [64] [153]. Given that the contact angle changes with the storage time, the irradiated PDMS surfaces were undisturbed for 30 min to stabilize the molecular bonding of the treated surfaces before using the sessile method [64] [153].

The Sessile method was used for all the fabricated PDMS surfaces for different gas flow rates and irradiation times to investigate their effect on wettability.

3.2.3 Wetting area estimation

Plasma patterning without a mask does not limit the wetting area. Therefore, it is necessary to identify the dimensions of the wetted area as a function of the investigated parameters such as the gas flow rate, and irradiation. In this study, estimation of the wetting size was performed using digital image of the moistened PDMS surface. The plasma treated PDMS surfaces were exposed to the water vapor produced by a humidifier, and it was imaged to estimate the diameter of the wetting area as shown in Figure 3.5.

All the irradiated PDMS surfaces were investigated for different gas flow rates and irradiation times using the aforementioned procedure to better understand the factors that influence the dimensions of mask-free plasma patterning.

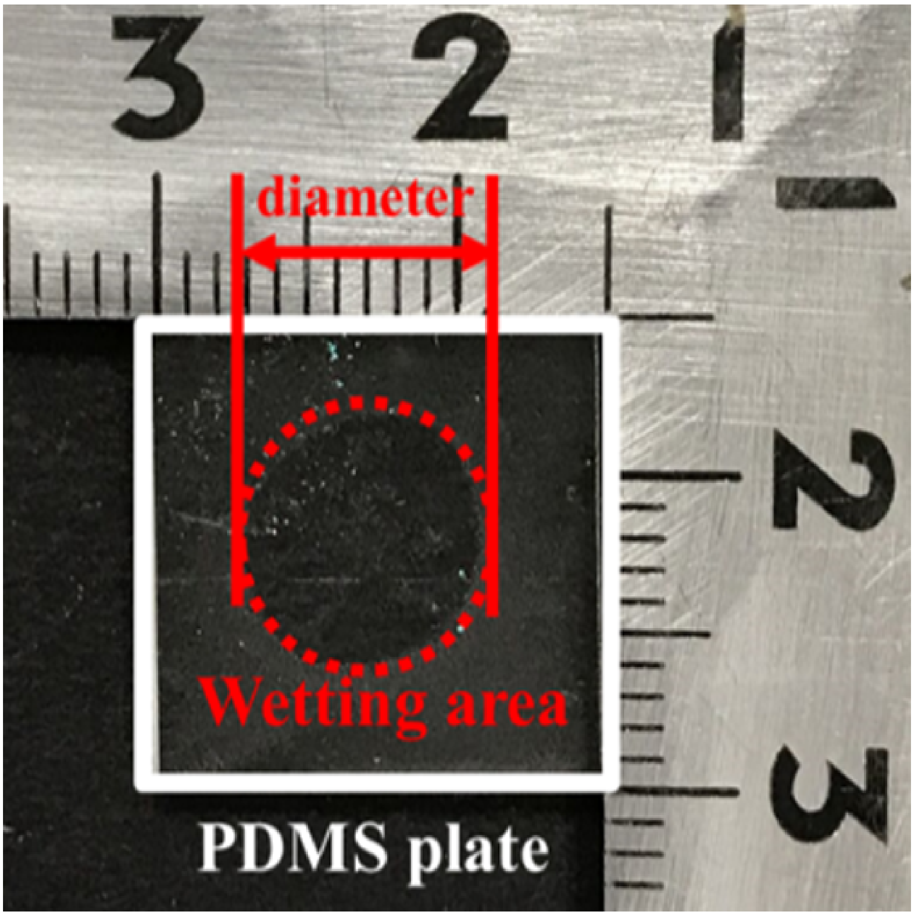

Figure 3.5: Digital image of moistened PDMS surface using humidifier [6]

3.2.4 HiPSC's cultivation

To confirm iPSCs cultivation on plasma treated PDMS surfaces, a cell cultivation procedure was performed. A spin-coated PDMS dish was irradiated at four points using APPJ without a mask and human induced pluripotent stem cell (hiPSCs) were seeded with serum medium to facilitate adhesion. A mixture of vitronectin and bovine serum albumin (BSA) dissolved in phosphate buffered saline solution was used in this study as the media for cell cultivation under laboratory condition [63] [64].

BSA serum was absorbed onto the hydrophobic surface whereas the untreated surfaces prevent cell adhesion. Vitronectin mediated cell adhesion on the plasma treated surfaces [63] [64]. A concentration of 20 μg/mL of vitronectin and 10 mg/mL of BSA was used, in addition to the gene-transferred hiPSCs (201B7) to seed the treated PDMS surfaces. Serum coated and hiPSCs seeded dishes were kept for two days to allow for cell cultivation before observation were made. Given that the cell-adhesion and non-adhesion surfaces are transparent, fluorescence spectroscopy was used to observe cell cultivation on the plasma treated surfaces.

3.3 Results and discussion

In this section, the observations of the hydrophilization properties of the treated PDMS surfaces for mask-free plasma patterning using APPJ and cell culturing on fabricated surfaces are discussed. The experimental procedures described in section 3.2 were used to obtain the experimental results.

3.3.1 Hydrophilization on PDMS surfaces using APPJ

In this study, the wettability of treated PDMS surfaces was expressed using the contact angle, as described in section 3.2.2. Figure 3.6 shows the contact angle for different irradiation times and gas flow rates.

As shown in Figure 3.6, an increase of the plasma irradiation time of the PDMS surface caused a decrease of the contact angle. Similar to the low-pressure plasma treatment on PDMS surfaces, APPJ irradiation on the surface of PDMS facilitated oxidization and improved the hydrophilicity. Compared to the low-pressure plasma treatment, APPJ irradiation allowed for quantitative evaluation of the impact of the irradiation time on the improvement of hydrophilicity [64].

An increase of the gas flow rate caused a decrease of the contact angle for

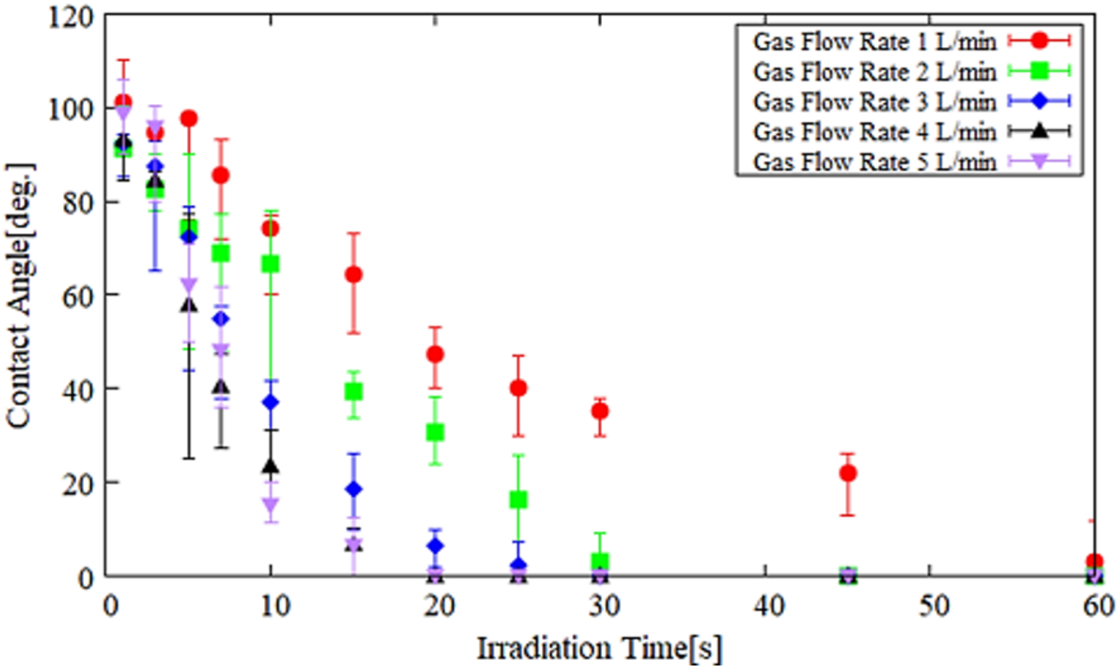

Figure 3.6: Contact angles on PDMS surfaces against irradiation time for different gas flow rates [6]

a given irradiation time. The increase of the gas flow rate increased the density of excited and reactive species as discussed in chapter 2. This is the reason for the drastic decrease of the contact angle. Oxidation of PDMS surfaces is impacted by the reactive oxygen and the increase of the gas flow rate will increase the density of reactive oxygen, thereby increasing the rate of oxidation.

The dimensions of the mask-free pattern sizes were estimated using the procedure described in section 3.2.3. The distribution of the wetting area diameter on the irradiated PDMS surface as a function of the irradiation time for different gas flow rates is shown in Figure 3.7.

As shown in Figure 3.7, the diameter of the wetted area increases as the irradiation time increases. The increase of the irradiation time increase the density of the excited or reactive species on the treated surface. Given that the reaction rate of oxidation is lower than the reaction rate for the production of reactive species on the treated surface, this results in the spread of an excess of reactive species over the irradiation point and an increase of the oxidization area.

The increase of the gas flow rate increases the size of the wetted area for a given irradiation time as shown in Figure 3.7. Similar to the explanation given for the decrease of the contact angle as a function of the gas flow rate, the increase of the gas flow rate increases the density of the reactive species of oxidization. This is

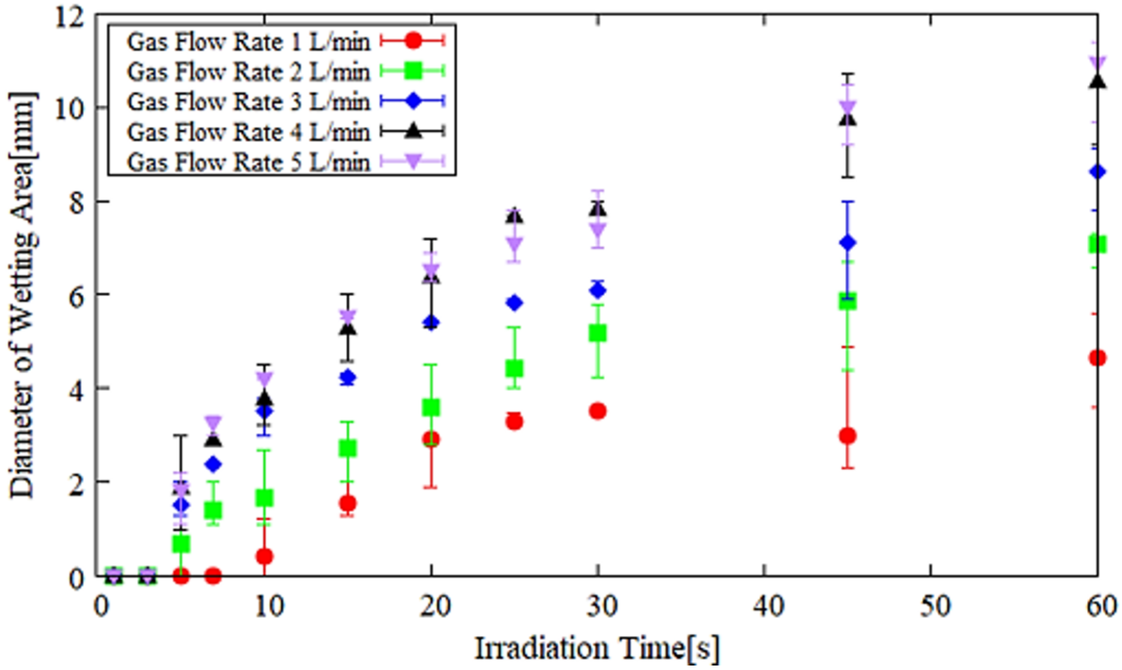

Figure 3.7: The diameter of wetted areas on treated PDMS surfaces versus irradiation time for different gas flow rates [6]

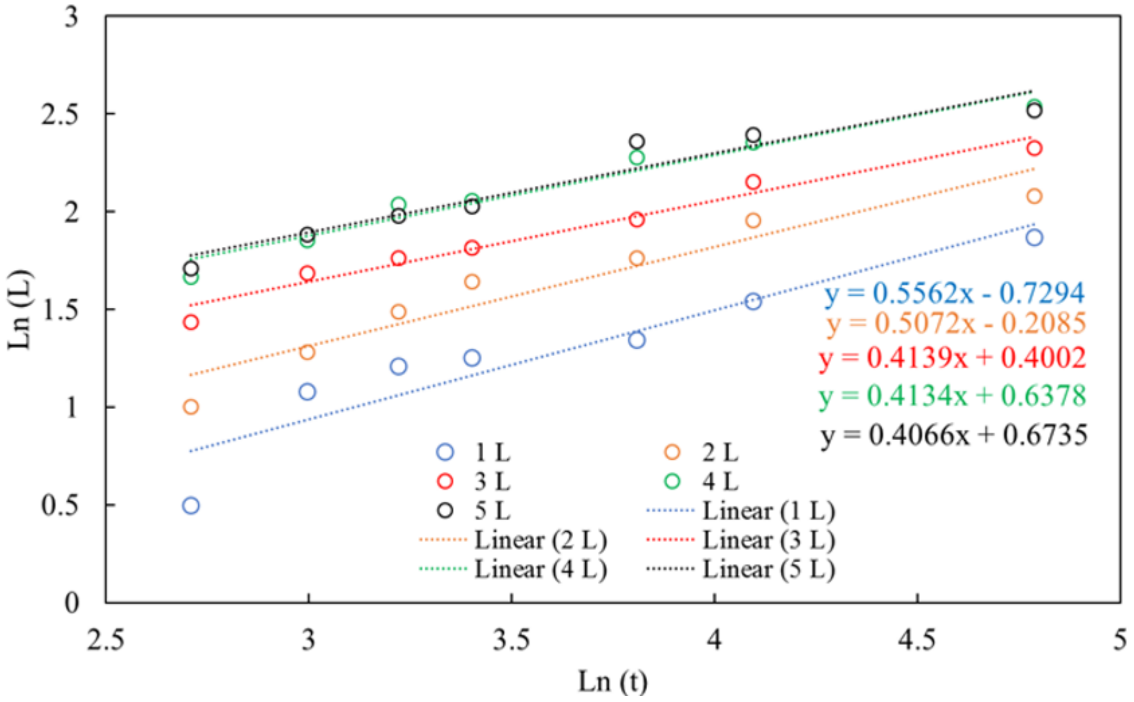

Figure 3.8: Logarithmic plot for the diameter of the plasma pattern as a function of the irradiation time and the fitted function (dash-line) for different gas flow rates

expected to increase the diffusion distribution of reactive species over the irradiation point, thereby increasing the diameter of the wetted area.

The spread of reactive species over the irradiation point follows a diffusion distribution. This limits the effective spreading area of oxidization, and causes saturation of the wetted area, as shown in Figure 3.7.

To evaluate the effect of the diffusion process on the size of the mask-free plasma patterns, the theoretical concepts presented in chapter 1.7.3 were investigated. The experimental data presented in Figure 3.7 were used in a logarithmic scale as defined by equation 1.16 and the analysis is shown in Figure 3.8.

As shown in Figure 3.8, the tangent of the fitted lines represents the effect of the irradiation time on the diffusion process. The expected theoretical value for diffusion as determined using equation 1.16 is 0.5 for ideal conditions. However, in the conducted experiments, the tangent values varied between 0.56 and 0.40, which is close to the expected value.

The experimental conditions generally deviated from the ideal conditions, and a shift of the tangent lines can generally be expected. This deviation can occur due to errors in the measurement of the wetting size, errors in time recording, and the non-effect of diffused radicals on surface modification.

3.3.2 Mask-free plasma patterning

HiPSC cultivation on the PDMS surface that was treated for 30 s using APPJ without a mask was performed as described in section 3.2.4. Figure 3.9 shows an overhead view of the cell culture dish and fluorescence image of the hiPSCs that were cultivated after two days of cell seeding.

As shown in Figure 3.9, mask-free plasma patterning of cell cultures is possible using the APPJ. The diameter of the cell culture area that was irradiated for 30 s was similar to the wetted diameter of approximately 5 mm, which was obtained for a gas flow rate of 3 L/min. These results confirm that APPJ produced reactive species that are similar to that of the low-pressure plasma for the oxidization of PDMS surfaces and hydrophilicity of the treated surfaces facilitated the adhesion of iPSCs.

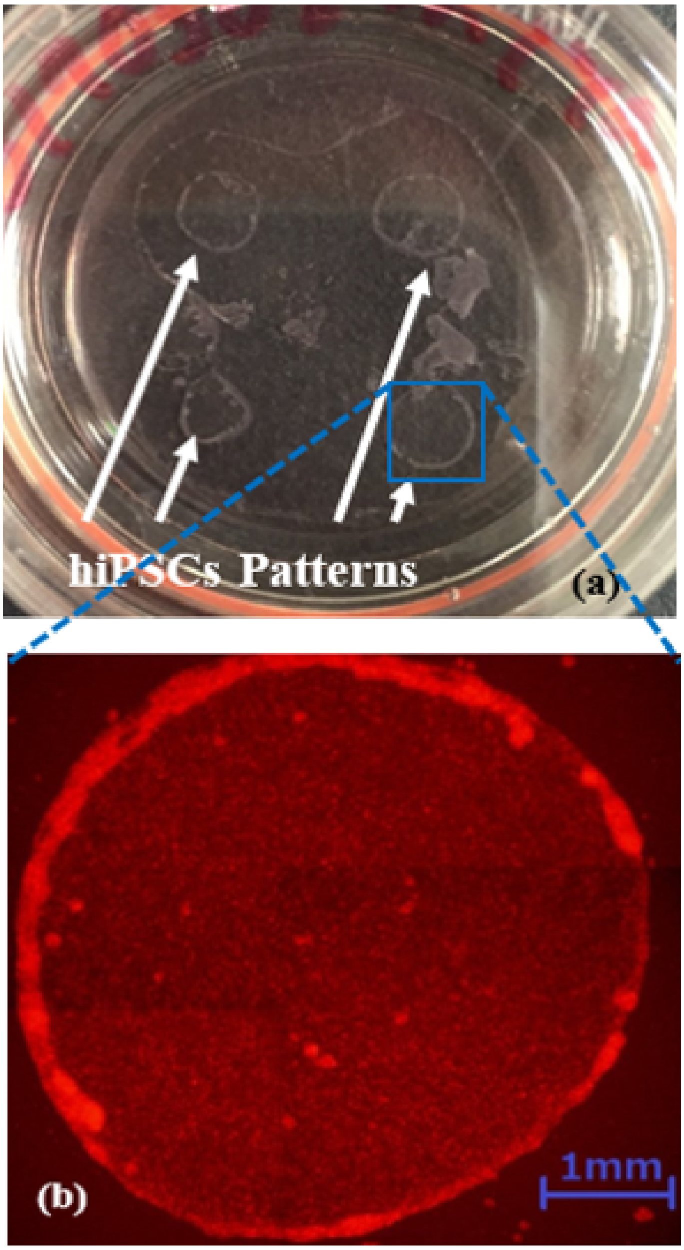

Figure 3.9: Overhead view of the hiPSCs cultured PDMS surface after two days; (a) patterned dish, and (b) fluorescence image of a single irradiation point [6]

3.4 Conclusion

The use of APPJ with mask-free plasma patterning compared to conventional low-pressure plasma patterning with a mask will lead to new opportunities in the field of cell culturing. Cell culturing on bio-compatible materials in laboratories is normally performed using low-pressure plasma patterning with a mask. Given that low-pressure plasma systems are expensive and the ability to change plasma parameters to investigate the effects of different parameters is limited, the use of APPJ as an alternative source can address these limitations. Therefore, in this chapter, the possibility of using atmospheric pressure plasma jets for plasma patterning without a mask was investigated for cell culturing on treated bio-compatible surfaces, as an alternative to conventional low-pressure plasma patterning. Cell culturing was investigated under laboratory conditions, with and without a mask for plasma patterning. The wettability of the plasma irradiated PDMS surfaces was investigated using the contact angle and the diameter of the mask-free plasma patterned area was estimated for different irradiation times and gas flow rates. Mask-free plasma treated PDMS surfaces were seeded with hiPSCs to cultivate cells using the APPJ source.

The experimental results presented in this chapter demonstrate that the hydrophilization changes of the treated PDMS surfaces using APPJ depend on the irradiation time and the gas flow rate. The increase in the irradiation time of the PDMS surfaces decreased the contact angle, which implied improvement of the hydrophilic property. The diameter of the wetted area also increased as the irradiation time increased.

In addition, the increase in the gas flow rate shifted the curve of the wetting area diameter as a function of the irradiation time upwards, while the contact angle curve was shifted downwards. The increase of the reactive species due to the increase of the gas flow rate was responsible for these shifts, and their distribution caused an increase of the wetted areas and saturation at a certain limit.

Chapter 4

Controllability of plasma patterning using APPJ

In this chapter, the use of a double electrode atmospheric pressure plasma jet was investigated with and without a ground connected additional floating pin electrode at the bottom of the plasma jet for plasma patterning and cell cultivation on treated polydimethylsiloxane surfaces. The effect of the electrode configurations, tube diameter, and the use of a mask for different irradiation times was investigated to better understand the parameters that control plasma patterning.

4.1 Introduction

In recent years, the applicability of plasma sources for biomedicine applications has attracted significant interest [3] [6] [9] [62] [99] [100] [102]. Plasma sources operating at room temperature known as atmospheric pressure plasma (APP) are among the main sources used for biomedicine applications [6] [9] [90] [98] [101] [102] [163]. To ability to generate radicals that facilitate biomedical applications at room temperature and obviate the need for complex vacuum systems results in notable advantages of APP compared to the other plasma sources. An example of a well-known APP technique is atmospheric pressure plasma jet (APPJ), which is widely used for biological applications due to its properties such as its cone shape, generation and propagation of reactive and excited particles along the jet, and its ability to focus the plasma jet to a localize position [8] [15] [73] [90] [154]. The investigation and improvement of the properties of APPJs have generated much interest in its application, especially in biomedicine fields.

Cell cultivation is an important area of medical application studies, as it is often the basis of patient-specific drug screening [147] [149] [164] as discussed in chapter 3. This process requires the use of culturing devises, of which the most notable biocompatible material for these devices is polydimethylsiloxane (PDMS) [84] [150]. PDMS has several useful properties including non-toxicity, chemical inertness, transparency, and gas permeability, which renders it as a suitable biocompatible material for many applications [82] [83] [84]. Although the surface of PDMS is hydrophobic, it can be hydrophilized using plasma irradiation [6] [63] [64] [149] [151] [153].

Generally, surface modification of PDMS is easily performed using low-pressure plasma with a mask for cell culturing [63] [64]. In this approach, the control of the size of the plasma-treated areas depends on the size of the mask, however, the effect of the irradiation time has not been considered [63] [64]. As discussed in chapter 3, these issues were addressed using an APPJ source without a mask as an alternative approach to plasma patterning and cell cultivation [6]. However, the effectiveness of APPJ with and without a mask for plasma patterning and cell cultivation requires further investigation.

Chapters 1 and 2 discussed the modification of the electrode configurations via the inclusion of an additional floating pin electrode connected to the ground voltage at the bottom of the plasma jet. This increased the length of the APPJ and the properties of the radical along the jet propagation direction [7] [144] [145]. These changes of the APPJ with respect to plasma patterning and cell cultivation must be investigated to better understand their effects, to improve the controllability of APPJ in plasma patterning.

In this chapter, several parameters that vary the wetting size due to plasma irradiation are investigated. The effect of electrode modification in the APPJ setup on PDMS surface fabrication and cell cultivation was investigated as a function of the irradiation time for different conditions. The tube diameter and the use of a mask in plasma patterning for cell cultivation were also investigated for different irradiation times to better understand the possible controlling parameters.

4.2 Methodology

In to investigate the controllability parameters for plasma pattern size, the parameters that affect the jet properties and the generation and propagation of radical needs to be considered. The parameters of electrode configuration, and tube diameter were considered to determine their effect on plasma patterning. In addition, the use of a mask instead of mask-free patterning was also investigated. The previous chapters in this dissertation discussed the effect of those parameters on the APPJ and its properties in the case of mask-free plasma patterning. In this section, the experimental methods and conditions used to investigate the controllability parameters are discussed.

4.2.1 Experimental condition

As discussed in chapter 2, a change in the electrode configuration caused a change in the properties of the plasma jet. Therefore, in this investigation, we used a double electrode configured APPJ with and without a ground connected additional floating pin electrode to generate a plasma jet (Figure 2.5). Helium with a purity of 99 % was used as the working gas and a 15 $\mathrm{kV_{P\text{-}P}}$ voltage with a frequency of 16 kHz was used to generate the plasma jet. As discussed in chapter 2, the increase of the jet length associated with the voltage is small compared to the configuration effect of the additional grounded pin electrode. Therefore, the investigation of the effect of the applied voltage as a controlling parameter was excluded in this study.

Plasma jet was generated using a commercially available quartz capillary tube with an outer diameter of 2.0 mm and an inner tube diameter of 1.0 mm (Hilgenberg GmbH). In addition, quartz capillary tubes with inner tube diameters of 120 μm and 60 μm at the nozzle exit were also used to generate plasma jets in this work. To fabricate quartz capillary tubes with micron-scale inner diameters, commercially available quartz capillary tubes with outer and inner diameters of 2.0 mm and 1.0 mm respectively, were used. Using these tubes, the outer and inner diameters were gradually reduced to develop inhouse capillaries, similar to the microcapillary tube reported by Kim *et al* [90], without an angled nozzle tip. In this work, the maximum plasma jet obtained in the laminar regime was used for the plasma treatment because the highest density of radicals is expected from these APPJs, as discussed in chapter 2.

Plasma irradiation was performed on spin-coated PDMS dishes in this work. The details of the PDMS (Sylgard 184 Silicone Elastomer Kit, Tokyo, Japan) used in this study has been previously reported by Yamada *et al* [63] [64]. To create PDMS coated dishes, approximately 0.1 mL PDMS was placed on a glass base cell culture dish (35 mm Tissue culture dishes, 93040, TPP, Switzerland) using a 1 mL syringe and spin coated at 1000 rpm for 60 seconds, followed by 3000 rpm for 120 seconds (MSA-100, Mikasa Corporation, Tokyo, Japan). The dishes were cured in an oven at 60 °C overnight.

4.2.2 Wettability of PDMS

In this work we used the sessile method, which was discussed in chapter 3.3.2, to measure the water contact angle of the irradiated PDMS surfaces as previously reported [6] [63] [64] [163]. Digital images of the droplets were acquired using a digital camera (Nikon D3100, with Micro-Nikkor-lens and 2x multiplier), and their

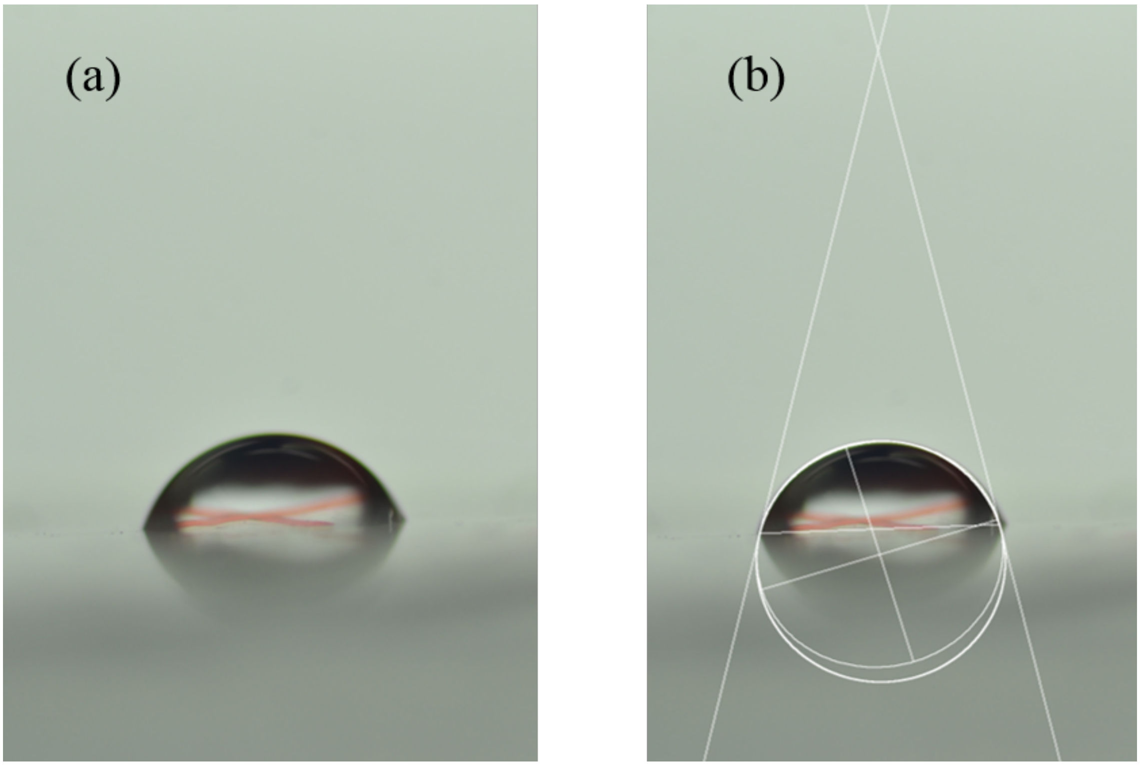

Figure 4.1: (a) Digital image of a water droplet and (b) digital image of ImageJ analyzed water droplet

contact angles were estimated using the ImageJ software [165]. Figure 4.1 shows a digital image of a water droplet on the treated PDMS surface and the resulting ImageJ analyzed image.

Plasma irradiation was conducted on the PDMS surfaces for 30, 60, 90, and 120 s using capillary tubes with different inner diameters and an additional floating pin electrode with and without a ground connection to estimate the contact angle. Water droplets were imaged after 5 mins after irradiation and measurements were performed for up to 96 hours (4 days) to analyze the hydrophilicity of the irradiated PDMS surfaces with against time.

4.2.3 Mouse cell cultivation

For this work, cultures and subculture of cells were produced using mouse osteoblast cells (MC3T3-E1) [166]that were obtained from the RIKEN BRC Cell Bank (RBRC-RCB1126, Tsukuba, Japan). The cells were cultured in serum medium composed of Dulbecco's modified Eagle's medium (043-30085, D-MEM High Glucose, FUJIFILM, Osaka, Japan), supplemented with 10 % fetal bovine serum and 1 % penicillin streptomycin (P4333-100ML, SIGMA-ALDRICH, Missouri, USA). For sub-culturing, the cells were washed 3 times using 1 mL PBS (Ca^{2+} - and Mg^{2+} - free phosphate buffered saline), then digested with 500 μL/well TrypLE select (12563-011, Life technologies, Carlsbad, USA). These cells were collected in a 15 mL centrifuge tube and centrifuged at 300 rpm for 3 minutes. The cells were then resuspended and inoculated in 2 mL of growth medium on 6-well culture plates (353046, FALCON, Cagno, Italia).

In this study, the coating procedure described by Yamada *et al* [63] [64] was utilized with a serum coating on treated PDMS surfaces for the cell cultures [164] [167]. Figure 4.2 shows the details of the procedure that was adopted for cell culturing after irradiation.

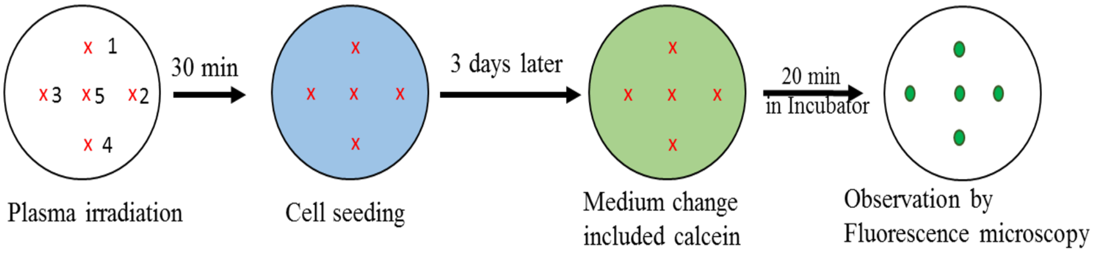

Figure 4.2: Procedure used for ell culture after fabrication of spin coated PDMS surfaces without a mask

Spin-coated PDMS dishes were used for surface treatment for cell culturing using the APPJ with and without additional pin grounded electrodes for irradiation times of 1, 3, 5, 7, 10, 30, 60, 90, and 120s. The plasma treated surfaces were used for the cell culture from 30 minutes to 1 hour after plasma treatment, during which the hydrophilicity of the PDMS surface was stable due to charging effect and the relaxation rate of the contact angle was low. The cells were inoculated at 1X10 ^{4} cells/cm^{2} with serum medium for each plasma irradiated position.

After 3 days of cell culturing, Calcein AM (C3100MP, Life technologies, Carlsbad, USA), a green fluorescent dye that can be transported into living cells, was added to the growth medium at a final concentration of 1 μM and incubated at 37 °C for 20 minutes. Living cells were observed with a fluorescence microscope (BZ-8100, KEYENCE, Osaka, Japan). To estimate the plasma patterning area, fluorescence images of the adhered cells stained with calcein AM after cell cultivation were investigated.

4.3 Results and discussion

The effect of the tube diameter, electrode configuration, and the use of a mask to control the plasma patterning and cell cultivation will be discuss in this section. The experimental results for the contact angle and plasma pattern sizes using cell cultivation were obtained using the experimental procedures described in section 4.2 to determine the relevant parameters.

4.3.1 Hydrophilicity on plasma treated surfaces

Hydrophilicity gives valuable information about the adhesion property of the plasma treated PDMS surfaces for cell culturing. To quantify the hydrophilicity of the plasma treated surfaces, the contact angle was estimated using the procedure described in section 4.2.2. The effect of the capillary tube diameter on the contact angle as a function of the irradiation time was investigated, and Figure 4.3 shows the estimated contact angles after 5 minutes of irradiation for different capillary tube configurations.

As shown in Figure 4.3, the hydrophilicity of the PDMS surfaces improved as the irradiation time increased, as reflected by the decrease of the contact angle. In addition, the contact angle tended to saturate at an angle of 15°for long irradiation times. The figure suggests that the behavior should be similar, irrespective of the inner tube diameter, except for an inner tube diameter of 60 μm This anomaly is expected due to the smaller wetted area, which is not able to contain the 2 μL water

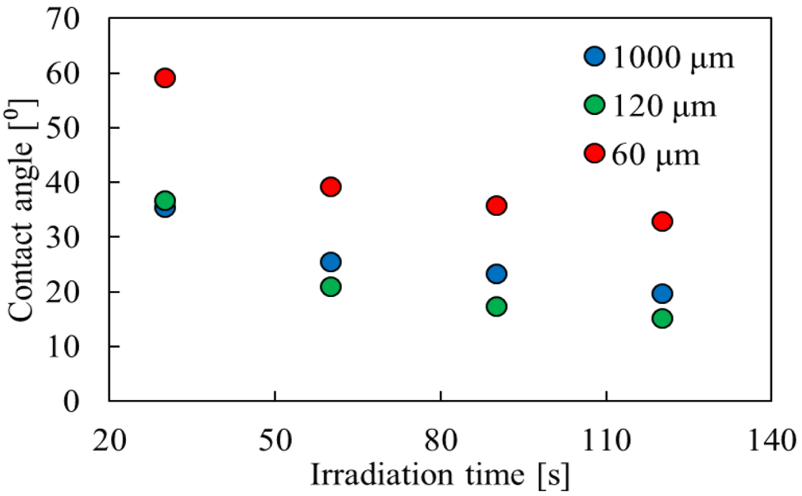

Figure 4.3: Variation of the contact angle for different irradiation times after 5 minutes of irradiation using the double electrode APPJ with an additional grounded pin electrode for different tube diameters

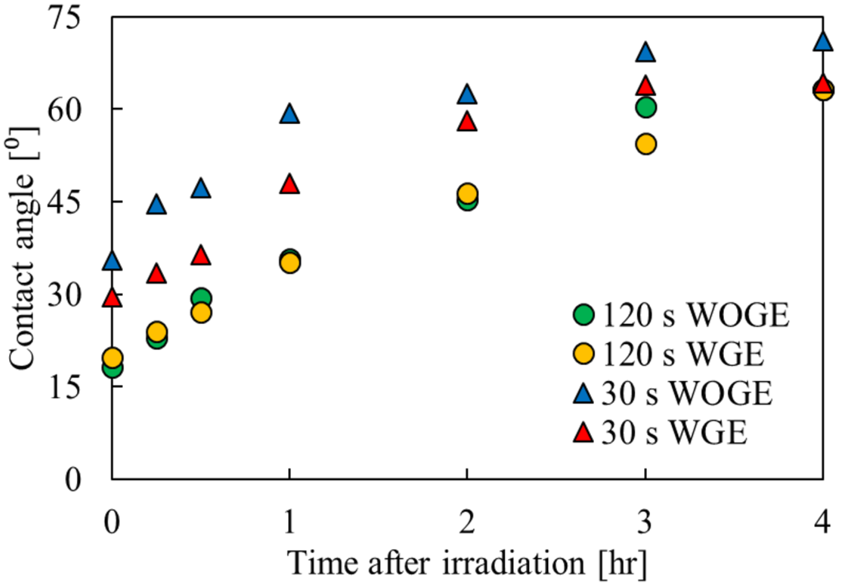

Figure 4.4: Contact angle versus time for irradiation of 120 s and 30 s for an inner tube diameter of 1.0 mm APPJ with (WGE) grounded pin electrode and with (WOGE) additional floating pin electrode

droplet in the irradiated area.

Plasma treated PDMS surfaces change their hydrophilic state to hydrophobic as relaxation occurs. Therefore, the expiration time of the hydrophilic condition

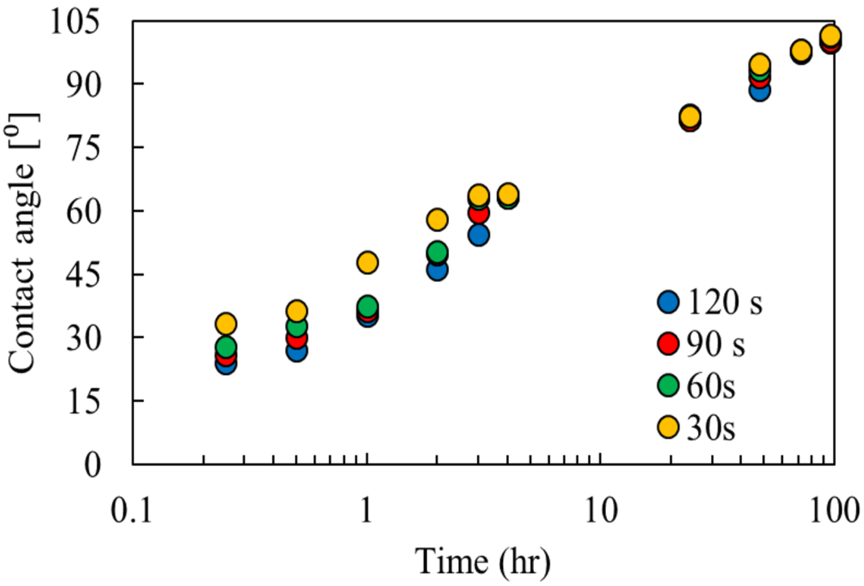

Figure 4.5: Relaxation of the contact angle as a function of time for irradiation of 30, 60, 90, and 120 s using capillary with an inner tube diameter of 1.0 mm for APPJ with a grounded additional pin electrode

of an irradiated PDMS surface was also investigated in this work. Figure 4.4 show the contact angle for a relaxation time of four hours, and for 120 s and 30 s irradiation time for the double electrode APPJ with and without a ground connected additional floating pin electrode, for an inner tube diameter of 1.0 mm.

As shown in Figure 4.4, as the time increases, the hydrophilic state changes to hydrophobic for the irradiated PDMS surfaces. An additional grounded pin electrode improved the hydrophilic property for a lower irradiation time (30 s) compared to a longer irradiation time (120 s).

Further observation of the relaxation of the hydrophilic state was conducted for four days. Figure 4.5 shows the relaxation of the hydrophilic condition for 96-hour rest time for 30, 60, 90, and 120 s irradiation time using APPJ with a ground connected additional floating pin electrode and a tube diameter of 1.0 mm.

As shown in Figure 4.5, the relaxation rate is approximately constant throughout the time scale of 1 hr and beyond. However, the relaxation rate of the contact angle is low during the first hour after irradiation. Further investigations were conducted for all the APPJ configurations used in this work to identify their impact on the relaxation time in the first two hours. A summary of the first two-hour relaxation is presented in Table 4.1.

Table 4.1: Variance of contact angle (CA) against time steps for different APPJ configurations

		APPJ Configuration															
		60 μm - WGE				120 μm - WGE				1000 μm - WGE				1000 μm - W0GE			
Irradiation time (s)		30	60	90	120	30	60	90	120	30	60	90	120	30	60	90	120
CA [°]	5 min	58.0	37.5	36.9	31.7	35.2	19.0	15.5	14.1	30.7	24.4	22.8	19.8	37.0	22.0	19.8	16.5
	30 min	62.0	45.4	41.6	37.1	52.8	32.4	31.9	28.1	36.2	31.7	28.7	26.3	48.2	37.0	32.4	29.5
CA variance between 5 min and 30 min [°]		4.0	7.9	4.7	5.4	17.6	13.4	16.4	14.0	5.5	7.3	5.9	6.5	11.2	15.0	12.6	13.0
CA [°]	1 hour	65.4	59.8	52.9	48.2	54.8	39.5	39.4	38.9	43.9	37.7	37.5	36.9	58.1	46.0	38.9	37.1
CA variance between 30 min and 1 hour [°]		3.4	14.4	11.3	11.1	2.0	7.1	7.5	10.8	7.7	6.0	8.8	10.6	9.9	9.6	6.5	7.6
CA [°]	2 hour	73.5	66.7	59.1	57.2	59.3	52.6	47.7	45.8	55.7	50.0	48.3	47.0	61.5	53.0	51.3	44.8
CA variance between 1 hour and 2 hour [°]		8.1	6.9	6.2	9.0	4.5	13.1	8.3	6.9	11.8	12.3	10.8	10.1	3.4	7.0	12.4	7.7

As shown in Table 4.1, the variation of the contact angle is reduced between 30 minutes and 1-hour. This indicates that the wettability of the treated surface is stable between 30 minutes and 1 hour for cell seeding.

4.3.2 Cell culture on mask-free plasma patterning

Similar to the discussion in chapter 3 and the procedure explained in section 4.2.4, cell cultivation was conducted on an irradiated PDMS surface. Fluorescence images of the cell cultivation for 0, 1, 3, 5, 7, 10, 30, 60, 90, and 120 s irradiation time are shown in Figure 4.6.

As shown in Figure 4.6, the mask free plasma pattering for cell cultivation is possible using the double electrode APPJ configuration. Increasing the irradiation time facilitated an increase of the area of the cell culture.

The results shown in section 4.3.1 indicate that an increase in the irradiation time causes a decrease of the contact angle, whereas Figure 4.6 shows that the plasma pattern size increases. The relationship between the contact angle and the size of the plasma pattern as a function of the irradiation is shown in Figure 4.7.

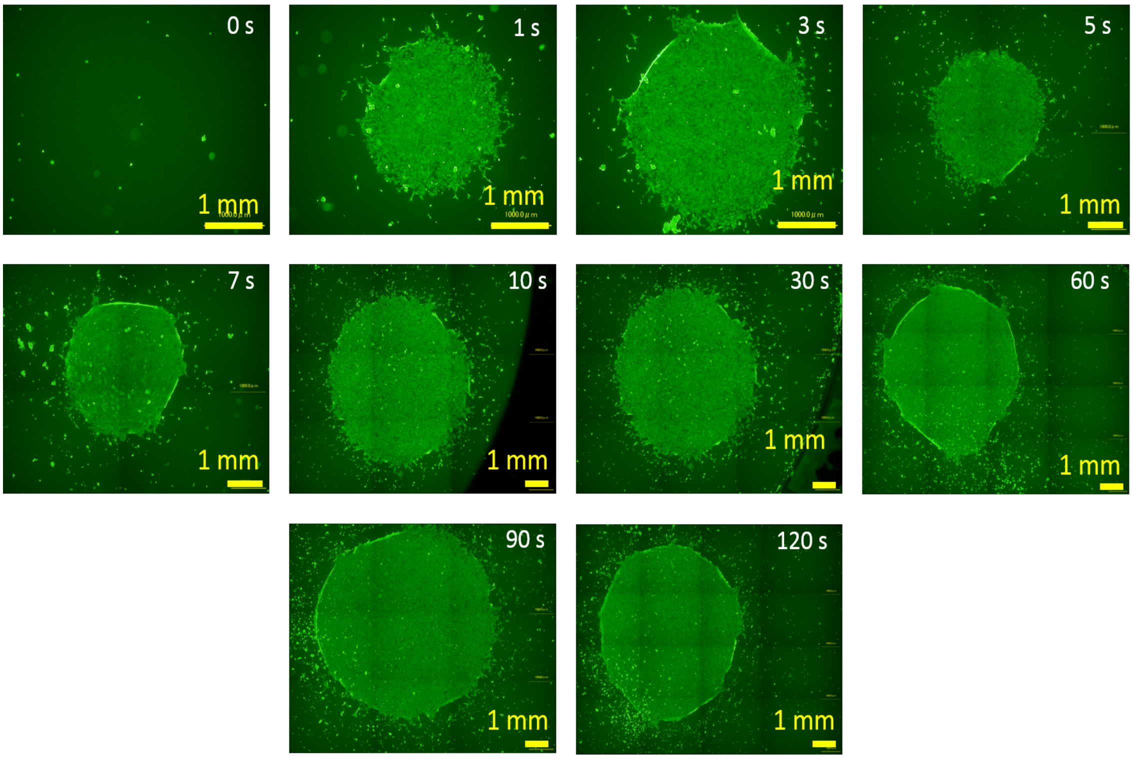

Figure 4.6: Fluorescence images of the Calcein AM induced mouse cells (MC3T3-E1) for 0, 1, 3, 5, 7, 10, 30, 60, 90, and 120 s irradiation time

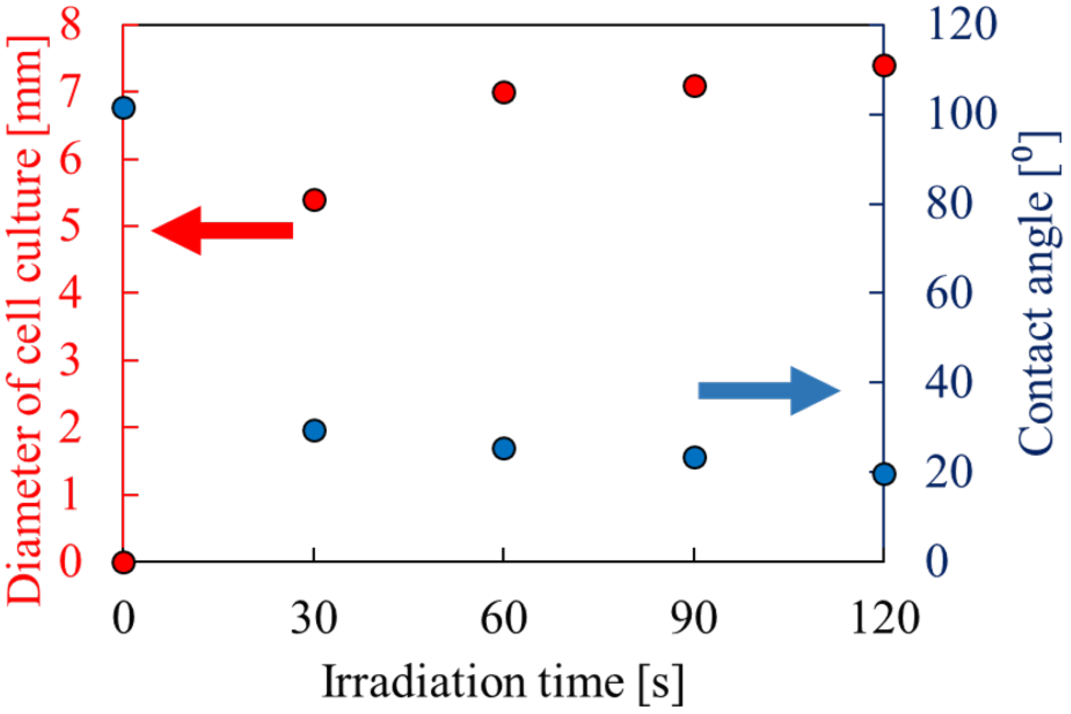

Figure 4.7: Diameter of cell culture and contact angle as a function of the irradiation time

The effect of the irradiation time on the PDMS surface increases the hydrophilic condition and its effective area as the irradiation time increases. Surface modification of the PDMS was expected due to the charged and excited electrons (e), hydroxyl (OH), nitrogen (N), and oxygen (O) [168] [169] [170]. Akishev *et al* [171] demonstrated that radicals of N, NO, and O are distributed along the surface of a substrate. Therefore, as the irradiation time increases, the density of the radicals increases and affects the PDMS surface modification process, causing the size of the wetted areas to increase, as explained in chapter 3.

4.3.3 Effect of additional floating pin electrode on cell culturing

The additional floating pin electrode connected to the ground voltage can improve the plasma jet properties as described in chapter 2. Therefore, in this study, we hypothesize that placing an additional grounded pin electrode at the bottom of the culture dish would cause an increase of the density of the species, in addition to focusing of the plasma plume at a localized point, leading to a decrease of the cell culturing area. Figure 4.8 shows the diameter of the cell culturing area for different irradiation times, for APPJ with and without a ground connected additional floating pin electrode.

For lower irradiation periods (less than 10 second), the additional pin grounded electrode caused an increase in the cell culturing area diameter compared to the area without the additional pin grounded electrode. As expected, the additional pin grounded electrode attracts a large number of radicals along the plasma jet to focus on the APPJ treated areas [172], causing an increase of the wetting diameter. The increase of irradiation time in both configurations is expected to increase the density of the species. The increase in the concentration of the species is expected to cause a saturation of the reactions for surface modification, and excess amounts of species to be distributed along the surface via diffusion distribution, to increase the wetting size. These phenomena need to be further investigated to confirm the proposed explanation for the increase of the wetting area as a function of the increase of the irradiation time for both the APPJ configurations.

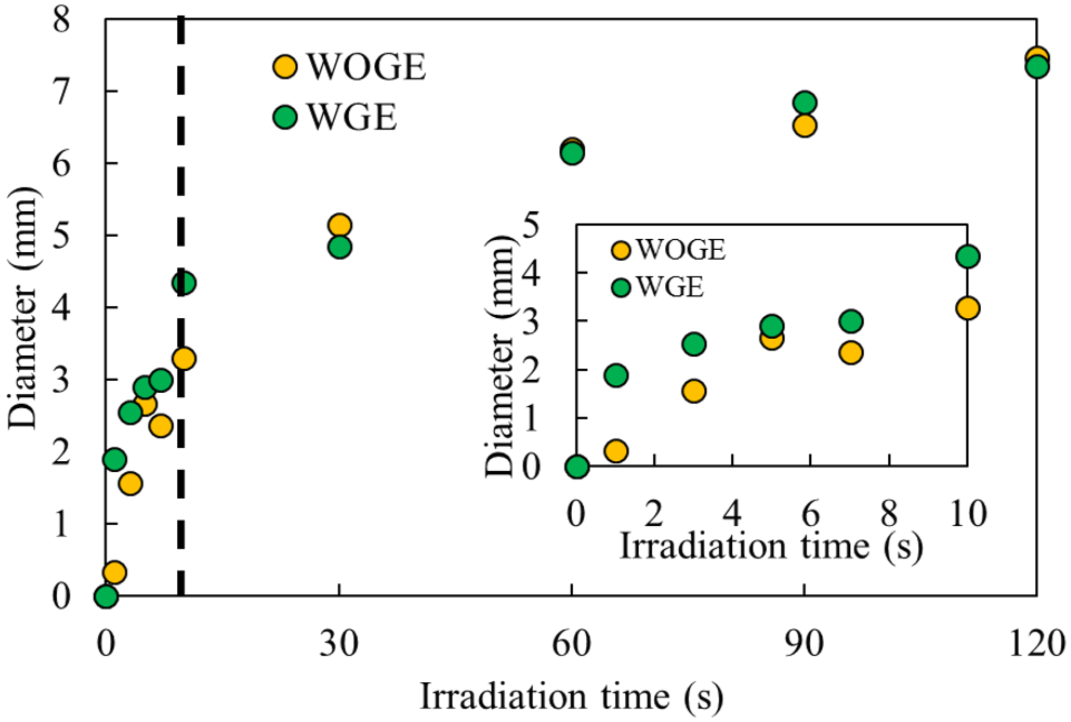

Figure 4.8: Diameter of cell culture as a function of irradiation times for 1.0 mm inner diameter capillary tube APPJs with (WGE) and without (WOGE) grounded connected additional pin electrode

4.3.4 Effect of tube diameter on cell culturing

A decrease in the tube diameter resulted in the generation of lower diameter visible APPJs. Therefore, the hypothesis of this study is that a decrease of the tube diameter for the double electrode APPJ configuration with plasma irradiation without a mask will cause a decrease of the plasma pattern size. Figure 4.9 shows the diameter of the cell culture areas as a function of the irradiation time for APPJ configurations with different diameters.

Although the smaller inner tube diameter reduces the radius of the visible APPJ, the spread of the radicals over the fabricated substrate was similar. This may be due to the spread of the radicals all over the surface, which is consistent with the results published by Akishev *et al* [171]. However, for lower irradiation times, the effect of the tube diameter caused a decrease of the diameter of the wetted area as the tube diameter decreased.

In addition, the decrease of the tube diameter caused a decrease of the effective plasma jet length and required the adjustment of the effective irradiation point to be closer to the nozzle exit. These conditions suggest an increase of the

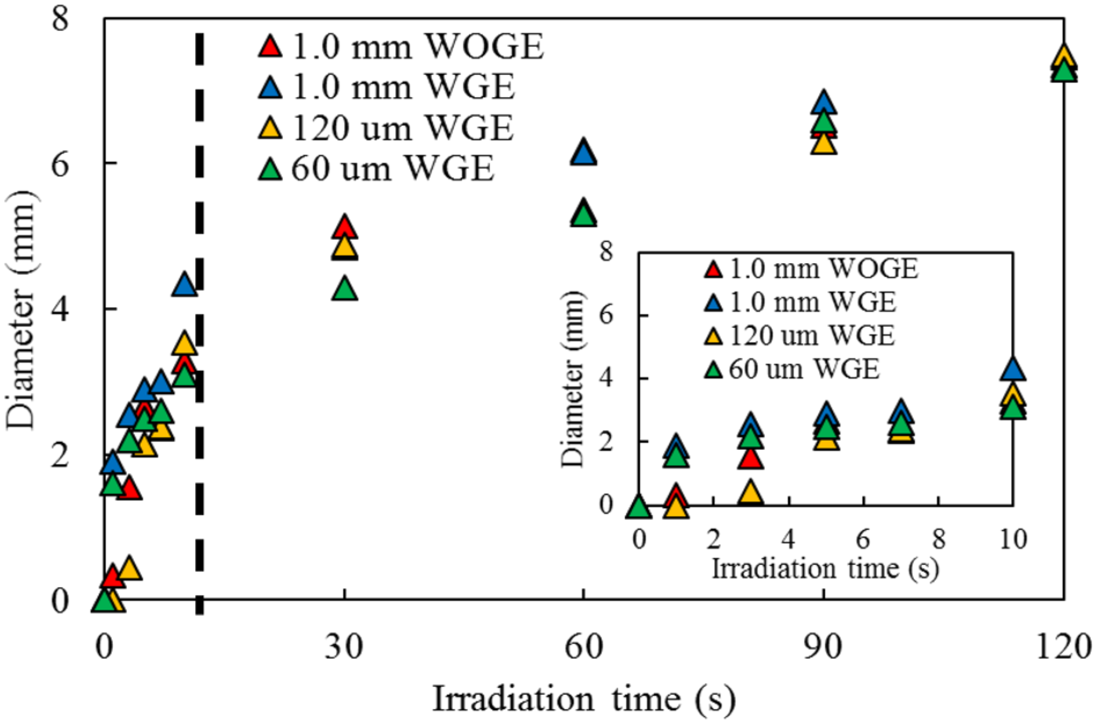

Figure 4.9: Diameter of cell culture as a function of the irradiation time for double electrode APPJ with (WGE) and without (WOGE) ground connected additional pin electrode configurations for different tube diameters

density of the species from the plasma at the fabricated surface of the PDMS and an increase of the diffusion process. Therefore, as shown in Figure 4.9, an increase of the cell culture area is expected. The irradiation required to obtain a certain pattern size decreases, irrespective of the diameter, as shown in Figure 4.9. This may be due to the effect of the density of the species generated at the surface of the PDMS. Similar to the discussion in the previous section (4.3.3), at longer irradiation times, the radicles are able to spread along the substrate, and thus the effect of the tube dimeter becomes ineffective as a function of the irradiation time in controlling the wetting size.

4.3.5 Mask effect on cell culturing

In conventional plasma patterning using a low-pressure plasma with a mask, due to the thorough spread of the plasma in the plasma chamber, the diameter of the wetted size is similar to the hole size of the mask [63] [64]. Such patterns were obtained using spin-coated PDMS dishes with a mask to pattern PDMS surfaces for cell culturing. The 0.5 mm thick PDMS sheets were cured in an oven at 60 °C overnight and these sheets were punched with 15 holes using 25 mm and 2 mm diameter belt punches (H.H.H. MANUFACTURING Corporation, Osaka, Japan) to produce masks. Masks with hole sizes of 1.0 mm and 2.0 mm were used in this study to investigate the effect of q mask on plasma patterning using APPJ. Given that the mask free plasma patterning sizes are on the order of millimeters, we hypothesize that the use of a mask facilitates plasma patterning on the order of the mask hole size. The process of irradiation and cell cultivation is similar to that described in section 4.2.4, except for the use of a mask during the irradiation process, as shown in Figure 4.10.

The microscopy and fluorescence images of the cell culture for different irradiation time using APPJ with

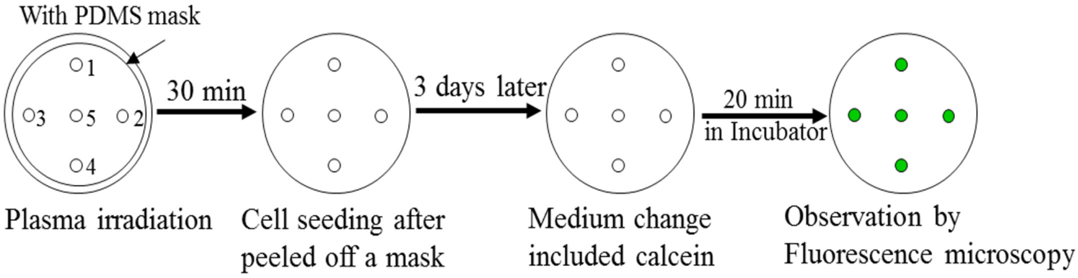

Figure 4.10: Procedure used for cell culture after fabrication of spin coated PDMS surfaces with a mask

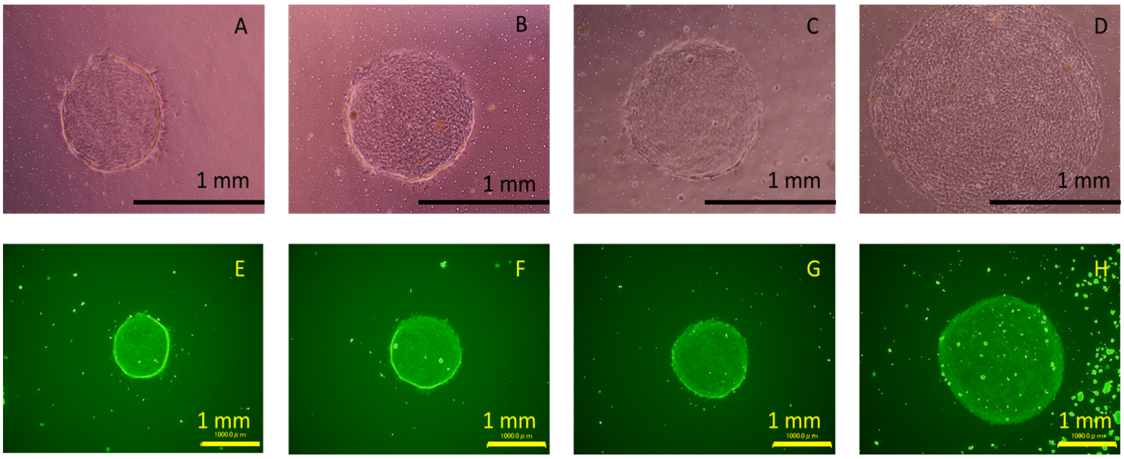

Figure 4.11: Phase-contrast microscopy images (A-D) of cell culture and fluorescence images (E-F, green color) of Calcein AM stained MC3T3-E1. The PDMS surfaces were irradiated by plasma using a mask with a hole size of 1.0 mm. A and E images are for 5 s; B and F images are for 7 s; C and G images are for 10 s; and D and H images are for 120 s irradiation

an additional grounded pin electrode for 1.0 mm inner diameter capillary tube with 1.0 mm mask size were captured and are shown in Figure 4.11.

As shown in Figure 4.11, the diameter of the cell culture increases as the irradiation time increases for lower irradiation times. When a specific irradiation time is exceeded, saturation of the pattern size to the limit of the mask size is observed. Charged particles that propagate through the APPJ are expected to be trapped in the mask holes resulting in shielding. This causes a decrease of the effective wetting size for shorter irradiation times. However, this temporary shielding is expected to be ineffective for irradiation times in excess of 30 s as the density of the charged particles increase, thereby diminishing the shielding effect via charge recombination. Such phenomena are expected to saturate the diameter of the cell culture to the same order of the mask after an irradiation time of 30 s or longer.

Further analysis was conducted to investigate the variation of the plasma patterning for different mask sizes. Figure 4.12 shows the diameter of the cell culture as a function of the irradiation time for masks with hole sizes of 1.0 mm and 2.0 mm.

As shown in Figure 4.12, an additional grounded pin electrode in the APPJ configuration and changes of tube diameter are ineffective compared to the mask effect. It was expecting that temporary shielding (Debye shield) occurred at shorter irradiation times around the masks, which reduced the wetting size to be less than the mask size. Decreasing the mask size causes a decrease of the plasma wetting size, and plasma patterning can be achieved for a size of a few hundred micrometers

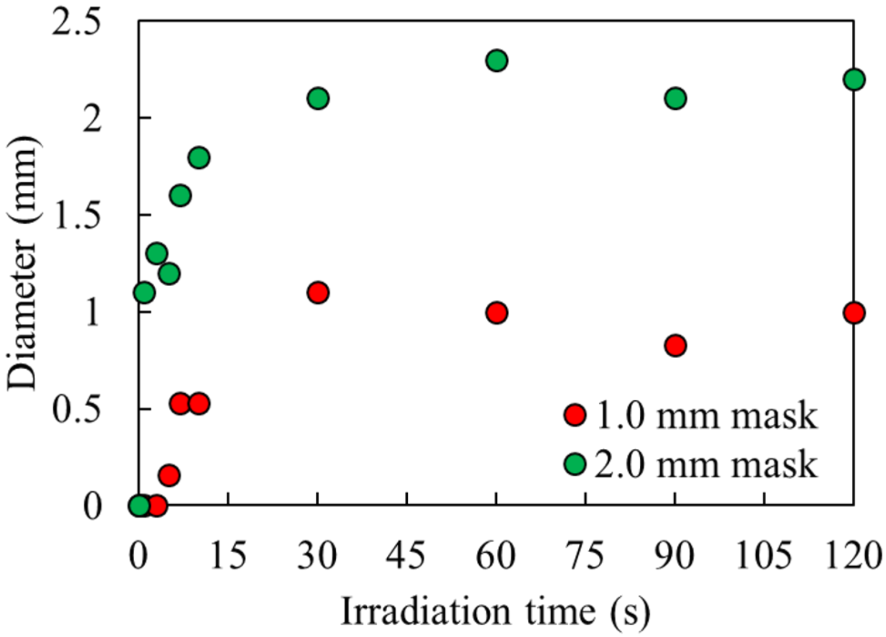

Figure 4.12: Diameter of the cell culture as a function of the irradiation time using the masks with hole sizes of 1.0 mm and 2.0 mm

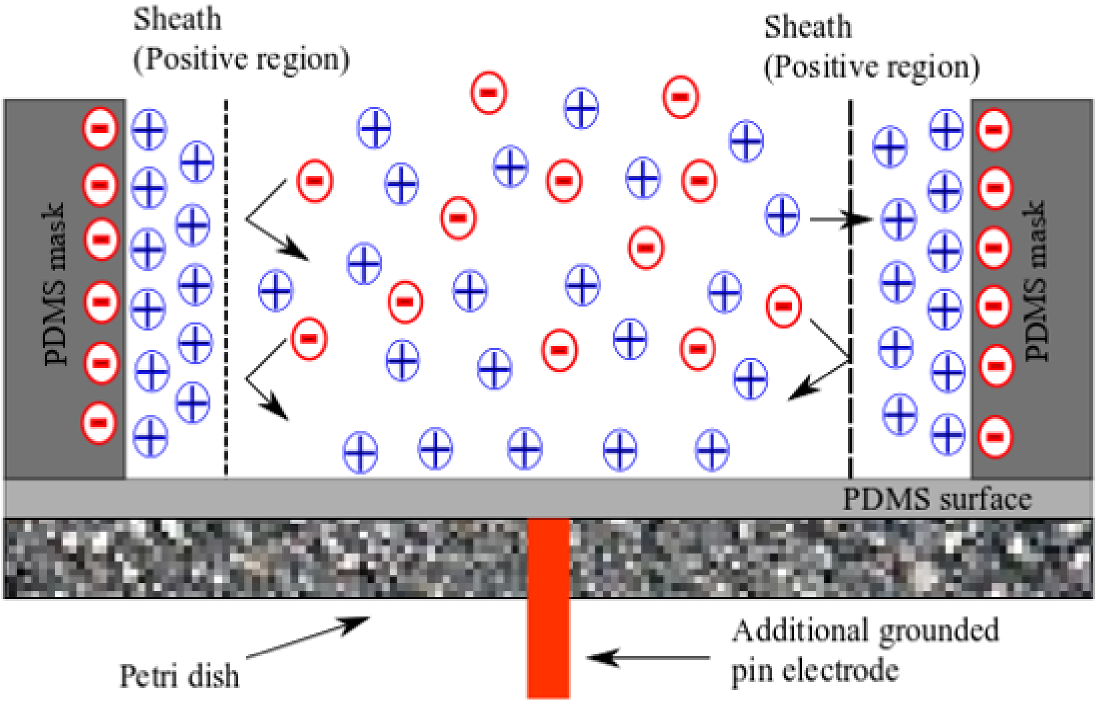

Figure 4.13: Formation of Debye sheath around the mask at shorter irradiation time

using a shorter irradiation time.

The illustration shown in Figure 4.13 depicts the expected events as mask patterning proceeds. As shown in Figure 4.13, a temporary shield is present for short irradiation times. An increase in the irradiation time causes an increase in the diffusion process, as discussed in chapter 3. Therefore, as the irradiation time increases, the diffusion process largely overcomes the shield that occurs during the mask patterning process. Hence, an increase in the irradiation time increases the pattern size.

The effect of the tube diameter on plasma patterning using a mask with a hole size of 1.0 mm was also investigated and Figure 4.14 shows the diameter of cell culture as a function of the irradiation time.

As shown in Figure 4.14, the decrease of tube diameter does not result in a decrease of the plasma patterning size for short irradiation times. The ability to decrease the wetting size is expected to mainly depend on the temporary shield that occur in the mask, due to the charge particles.

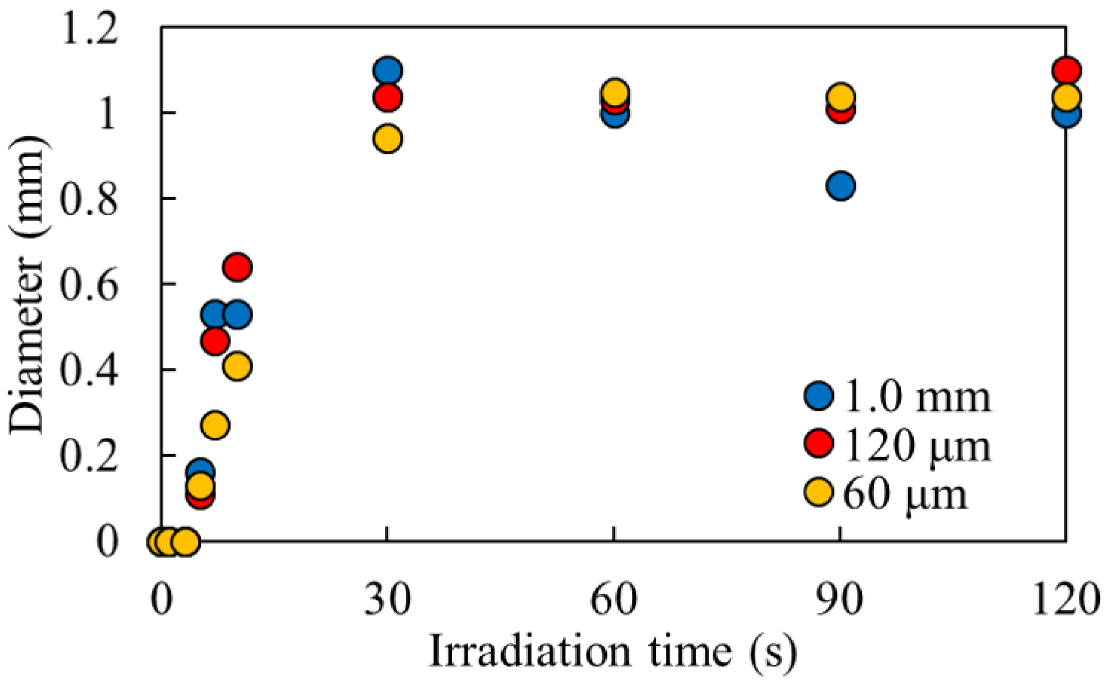

Figure 4.14: Diameter of the cell culture as a function of the irradiation time for different APPJ configurations using a mask with a hole size of 1.0 mm

4.4 Conclusion

Control of plasma patterning provides value to researchers in the culturing of cells on bio-compatible surface. In addition, the use of APPJ for plasma patterning addresses many of the limitations associated with current plasma patterning using low-pressure plasma. Chapter 3 discussed the possibility of using APPJ for the fabrication of bio-compatible materials for cell culturing. Given that this is a novel approach for plasma patterning, the control of the plasma pattern size was investigated. This chapter focused on the investigation of the use a double electrode APPJ for plasma patterning for cell culturing, and considered the parameters that affect the control of the plasma pattering size. The parameters of electrode configuration, tube diameter, and the use of a mask were investigated to better analyze the wettability of the treated surfaces and cell culturing.

Double electrode APPJ facilitates the improvement of the adhesion properties of PDMS for cell culturing. The hydrophilicity of the fabricated PDMS surfaces increased as the irradiation time increased along with the diameter of the cell culturing area. In this study, the experimental results indicate that the controllability of plasma patterning mainly depends on a shorter irradiation time. The use of a mask with the APPJ caused a decrease of the wetting size to a lower order than the mask hole size for a short irradiation time. It is expected that temporal shielding occurred in the mask because a short irradiation time facilitates the control of the wetting size. However, this phenomenon needs to investigated further to confirm its occurrence. The additional floating pin electrode connected to the ground voltage for the double electrode APPJ configuration and the inner tube diameter slightly affected the control of the wetting size, but its size was in millimeter range. Compared to the mask effect, the tube diameter and the inclusion of an additional grounded pin electrode were determined to be ineffective.

Chapter 5

Overall conclusions

This chapter summaries the conclusions of all the investigation conducted as part of the background and experimental work in this study in addition to potential future investigations.

A novel approach for mask-free plasma patterning of cell culture using atmospheric pressure plasma jet was investigated. In addition, parameter investigation was also conducted to identify the controllability of the plasma patterning size. To achieve these objectives, a background study was conducted on the properties of plasma jet such as the jet length, radical generation, and propagation along the jet, and the thermodynamic distribution. These properties were investigated for the effective parameters of electrode configuration, electrode polarity, capillary tube diameter, gas flow rate, and applied voltage to better understand the suitability of a plasma jet for mask-free plasma patterning.

The different chapters of this dissertation cover the background of possible mask-free plasma patterning for cell culture, the effect of different parameters on the jet properties, and the achievement of mask-free plasma patterning using APPJ. Chapter 1 in this study was focused on understanding the breakdown process of APPJ's, plasma spectroscopy in the identification of radicals, and the properties of microdevices used for cell culture. Chapters 2 to 4 was focused on the experimental investigations for the effective parameters of plasma jet length, generation and propagation of reactive species, the possibility of mask-free plasma patterning, and control of the pattern sizes.

Atmospheric pressure plasma jets used in this study exhibit low-frequency AC glow discharge. Parallel electrode and double electrode configured APPJs have been used for plasma irradiation of bio-compatible PDMS surfaces for cell culturing. Experimental results for both the plasma jets reveal that the double electrode configured APPJ has a longer plasma jet compared to the parallel electrode configuration because of the increase in the external electric field strength along the plasma jet propagation direction. The generated reactive species are also changed by the alignment of electrodes, as the double electrode is able to increase the reaction cross-section to generate dense reactive species when compared to the parallel electrode configuration.

The addition of the pin electrode at the bottom of the double electrode plasma jet improved the jet properties. The experimental evidence revealed that the additional grounded pin electrode caused an increase of the plasma jet length as well as the density of the species. Similar to the breakdown process in the double electrode configuration, the additional grounded pin electrode caused the plasma jet to undergo a streamer triggered glow discharge. A change in the ground connection with a high voltage for the additional pin electrode revealed similar jet properties. Hence, considering the safety of the experimental conditions for the intended application, this study considers the use of a double electrode configured APPJ with an additional grounded pin electrode at the bottom of the plasma jet. The investigation of radical generation and propagation and the controlling parameters of the pattern size was performed using the double electrode with an additional grounded pin electrode configured APPJ. The optical emission from the radicals was enhanced compared to the ordinary APPJs and the floating one. From the experimental results, it is expected that the additional grounded pin electrode can improve the plasma jet properties according to the electric field strength at the end of the plasma jet. It might increase the propagation velocity and the jet length. In addition, the spectra for the N_2^+ and O_2^+ species were observed in the vicinity of the pin electrode. This may be because penning ionization occurs on the pin electrode.

The plasma jet properties were found to be affected by the capillary tube diameter and flow rate. The change in the flow behavior from the laminar regime to the turbulent regime caused a change of the plasma jet properties in terms of the jet length as well as radical generation and propagation. The jet length and the densities of the radical were maximized when the plasma jet laminar flow regime reached its upper limit. Capillary tubes with diameters of 1.4 mm and 1.0 mm generated the longest plasma jets in the laminar regime. An increase in the gas flow rate in the laminar regime caused a shift of the peak position of N_2 (337 nm) and O (777 nm) along with the plasma jet, because the plasma jet velocity affects the radical's temporal and spatial distributions.

Many studies have shown that an increase of the applied voltage affects the plasma jet properties. This confirms its effect on the plasma jet. Considering the effect of the additional grounded pin electrode on the plasma jet properties, the impact of the voltage on the plasma jet properties is less based on the experimental results. The generation and propagation of radicals along with the plasma jet in the laminar regime for voltage effect show similar shapes, although they shift to higher densities as the voltage is increased.

Optical spectra from the APPJ revealed the presence of reactive oxygen species, which caused oxidization of the PDMS surfaces to improve the hydrophilic property. To identify the effect of reactive oxygen on the surface modification of PDMS, a parallel electrode configured APPJ was used. The result indicated that the wettability improved as the contact angle decreased when the irradiation time was increased. In addition, the APPJ treated PDMS surfaces were used to cultivate hiPSCs. The results reveal that the cells were cultured on the mask-free plasma patterned area.

Investigation of mask-free plasma patterning was performed by using a double electrode configured APPJ with and without a ground connected additional pin electrode. It was determined that jet properties were improved. Similar to the parallel electrode, the double electrode APPJs was also able to demonstrate mask-free plasma patterning for cell culturing. Although, the double electrode configured APPJ improves the jet properties, the diameter of the cell culture for both the electrode configurations tended to increase as the irradiation time was increased. Such a tendency was observed for all the APPJ configurations used in this study. The behavior of the diffusion process can be considered as a candidate to account for such behavior. As the irradiation time increased, the density of the reactive radicals for surface modification will increase and spread throughout the irradiate point to increase the wetting areas.

Plasma jet in the highest laminar flow due to different capillary tube diameters also exhibit similar plasma wetting sizes for different irradiation times. However, the use of a mask in the vicinity of the irradiation point decreased the diameter of the wetting area at shorter irradiation times. For shorter irradiation, it is expecting to generate a temporal Debye sheath around the mask due to charge particles for the interaction of reactive radicals with the surface of PDMS. As the irradiation time increases, the diffusion process overcomes the Debye shield to increase the plasma patterning size.

Finally, in this work, mask-free plasma patterning using APPJ was successful compared to the conventional low-pressure plasma patterning with a mask for cell cultivation. Plasma pattern sizes can be reduced to a few hundred-micrometer for APPJ irradiation with a short irradiation time using a mask. Regarding future work, the investigation of the spread of reactive species around the PDMS surface, the shielding effect that occurred in the mask for a low irradiation time, and the contact angle variation around the surface of the irradiation point can be investigated based on experimental and numerical studies.

Bibliography

[1] C. Tendero, C. Tixier, P. Tristant, J. Desmaison, and P. Leprince, "Atmospheric pressure plasmas: A review," *Spectrochimica Acta Part B: Atomic Spectroscopy*, vol. 61, no. 1, pp. 2–30, 2006.

[2] H. Conrads and M. Schmidt, "Plasma generation and plasma sources," *Plasma Sources Science and Technology*, vol. 9, no. 4, p. 441, 2000.

[3] K.-D. Weltmann and T. von Woedtke, "Plasma medicine—current state of research and medical application," *Plasma Physics and Controlled Fusion*, vol. 59, p. 014031, nov 2016.

[4] P. V. Thai, S. Abe, K. Kosugi, N. Saito, K. Takahashi, T. Sasaki, and T. Kikuchi, "Interaction and transfer of charged particles from an alternating current glow discharge in liquids: Application to silver nanoparticle synthesis," *Journal of Applied Physics*, vol. 125, no. 6, p. 063303, 2019.

[5] P. V. Thai, S. Abe, K. Kosugi, N. Saito, K. Takahashi, T. Sasaki, and T. Kikuchi, "Size/shape control of gold nanoparticles synthesized by alternating current glow discharge over liquid: the role of pH," *Materials Research Express*, vol. 6, p. 095074, jul 2019.

[6] W. T. L. S. Fernando, G. Kato, S. Miyazaki, K. Maruyama, K. Takahashi, T. Kikuchi, K. Ohnuma, and T. Sasaki, "Mask-free plasma patterning for biocompatible material using atmospheric pressure plasma jet," *IEEE Transactions on Radiation and Plasma Medical Sciences*, vol. 4, no. 1, pp. 108–112, 2020.

[7] W. T. L. S. Fernando, K. Motito, G. Kato, K. Ohnuma, K. Takahashi, T. Kikuchi, and T. Sasaki, "Effect of the additional ground electrode in double electrode configuration in maintaining stable atmospheric pressure plasma jet for bio-applications," 2018.

[8] I. Motrescu, A. Ogino, and M. Nagatsu, "Micro-patterning of functional groups onto polymer surface using capillary atmospheric pressure plasma jet,"

Journal of Photopolymer Science and Technology, vol. 25, no. 4, pp. 529–534, 2012.

[9] R. Wolf and A. C. Sparavigna, “Role of plasma surface treatments on wetting and adhesion,” *Engineering*, vol. 2, no. 6, pp. 397–402, 2010.

[10] N. S. J. Braithwaite, “Introduction to gas discharges,” *Plasma Sources Science and Technology*, vol. 9, pp. 517–527, oct 2000.

[11] R. Brandenburg, “Dielectric barrier discharges: progress on plasma sources and on the understanding of regimes and single filaments,” *Plasma Sources Science and Technology*, vol. 26, p. 053001, mar 2017.

[12] F. Paschen, “Ueber die zum funkenübergang in luft, wasserstoff und kohlensäure bei verschiedenen drucken erforderliche potentialdifferenz,” *Annalen der Physik*, vol. 273, no. 5, pp. 69–96, 1889.

[13] M. A. Lieberman and A. J. Lichtenberg, *Introduction*, ch. 1, pp. 1–22. John Wiley Sons, Ltd, 2005.

[14] S. P. Das, G. Dalei, and A. Barik, “A dielectric barrier discharge (DBD) plasma reactor: An efficient tool to measure the sustainability of non-thermal plasmas through the electrical breakdown of gases,” *IOP Conference Series: Materials Science and Engineering*, vol. 410, p. 012004, sep 2018.

[15] X. Lu, G. Naidis, M. Laroussi, S. Reuter, D. Graves, and K. Ostrikov, “Reactive species in non-equilibrium atmospheric-pressure plasmas: Generation, transport, and biological effects,” *Physics Reports*, vol. 630, pp. 1 – 84, 2016. Reactive species in non-equilibrium atmospheric-pressure plasmas: Generation, transport, and biological effects.

[16] M. Laroussi and T. Akan, “Arc-free atmospheric pressure cold plasma jets: A review,” *Plasma Processes and Polymers*, vol. 4, no. 9, pp. 777–788, 2007.

[17] X. Lu, M. Laroussi, and V. Puech, “On atmospheric-pressure non-equilibrium plasma jets and plasma bullets,” *Plasma Sources Science and Technology*, vol. 21, p. 034005, apr 2012.

[18] M. Teschke, J. Kedzierski, E. G. Finantu-Dinu, D. Korzec, and J. Engemann, “High-speed photographs of a dielectric barrier atmospheric pressure plasma jet,” *IEEE Transactions on Plasma Science*, vol. 33, no. 2, pp. 310–311, 2005.

[19] X. Lu and M. Laroussi, “Dynamics of an atmospheric pressure plasma plume generated by submicrosecond voltage pulses,” *Journal of Applied Physics*, vol. 100, no. 6, p. 063302, 2006.

[20] N. Mericam-Bourdet, M. Laroussi, A. Begum, and E. Karakas, “Experimental investigations of plasma bullets,” *Journal of Physics D: Applied Physics*, vol. 42, p. 055207, feb 2009.

[21] A. Schutze, J. Y. Jeong, S. E. Babayan, Jaeyoung Park, G. S. Selwyn, and R. F. Hicks, “The atmospheric-pressure plasma jet: a review and comparison to other plasma sources,” *IEEE Transactions on Plasma Science*, vol. 26, no. 6, pp. 1685–1694, 1998.

[22] C. F. Gallo, “Coronas and gas discharges in electrophotography: A review,” *IEEE Transactions on Industry Applications*, vol. IA-11, no. 6, pp. 739–748, 1975.

[23] A. Anders, “Tracking down the origin of arc plasma science-ii. early continuous discharges,” *IEEE Transactions on Plasma Science*, vol. 31, no. 5, pp. 1060–1069, 2003.

[24] P. Fauchais and A. Vardelle, “Thermal plasmas,” *IEEE Transactions on Plasma Science*, vol. 25, no. 6, pp. 1258–1280, 1997.

[25] R. W. Smith, D. Wei, and D. Apelian, “Thermal plasma materials processing—applications and opportunities,” *Plasma Chem Plasma Process*, vol. 9, no. 1, p. 135S–165S, 1989.

[26] D. R. Mac Rae, “Plasma arc process systems, reactors, and applications,” *Plasma Chem Plasma Process*, vol. 9, no. 1, p. 85S–118S, 1989.

[27] A. Bogaerts, “The glow discharge: an exciting plasma,” *J. Anal. At. Spectrom.*, vol. 14, pp. 1375–1384, 1999.

[28] M. J. Druyvesteyn and F. M. Penning, “The mechanism of electrical discharges in gases of low pressure,” *Rev. Mod. Phys.*, vol. 12, pp. 87–174, Apr 1940.

[29] M. Goldman and R. S. Sigmond, “Corona and insulation,” *IEEE Transactions on Electrical Insulation*, vol. EI-17, no. 2, pp. 90–105, 1982.

[30] J. . Chang, P. A. Lawless, and T. Yamamoto, “Corona discharge processes,” *IEEE Transactions on Plasma Science*, vol. 19, no. 6, pp. 1152–1166, 1991.

[31] N. Jiang, A. Ji, and Z. Cao, “Atmospheric pressure plasma jet: Effect of electrode configuration, discharge behavior, and its formation mechanism,” *Journal of Applied Physics*, vol. 106, no. 1, p. 013308, 2009.

[32] T. Shao, W. Yang, C. Zhang, Z. Fang, Y. Zhou, and E. Schamiloglu, “Temporal evolution of atmosphere pressure plasma jets driven by microsecond pulses with positive and negative polarities,” *EPL (Europhysics Letters)*, vol. 107, p. 65004, sep 2014.

[33] S. Reuter, J. Winter, S. Iseni, S. Peters, A. Schmidt-Bleker, M. Dünnbier, J. Schäfer, R. Foest, and K.-D. Weltmann, “Detection of ozone in a MHz argon plasma bullet jet,” *Plasma Sources Science and Technology*, vol. 21, p. 034015, may 2012.

[34] R. Bussiahn, E. Kindel, H. Lange, and K.-D. Weltmann, “Spatially and temporally resolved measurements of argon metastable atoms in the effluent of a cold atmospheric pressure plasma jet,” *Journal of Physics D: Applied Physics*, vol. 43, p. 165201, apr 2010.

[35] A. Begum, M. Laroussi, and M. R. Pervez, “Atmospheric pressure He-air plasma jet: Breakdown process and propagation phenomenon,” *AIP Advances*, vol. 3, no. 6, p. 062117, 2013.

[36] G. B. Sretenović, I. B. Krstić, V. V. Kovačević, B. M. Obradović, and M. M. Kuraica, “Spatio-temporally resolved electric field measurements in helium plasma jet,” *Journal of Physics D: Applied Physics*, vol. 47, p. 102001, feb 2014.

[37] P. J. Bruggeman, N. Sadeghi, D. C. Schram, and V. Linss, “Gas temperature determination from rotational lines in non-equilibrium plasmas: a review,” *Plasma Sources Science and Technology*, vol. 23, p. 023001, apr 2014.

[38] R. van Rooij, J. S. Borbely, J. Simonet, M. D. Hoogerland, K. S. E. Eikema, R. A. Rozendaal, and W. Vassen, “Frequency metrology in quantum degenerate helium: Direct measurement of the $2^3S_1 \longrightarrow 2\ ^1S_0$ transition,” *Science*, vol. 333, no. 6039, pp. 196–198, 2011.

[39] “Nist atomic spectra database (version 5.6.1),” 2018.

[40] T. Murakami, K. Niemi, T. Gans, D. OConnell, and W. G. Graham, “Chemical kinetics and reactive species in atmospheric pressure helium–oxygen plasmas with humid-air impurities,” *Plasma Sources Science and Technology*, vol. 22, p. 015003, dec 2012.

[41] Y. Sakiyama and D. B. Graves, “Neutral gas flow and ring-shaped emission profile in non-thermal RF-excited plasma needle discharge at atmospheric pressure,” *Plasma Sources Science and Technology*, vol. 18, p. 025022, mar 2009.

[42] D. S. Stafford and M. J. Kushner, “$O_2(\Delta_1)$ production in He / O_2 mixtures in flowing low pressure plasmas,” *Journal of Applied Physics*, vol. 96, no. 5, pp. 2451–2465, 2004.

[43] Y. B. Golubovskii, V. A. Maiorov, J. Behnke, and J. F. Behnke, “Modelling of the homogeneous barrier discharge in helium at atmospheric pressure,” *Journal of Physics D: Applied Physics*, vol. 36, pp. 39–49, dec 2002.

[44] W. C. Richardson and D. W. Setser, “Penning ionization optical spectroscopy: Metastable helium (He 2^3S) atoms with nitrogen, carbon monoxide, oxygen, hydrogen chloride, hydrogen bromide, and chlorine,” *The Journal of Chemical Physics*, vol. 58, no. 5, pp. 1809–1825, 1973.

[45] V. Linss, “Spatial distribution of the neutral gas temperature in rf and dc magnetron sputter discharges determined by fitting rotational spectra of the N_2^+ using a two-temperature fit,” *Spectrochimica Acta*, vol. 60, pp. 253–263, Feb. 2005.

[46] P. Bruggeman and D. C. Schram, “On OH production in water containing atmospheric pressure plasmas,” *Plasma Sources Science and Technology*, vol. 19, p. 045025, jul 2010.

[47] J. T. Gudmundsson and E. G. Thorsteinsson, “Oxygen discharges diluted with argon: dissociation processes,” *Plasma Sources Science and Technology*, vol. 16, pp. 399–412, apr 2007.

[48] P. C. Cosby, “Electron-impact dissociation of oxygen,” *The Journal of Chemical Physics*, vol. 98, no. 12, pp. 9560–9569, 1993.

[49] K. Niemi, J. Waskoenig, N. Sadeghi, T. Gans, and D. OConnell, “The role of helium metastable states in radio-frequency driven helium–oxygen atmospheric pressure plasma jets: measurement and numerical simulation,” *Plasma Sources Science and Technology*, vol. 20, p. 055005, aug 2011.

[50] R. J. Vidmar, “On the use of atmospheric pressure plasmas as electromagnetic reflectors and absorbers,” *IEEE Transactions on Plasma Science*, vol. 18, no. 4, pp. 733–741, 1990.

[51] R. S. Berry, “The theory of penning ionization,” *Radiation Research*, vol. 59, no. 2, pp. 367–375, 1974.

[52] Riahi, R., Teulet, Ph., Ben Lakhdar, Z., and Gleizes, A., “Cross-section and rate coefficient calculation for electron impact excitation, ionisation and dissociation of H_2 and OH molecules,” *The European Physical Journal D - Atomic, Molecular, Optical and Plasma Physic*, vol. 40, no. 2, pp. 223–230, 2006.

[53] Y. Itikawa and N. Mason, “Cross sections for electron collisions with water molecules,” *Journal of Physical and Chemical Reference Data*, vol. 34, no. 1, pp. 1–22, 2005.

[54] B. R. Rowe, F. Vallée, J. L. Queffelec, J. C. Gomet, and M. Morlais, “The yield of oxygen and hydrogen atoms through dissociative recombination of H_2O^+ ions with electrons,” *The Journal of Chemical Physics*, vol. 88, no. 2, pp. 845–850, 1988.

[55] Millar, T. J., Farquhar, P. R. A., and Willacy, K., "The umist database for astrochemistry 1995*," *Astron. Astrophys. Suppl. Ser.*, vol. 121, no. 1, pp. 139–185, 1997.

[56] G. Dilecce, M. Simek, and S. D. Benedictis, "The $N_2(A^3\Sigma_u^+)$ energy transfer to OH($A^2\Sigma^+$) in low-pressure pulsed RF discharges," *Journal of Physics D: Applied Physics*, vol. 34, pp. 1799–1806, jun 2001.

[57] J. Bacri and A. Medani, "Electron diatomic molecule weighted total cross section calculation: Iii. main inelastic processes for N_2 and N_2^+," *Physica B+C*, vol. 112, no. 1, pp. 101 – 118, 1982.

[58] Y. S. Cao and R. Johnsen, "Recombination of N_4^+ ions with electrons," *The Journal of Chemical Physics*, vol. 95, no. 10, pp. 7356–7359, 1991.

[59] L. G. Piper, "State-to-state $\mathrm{N}_2(A^3\Sigma_u^+)$ energy-pooling reactions. i. the formation of $\mathrm{N}_2(C^3\Pi_u)$ and the herman infrared system," *The Journal of Chemical Physics*, vol. 88, no. 1, pp. 231–239, 1988.

[60] Y. Akishev, M. Grushin, V. Karalnik, A. Petryakov, and N. Trushkin, "On basic processes sustaining constricted glow discharge in longitudinal N_2 flow at atmospheric pressure," *Journal of Physics D: Applied Physics*, vol. 43, p. 215202, may 2010.

[61] J. R. Hall, C. A. L. Westerdahl, A. T. Devine, and M. J. Bodnar, "Activated gas plasma surface treatment of polymers for adhesive bonding," *Journal of Applied Polymer Science*, vol. 13, no. 10, pp. 2085–2096, 1969.

[62] W. Petasch, B. Kegel, H. Schmid, K. Lendenmann, and H. Keller, "Low-pressure plasma cleaning: a process for precision cleaning applications," *Surface and Coatings Technology*, vol. 97, no. 1, pp. 176 – 181, 1997.

[63] R. Yamada, K. Hattori, M. Tagaya, T. Sasaki, D. Miyamoto, K. Nakazawa, S. Sugiura, T. Kanamori, and K. Ohnuma, "Plasma-patterned polydimethylsiloxane surface with single-step coating with a mixture of vitronectin and albumin enables the formation of small discs and spheroids of human induced pluripotent stem cells," *Plasma Medicine*, vol. 4, no. 1-4, pp. 165–176, 2014.

[64] R. Yamada, K. Hattori, S. Tachikawa, M. Tagaya, T. Sasaki, S. Sugiura, T. Kanamori, and K. Ohnuma, "Control of adhesion of human induced pluripotent stem cells to plasma-patterned polydimethylsiloxane coated with vitronectin and γ-globulin," *Journal of Bioscience and Bioengineering*, vol. 118, no. 3, pp. 315 – 322, 2014.

[65] J. C. McDonald, D. C. Duffy, J. R. Anderson, D. T. Chiu, H. Wu, O. J. A. Schueller, and G. M. Whitesides, "Fabrication of microfluidic systems in

poly(dimethylsiloxane)," *ELECTROPHORESIS*, vol. 21, no. 1, pp. 27–40, 2000.

[66] Z.-S. Chang, G.-J. Zhang, X.-J. Shao, and Z.-H. Zhang, "Diagnosis of gas temperature, electron temperature, and electron density in helium atmospheric pressure plasma jet," *Physics of Plasmas*, vol. 19, no. 7, p. 073513, 2012.

[67] A. Yanguas-Gil, J. Cotrino, and A. R. González-Elipe, "Measuring the electron temperature by optical emission spectroscopy in two temperature plasmas at atmospheric pressure: A critical approach," *Journal of Applied Physics*, vol. 99, no. 3, p. 033104, 2006.

[68] V. Colombo, E. Ghedini, and P. Sanibondi, "Thermodynamic and transport properties in non-equilibrium argon, oxygen and nitrogen thermal plasmas," *Progress in Nuclear Energy*, vol. 50, no. 8, pp. 921 – 933, 2008. In Honour of Prof. Bruno Montagnini.

[69] Q. Y. Zhang, D. Q. Shi, W. Xu, C. Y. Miao, C. Y. Ma, C. S. Ren, C. Zhang, and Z. Yi, "Determination of vibrational and rotational temperatures in highly constricted nitrogen plasmas by fitting the second positive system of N_2 molecules," *AIP Advances*, vol. 5, no. 5, p. 057158, 2015.

[70] C. Biloiu, X. Sun, Z. Harvey, and E. Scime, "Determination of rotational and vibrational temperatures of a nitrogen helicon plasma," *Review of Scientific Instruments*, vol. 77, no. 10, p. 10F117, 2006.

[71] A. Sarani, A. Y. Nikiforov, and C. Leys, "Atmospheric pressure plasma jet in ar and Ar/H_2O mixtures: Optical emission spectroscopy and temperature measurements," *Physics of Plasmas*, vol. 17, no. 6, p. 063504, 2010.

[72] D. Mariotti, Y. Shimizu, T. Sasaki, and N. Koshizaki, "Gas temperature and electron temperature measurements by emission spectroscopy for an atmospheric microplasma," *Journal of Applied Physics*, vol. 101, no. 1, p. 013307, 2007.

[73] I. Jõgi, R. Talviste, J. Raud, K. Piip, and P. Paris, "The influence of the tube diameter on the properties of an atmospheric pressure he micro-plasma jet," *Journal of Physics D: Applied Physics*, vol. 47, p. 415202, sep 2014.

[74] V. Massereau-Guilbaud, I. Géraud-Grenier, and A. Plain, "Determination of the electron temperature by optical emission spectroscopy in a 13.56 MHz dusty methane plasma: Influence of the power," *Journal of Applied Physics*, vol. 106, no. 11, p. 113305, 2009.

[75] J. Jaroslav, Q. Algwari, D. O'Connell, and A. Bourdon, "Experimental-modeling study of an atmospheric-pressure helium discharge propagating in a

thin dielectric tube," *IEEE transactions on plasma science*, vol. 40, pp. 2912–2919, Nov. 2012. © 2012 IEEE.

[76] J. Jánský, P. L. Delliou, F. Tholin, P. Tardiveau, A. Bourdon, and S. Pasquiers, "Experimental and numerical study of the propagation of a discharge in a capillary tube in air at atmospheric pressure," *Journal of Physics D: Applied Physics*, vol. 44, p. 335201, aug 2011.

[77] J. Jánský, F. Tholin, Z. Bonaventura, and A. Bourdon, "Simulation of the discharge propagation in a capillary tube in air at atmospheric pressure," *Journal of Physics D: Applied Physics*, vol. 43, p. 395201, sep 2010.

[78] J. Jánský and A. Bourdon, "Simulation of helium discharge ignition and dynamics in thin tubes at atmospheric pressure," *Applied Physics Letters*, vol. 99, no. 16, p. 161504, 2011.

[79] Y. Yamashita, F. Yamazaki, A. Nezu, and H. Akatsuka, "Diagnostics of low-pressure discharge argon plasma by multi-optical emission line analysis based on the collisional-radiative model," *Japanese Journal of Applied Physics*, vol. 58, p. 016004, jan 2019.

[80] G. Uchida, K. Takenaka, K. Kawabata, and Y. Setsuhara, "Influence of he gas flow rate on optical emission characteristics in atmospheric dielectric-barrier-discharge plasma jet," *IEEE Transactions on Plasma Science*, vol. 43, pp. 737–744, 2015.

[81] J. A. Byrne, "Overcoming clinical hurdles for autologous pluripotent stem cell-based therapies," *OA Stem Cells*, vol. 01, p. 1(1):3, 2013.

[82] J. El-Ali, P. Sorger, and K. Jensen, "Cells on chips," *Nature*, vol. 442, pp. 403–411, 2006.

[83] K. Gupta, D.-H. Kim, D. Ellison, C. Smith, A. Kundu, J. Tuan, K.-Y. Suh, and A. Levchenko, "Lab-on-a-chip devices as an emerging platform for stem cell biology," *Lab Chip*, vol. 10, pp. 2019–2031, 2010.

[84] D. C. Duffy, J. C. McDonald, O. J. A. Schueller, and G. M. Whitesides, "Rapid Prototyping of Microfluidic Systems in Poly(dimethylsiloxane)," *Analytical Chemistry*, vol. 70, no. 23, pp. 4974–4984, 1998. PMID: 21644679.

[85] M. Nendza, "Hazard assessment of silicone oils (polydimethylsiloxanes, PDMS) used in antifouling-/foul-release-products in the marine environment," *Marine pollution bulletin*, vol. 54, August 2007.

[86] "Elevflow," 2020.

[87] I. Onyshchenko, A. Yu Nikiforov, N. De Geyter, and R. Morent, “Local Analysis of Pet Surface Functionalization by an Atmospheric Pressure Plasma Jet,” *Plasma Processes and Polymers*, vol. 12, no. 5, pp. 466–476, 2015.

[88] I. Onyshchenko, N. De Geyter, and R. Morent, “Improvement of the plasma treatment effect on PET with a newly designed atmospheric pressure plasma jet,” *Plasma Processes and Polymers*, vol. 14, no. 8, p. 1600200, 2017.

[89] L. Potočňáková, J. Hnilica, and V. Kudrle, “Spatially resolved spectroscopy of an atmospheric pressure microwave plasma jet used for surface treatment,” *Open Chemistry*, no. 1, 2014.

[90] J. Y. Kim, Y. Wei, J. Li, and S.-O. Kim, “15-μm-sized single-cellular-level and cell-manipulatable microplasma jet in cancer therapies,” *Biosensors amp; bioelectronics*, vol. 26, p. 555—559, October 2010.

[91] “Effects of surface wettability and contact time on protein adhesion to biomaterial surfaces,” *Biomaterials*, vol. 28, no. 22, pp. 3273 – 3283, 2007.

[92] J. Shohet, “Plasma science and engineering,” in *Encyclopedia of Physical Science and Technology (Third Edition)* (R. A. Meyers, ed.), pp. 401 – 423, New York: Academic Press, third edition ed., 2003.

[93] I. H. Hutchinson, *Principles of Plasma Diagnostics.* Cambridge University Press, 2 ed., 2002.

[94] A. Bogaerts, E. Neyts, R. Gijbels, and J. Mullen, van der, “Gas discharge plasmas and their applications,” *Spectrochimica Acta. Part B : Atomic Spectroscopy*, vol. 57, no. 4, pp. 609–658, 2002.

[95] M. Laroussi, “Nonthermal decontamination of biological media by atmospheric-pressure plasmas: review, analysis, and prospects,” *IEEE Transactions on Plasma Science*, vol. 30, no. 4, pp. 1409–1415, 2002.

[96] J. Ehlbeck, U. Schnabel, M. Polak, J. Winter, T. von Woedtke, R. Brandenburg, T. von dem Hagen, and K.-D. Weltmann, “Low temperature atmospheric pressure plasma sources for microbial decontamination,” *Journal of Physics D: Applied Physics*, vol. 44, p. 013002, dec 2010.

[97] J. Goree, B. Liu, D. Drake, and E. Stoffels, “Killing of s. mutans bacteria using a plasma needle at atmospheric pressure,” *IEEE Transactions on Plasma Science*, vol. 34, no. 4, pp. 1317–1324, 2006.

[98] X. Lu, Z. Jiang, Q. Xiong, Z. Tang, and Y. Pan, “A single electrode room-temperature plasma jet device for biomedical applications,” *Applied Physics Letters*, vol. 92, no. 15, p. 151504, 2008.

[99] K. D. Weltmann, E. Kindel, T. von Woedtke, M. Hähnel, M. Stieber, and R. Brandenburg, "Atmospheric-pressure plasma sources: Prospective tools for plasma medicine," *Pure and Applied Chemistry*, vol. 82, no. 6, pp. 1223 – 1237, 2010.

[100] J. Y. Kim, J. Ballato, P. Foy, T. Hawkins, Y. Wei, J. Li, and S.-O. Kim, "Apoptosis of lung carcinoma cells induced by a flexible optical fiber-based cold microplasma," *Biosensors amp; bioelectronics*, vol. 28, p. 333—338, October 2011.

[101] R. Brandenburg, J. Ehlbeck, M. Stieber, T. v. Woedtke, J. Zeymer, O. Schlüter, and K.-D. Weltmann, "Antimicrobial treatment of heat sensitive materials by means of atmospheric pressure rf-driven plasma jet," *Contributions to Plasma Physics*, vol. 47, no. 1-2, pp. 72–79, 2007.

[102] D. Ye, S.-Q. Wu, Y. Yu, L. Liu, X.-P. Lu, and Y. Wu, "Patterned graphene functionalization via mask-free scanning of micro-plasma jet under ambient condition," *Applied Physics Letters*, vol. 104, no. 10, p. 103105, 2014.

[103] Onyshchenko, Iuliia, Nikiforov, Anton Yu., De Geyter, Nathalie, and Morent, Rino, "The plasma footprint of an atmospheric pressure plasma jet on a flat polymer substrate and its relation to surface treatment*," *Eur. Phys. J. Appl. Phys.*, vol. 75, no. 2, p. 24712, 2016.

[104] K.-D. Weltmann, M. Polak, K. Masur, T. von Woedtke, J. Winter, and S. Reuter, "Plasma processes and plasma sources in medicine," *Contributions to Plasma Physics*, vol. 52, no. 7, pp. 644–654, 2012.

[105] J. F. Kolb, A.-A. H. Mohamed, R. O. Price, R. J. Swanson, A. Bowman, R. L. Chiavarini, M. Stacey, and K. H. Schoenbach, "Cold atmospheric pressure air plasma jet for medical applications," *Applied Physics Letters*, vol. 92, no. 24, p. 241501, 2008.

[106] J. L. Walsh, F. Iza, N. B. Janson, V. J. Law, and M. G. Kong, "Three distinct modes in a cold atmospheric pressure plasma jet," *Journal of Physics D: Applied Physics*, vol. 43, p. 075201, feb 2010.

[107] S. Förster, C. Mohr, and W. Viöl, "Investigations of an atmospheric pressure plasma jet by optical emission spectroscopy," *Surface and Coatings Technology*, vol. 200, no. 1, pp. 827 – 830, 2005. PSE 2004.

[108] M. Laroussi and X. Lu, "Room-temperature atmospheric pressure plasma plume for biomedical applications," *Applied Physics Letters*, vol. 87, no. 11, p. 113902, 2005.

[109] H. Min Joh, S. Ja Kim, T. H. Chung, and S. H. Leem, "Reactive oxygen species-related plasma effects on the apoptosis of human bladder cancer cells

in atmospheric pressure pulsed plasma jets," *Applied Physics Letters*, vol. 101, no. 5, p. 053703, 2012.

[110] Q. Xiong, A. Y. Nikiforov, M. Á. González, C. Leys, and X. P. Lu, "Characterization of an atmospheric helium plasma jet by relative and absolute optical emission spectroscopy," *Plasma Sources Science and Technology*, vol. 22, p. 015011, dec 2012.

[111] E. Karakas, M. Koklu, and M. Laroussi, "Correlation between helium mole fraction and plasma bullet propagation in low temperature plasma jets," *Journal of Physics D: Applied Physics*, vol. 43, p. 155202, mar 2010.

[112] Q. Li, J.-T. Li, W.-C. Zhu, X.-M. Zhu, and Y.-K. Pu, "Effects of gas flow rate on the length of atmospheric pressure nonequilibrium plasma jets," *Applied Physics Letters*, vol. 95, no. 14, p. 141502, 2009.

[113] K. Urabe, T. Morita, K. Tachibana, and B. N. Ganguly, "Investigation of discharge mechanisms in helium plasma jet at atmospheric pressure by laser spectroscopic measurements," *Journal of Physics D: Applied Physics*, vol. 43, p. 095201, feb 2010.

[114] J.-S. Oh, Y. Aranda-Gonzalvo, and J. W. Bradley, "Time-resolved mass spectroscopic studies of an atmospheric-pressure helium microplasma jet," *Journal of Physics D: Applied Physics*, vol. 44, p. 365202, aug 2011.

[115] J.-P. Boeuf, L. L. Yang, and L. C. Pitchford, "Dynamics of a guided streamer ('plasma bullet') in a helium jet in air at atmospheric pressure," *Journal of Physics D: Applied Physics*, vol. 46, p. 015201, nov 2012.

[116] H. Guo, X.-N. Zhang, J. Chen, H. ping Li, and K. K. Ostrikov, "Non-equilibrium synergistic effects in atmospheric pressure plasmas," *Scientific Reports*, vol. 8, 2018.

[117] Q. Wang, D. J. Economou, and V. M. Donnelly, "Simulation of a direct current microplasma discharge in helium at atmospheric pressure," *Journal of Applied Physics*, vol. 100, no. 2, p. 023301, 2006.

[118] K. Takeda, T. Kumakura, K. Ishikawa, H. Tanaka, M. Sekine, and M. Hori, "Behavior of absolute densities of atomic oxygen in the gas phase near an object surface in an AC-excited atmospheric pressure he plasma jet," *Applied Physics Express*, vol. 10, p. 036201, feb 2017.

[119] G. B. Sretenovic, I. B. Krstic, V. V. Kovacevic, B. M. Obradovic, and M. M. Kuraica, "Spectroscopic study of low-frequency helium dbd plasma jet," *IEEE Transactions on Plasma Science*, vol. 40, no. 11, pp. 2870–2878, 2012.

[120] S. Wu, X. Lu, Y. Yue, X. Dong, and X. Pei, "Effects of the tube diameter on the propagation of helium plasma plume via electric field measurement," *Physics of Plasmas*, vol. 23, no. 10, p. 103506, 2016.

[121] H. Cheng, X. Lu, and D. Liu, "The effect of tube diameter on an atmospheric-pressure micro-plasma jet," *Plasma Processes and Polymers*, vol. 12, no. 12, pp. 1343–1347, 2015.

[122] B. Niermann, T. Hemke, N. Y. Babaeva, M. Böke, M. J. Kushner, T. Mussenbrock, and J. Winter, "Spatial dynamics of helium metastables in sheath or bulk dominated rf micro-plasma jets," *Journal of Physics D: Applied Physics*, vol. 44, p. 485204, nov 2011.

[123] D. Breden, K. Miki, and L. L. Raja, "Self-consistent two-dimensional modeling of cold atmospheric-pressure plasma jets/bullets," *Plasma Sources Science and Technology*, vol. 21, p. 034011, may 2012.

[124] A. Ranjan and P. L. G. Ventzek, "Simulations of hybrid direct current radiofrequency (dc/rf) capacitively coupled plasmas," *Japanese Journal of Applied Physics*, vol. 58, p. 036001, feb 2019.

[125] R. Xiong, Q. Xiong, A. Y. Nikiforov, P. Vanraes, and C. Leys, "Influence of helium mole fraction distribution on the properties of cold atmospheric pressure helium plasma jets," *Journal of Applied Physics*, vol. 112, no. 3, p. 033305, 2012.

[126] I. Jõgi, R. Talviste, S. Raud, J. Raud, T. Plank, L. Moravský, M. Klas, and Matejčík, "Comparison of two cold atmospheric pressure plasma jet configurations in argon," *Contributions to Plasma Physics*, vol. 60, no. 3, p. e201900127, 2020.

[127] Q. Algwari and D. O'Connell, "Electron dynamics and plasma jet formation in a helium atmospheric pressure dielectric barrier discharge jet," *Applied Physics Letters*, vol. 99, pp. 1–3, Sept. 2011.

[128] C. Cheng, Z. Liye, and R.-J. Zhan, "Surface modification of polymer fibre by the new atmospheric pressure cold plasma jet," *Surface and Coatings Technology*, vol. 200, no. 24, pp. 6659 – 6665, 2006.

[129] Y.-H. Choi, J.-H. Kim, K.-H. Paek, W.-T. Ju, and Y. Hwang, "Characteristics of atmospheric pressure n2 cold plasma torch using 60-hz ac power and its application to polymer surface modification," *Surface and Coatings Technology*, vol. 193, no. 1, pp. 319 – 324, 2005. Asian-European International Conference on Plasma Surface Engineering 2003.

[130] X. Deng, J. Shi, and M. G. Kong, "Physical mechanisms of inactivation of bacillus subtilis spores using cold atmospheric plasmas," *IEEE Transactions on Plasma Science*, vol. 34, no. 4, pp. 1310–1316, 2006.

[131] H. Koinuma, H. Ohkubo, T. Hashimoto, K. Inomata, T. Shiraishi, A. Miyanaga, and S. Hayashi, "Development and application of a microbeam plasma generator," *Applied Physics Letters*, vol. 60, no. 7, pp. 816–817, 1992.

[132] J. Park, I. Henins, H. W. Herrmann, G. S. Selwyn, J. Y. Jeong, R. F. Hicks, D. Shim, and C. S. Chang, "An atmospheric pressure plasma source," *Applied Physics Letters*, vol. 76, no. 3, pp. 288–290, 2000.

[133] A. Bilgic, C. Prokisch, J. Broekaert, and E. Voges, "Design and modelling of a modified 2.45 ghz coaxial plasma torch for atomic spectrometry," *Spectrochimica Acta Part B: Atomic Spectroscopy*, vol. 53, no. 5, pp. 773 – 777, 1998.

[134] K. e. a. Kobashi, "Fibrous structures on diamond and carbon surfaces formed by hydrogen plasma under direct current bias and field electron-emission properties," *JOURNAL OF MATERIALS RESEARCH*, vol. 18, no. 2, 2003.

[135] Q. Xiong, X. Lu, Y. Xian, J. Liu, C. Zou, Z. Xiong, W. Gong, K. Chen, X. Pei, F. Zou, J. Hu, Z. Jiang, and Y. Pan, "Experimental investigations on the propagation of the plasma jet in the open air," *Journal of Applied Physics*, vol. 107, no. 7, p. 073302, 2010.

[136] S. S. Hodgman, R. G. Dall, L. J. Byron, K. G. H. Baldwin, S. J. Buckman, and A. G. Truscott, "Metastable helium: A new determination of the longest atomic excited-state lifetime," *Phys. Rev. Lett.*, vol. 103, p. 053002, Jul 2009.

[137] A. Lofthus and P. H. Krupenie, "The spectrum of molecular nitrogen," *Journal of Physical and Chemical Reference Data*, vol. 6, no. 1, pp. 113–307, 1977.

[138] W. T. L. S. Fernando, K. Takahashi, T. Kikuchi, and T. Sasaki, "Effect of additional pin electrode placing at the bottom of the plasma jet and flow behavior on radical generation and propagation," *IEEE Transactions on Plasma Science*, pp. 1–8, 2020.

[139] E. Robert, V. Sarron, T. Darny, D. Riès, S. Dozias, J. Fontane, L. Joly, and J.-M. Pouvesle, "Rare gas flow structuration in plasma jet experiments," *Plasma Sources Science and Technology*, vol. 23, p. 012003, jan 2014.

[140] Y. P. Raizer, *Gas discharge physics*. Berlin ; New York: Springer-Verlag, 1991.

[141] C. Lukas, M. Spaan, V. S. von der Gathen, M. Thomson, R. Wegst, H. F. Döbele, and M. Neiger, "Dielectric barrier discharges with steep voltage rise: mapping of atomic nitrogen in single filaments measured by laser-induced

fluorescence spectroscopy," *Plasma Sources Science and Technology*, vol. 10, pp. 445–450, jun 2001.

[142] P. Paris, M. Aints, F. Valk, T. Plank, A. Haljaste, K. V. Kozlov, and H.-E. Wagner, "Intensity ratio of spectral bands of nitrogen as a measure of electric field strength in plasmas," *Journal of Physics D: Applied Physics*, vol. 38, pp. 3894–3899, oct 2005.

[143] L. S. Waldrop, R. Kerr, and P. Richards, "Photoelectron impact excitation of O I 8446 åÅ emission observed from arecibo observatory," *Journal of Geophysical Research: Space Physics*, vol. 113, no. A1, 2008.

[144] W. T. L. S. Fernando, K. Takahashi, and T. K. ana Toru Sasaki, "Radical distribution along the plasma jet for double electrode appj with additional pin ground electrode," 2019.

[145] W. T. L. S. Fernando, K. Takahashi, and T. K. ana Toru Sasaki, "Behavior of atmospheric pressure plasma jet using double electrode with additional ground electrode," 2019.

[146] J.-J. Qiao, L. Zhang, D.-Z. Yang, Z.-X. Jia, Y. Song, Z.-L. Zhao, H. Yuan, Y. Xia, and W.-C. Wang, "Temporal evolution of the relative vibrational population of N2 ($C^3\Pi_u$) and optical emission spectra of atmospheric pressure plasma jets in He mixtures," *Journal of Physics D: Applied Physics*, vol. 52, p. 285203, may 2019.

[147] K. Takahashi, K. Tanabe, M. Ohnuki, M. Narita, T. Ichisaka, K. Tomoda, and S. Yamanaka, "Induction of pluripotent stem cells from adult human fibroblasts by defined factors," *Cell*, vol. 131, p. 861—872, November 2007.

[148] M. Jedrzejczak-Silicka, *History of Cell Culture*. IntechOpen.

[149] S. Sugiura, K. Nakazawa, T. Kanamori, and K. Ohnuma, "Application of microfluidics in stem cell culture," in *Advances in Microfluidics* (X.-Y. Yu, ed.), ch. 3, Rijeka: IntechOpen, 2016.

[150] J. Zhou, A. V. Ellis, and N. H. Voelcker, "Recent developments in pdms surface modification for microfluidic devices," *ELECTROPHORESIS*, vol. 31, no. 1, pp. 2–16, 2010.

[151] H. M. Tan, H. Fukuda, T. Akagi, and T. Ichiki, "Surface modification of poly(dimethylsiloxane) for controlling biological cells' adhesion using a scanning radical microjet," *Thin Solid Films*, vol. 515, no. 12, pp. 5172 – 5178, 2007. The Third International Symposium on Dry Process (DPS 2005).

[152] B. . Jo, L. M. Van Lerberghe, K. M. Motsegood, and D. J. Beebe, “Three-dimensional micro-channel fabrication in polydimethylsiloxane (pdms) elastomer,” *Journal of Microelectromechanical Systems*, vol. 9, no. 1, pp. 76–81, 2000.

[153] S. Pinto, P. Alves, C. Matos, A. Santos, L. Rodrigues, J. Teixeira, and M. Gil, “Poly(dimethyl siloxane) surface modification by low pressure plasma to improve its characteristics towards biomedical applications,” *Colloids and Surfaces B: Biointerfaces*, vol. 81, no. 1, pp. 20 – 26, 2010.

[154] S. Nakao, E. Stamate, and H. Sugai, “Plasma parameters in the vicinity of the quartz window of a low pressure surface wave discharge produced in o2,” *Thin Solid Films*, vol. 515, no. 12, pp. 4869 – 4873, 2007. The Third International Symposium on Dry Process (DPS 2005).

[155] J. B. Gurdon, “The developmental capacity of nuclei taken from intestinal epithelium cells of feeding tadpoles,” *Development*, vol. 10, no. 4, pp. 622–640, 1962.

[156] J. Gurdon and V. Uehlinger, “”fertile” intestine nuclei,” *Nature*, vol. 210, p. 1240—1241, June 1966.

[157] I. Wilmut, A. Schnieke, J. McWhir, A. Kind, and K. Campbell, “Viable offspring derived from fetal and adult mammalian cells,” *Cloning and Stem Cells*, vol. 9, no. 1, pp. 3–7, 2007. PMID: 17386005.

[158] M. J. Munsie, A. E. Michalska, C. M. O’Brien, A. O. Trounson, M. F. Pera, and P. S. Mountford, “Isolation of pluripotent embryonic stem cells from reprogrammed adult mouse somatic cell nuclei,” *Current Biology*, vol. 10, no. 16, pp. 989 – 992, 2000.

[159] J. Byrne, D. Pedersen, L. Clepper, M. Nelson, W. Sanger, S. Gokhale, D. Wolf, and S. Mitalipov, “Producing primate embryonic stem cells by somatic cell nuclear transfer,” *Nature*, vol. 450, p. 497—502, November 2007.

[160] M. Tachibana, P. Amato, M. Sparman, N. Gutierrez, R. Tippner-Hedges, H. Ma, E. Kang, A. Fulati, H. Lee, H. Sritanaudomchai, K. Masterson, J. Larson, D. Eaton, K. Sadler-Fredd, D. Battaglia, D. Lee, D. Wu, J. Jensen, P. Patton, S. Gokhale, R. Stouffer, D. Wolf, and S. Mitalipov, “Human embryonic stem cells derived by somatic cell nuclear transfer,” *Cell*, vol. 153, pp. 1228–1238, June 2013.

[161] K. Takahashi and S. Yamanaka, “Induction of pluripotent stem cells from mouse embryonic and adult fibroblast cultures by defined factors,” *Cell*, vol. 126, p. 663—676, August 2006.

[162] J. A. Thomson, J. Itskovitz-Eldor, S. S. Shapiro, M. A. Waknitz, J. J. Swiergiel, V. S. Marshall, and J. M. Jones, “Embryonic stem cell lines derived from human blastocysts,” *Science*, vol. 282, no. 5391, pp. 1145–1147, 1998.

[163] G. Kato, K. Morito, S. Miyazaki, K. Takahashi, T. Sasaki, T. Kikuchi, and a. K. Ohnuma, “Behavior of atmospheric pressure plasma jet using double electrode with additional ground electrode,” 2017.

[164] K. Ohnuma, A. Fujiki, K. Yanagihara, S. Tachikawa, Y. Hayashi, Y. Ito, Y. Onuma, T. Chan, T. Michiue, M. K. Furue, and M. Asashima, “Enzyme-free passage of human pluripotent stem cells by controlling divalent cations,” *Scientific reports*, vol. 4, p. 4646, 2014.

[165] W. Rasband, “Imagej,” 1997-2019.

[166] H. Sudo, H. A. Kodama, Y. Amagai, S. Yamamoto, and S. Kasai, “In vitro differentiation and calcification in a new clonal osteogenic cell line derived from newborn mouse calvaria.,” *Journal of Cell Biology*, vol. 96, pp. 191–198, 01 1983.

[167] R. Kobayashi, K. Maruyama, and a. K. Ohnuma, “Pattern culture using serum medium does not require a composite coat,” 2019.

[168] D. Xiao, H. Zhang, and M. Wirth, “Chemical modification of the surface of poly(dimethylsiloxane) by atom-transfer radical polymerization of acrylamide,” *Langmuir*, vol. 18, no. 25, pp. 9971–9976, 2002.

[169] S. Hong, S. Kim, J. Kim, and H. Hwang, “Hydrophilic surface modification of pdms using atmospheric rf plasma,” *Journal of Physics: Conference Series*, vol. 34, pp. 656–661, Apr. 2006.

[170] W.-S. Bae and M. W. Urban, “Reactions of antimicrobial species to imidazole-microwave plasma reacted poly(dimethylsiloxane) surfaces,” *Langmuir : the ACS journal of surfaces and colloids*, vol. 20, p. 8372—8378, September 2004.

[171] Y. S. Akishev, V. B. Karalnik, A. V. Petryakov, K. B. Popov, O. N. Sattarov, and N. I. Trushkin, “Optical spectrum of the coaxial DBD forming the plasma jet in fast air flow at atmospheric pressure,” *Journal of Physics: Conference Series*, vol. 1112, p. 012010, nov 2018.

[172] Y. S. Akishev, V. B. Karalnik, M. A. Medvedev, A. V. Petryakov, N. I. Trushkin, and A. G. Shafikov, “How ionization waves (plasma bullets) in helium plasma jet interact with a dielectric and metallic substrate,” *Journal of Physics: Conference Series*, vol. 927, p. 012040, nov 2017.